Master's thesis

NTNU
Norwegian University of Science and Technology
Faculty of Engineering
Department of Structural Engineering

Mikael Rosendahl

Comparison of Strut-and-Tie Modeling and Nonlinear Finite Element Analysis Approaches for Concrete Wall-to-Wall Connections

Master's thesis in Civil and Environmental Engineering
Supervisor: Max Hendriks and Reignard Tan
June 2020

NTNU
Norwegian University of
Science and Technology

Mikael Rosendahl

Comparison of Strut-and-Tie Modeling and Nonlinear Finite Element Analysis Approaches for Concrete Wall-to-Wall Connections

Master's thesis in Civil and Environmental Engineering
Supervisor: Max Hendriks and Reignard Tan
June 2020

Norwegian University of Science and Technology
Faculty of Engineering
Department of Structural Engineering

NTNU
Norwegian University of
Science and Technology

Preface

This master's thesis is written at the Department of Structural Engineering at the Norwegian University of Science and Technology (NTNU), Trondheim. The thesis has been carried out during the spring semester of 2020 and concludes a period of five great years in Trondheim.

With this thesis I have had the possibility of studying two modeling approaches in structural concrete which interests me greatly. Working with the thesis and trying to find solutions for the Matlab code described in the thesis has been very interesting.

I would like to thank supervisor Professor Max Hendriks (NTNU) and co-supervisor Adjunct Associate Professor Reignard Tan (NTNU and Multiconsult) for all help and guidance I have received throughout the semester.

I also want to thank my family and friends for all support they have given me during my time at NTNU.

Trondheim, June 2020

Mikael Rosendahl

Abstract

In concrete structures, one will find regions with a nonlinear response caused by sudden changes in geometry or loading. Two modeling approaches for such regions, called D-regions, are nonlinear finite element analysis and strut-and-tie modeling. The objective of the thesis is to compare these two methods applied to a concrete D-region.

Large concrete structures typically include many D-regions possibly exposed to a large number of load combinations. With this in mind, the strut-and-tie modeling has been solved with a Matlab code [1] capable of generating and calculating models for many load cases at a rapid speed. The code calculates through several possible strut-and-tie models for each load case, and finally chooses the most optimal model based on minimum strain energy. The resulting strut-and-tie models for each load case are compared to nonlinear finite element analyses in two different softwares: DIANA [2] and IDEA StatiCa [3].

The D-region assessed in this thesis is a T-connection between two walls. Three load cases have been tested and the calculation time used by the Matlab code for all three load cases is 0.1-0.2 seconds in total. For the nonlinear finite element analyses, base models have been made in the two softwares, providing six analyses. With the desire of testing the effect of the tensile softening behavior of the concrete, an additional DIANA analysis has been run for the load case exposing the D-region to a dominating tension force. This gives in total seven nonlinear finite element analyses. Five of these showed a capacity larger than what was found in the strut-and-tie models. One of the seven reached failure at a load factor of 1.00. The final analysis reached a maximum load factor of 0.631. Some unexpected cracking was observed at the loading in this analysis. It is argued that this is caused by the arc-length procedure inducing a premature unloading as neither concrete crushing nor reinforcement rupture is observed at the ultimate load factor. The fact that for this load case, the largest difference ($\Delta_3 = 0.449$) in load factor between the two softwares was observed, substantiates the argument. The difference in load factors between the analyses of the two other load cases were significantly less ($\Delta_1 = 0.08$ & $\Delta_2 = 0.02$).

The different approaches to reduction in concrete compressive strength due to transverse tensile strains have been assessed for both the nonlinear finite element analyses and strut-and-tie models. A comparison of the results show that in the most critical compression fields of the strut-and-tie models, the reductions are on the conservative side of what is observed in the nonlinear finite element analyses. However, in areas with little compression stresses, the latter shows larger reductions than what is recommended by Eurocode 2 [4] for the nodes of the strut-and-tie models. All things considered, the results in this thesis suggest that strut-and-tie modeling gives conservative results with respect to the nonlinear finite element analyses.

Sammendrag

I betongkonstruksjoner vil man finne regioner med en ikkelineær respons forårsaket av plutselige endringer i geometri eller last. To tilnærminger for modellering av slike regioner, kalt D-regioner, er ikkelineære elementanalyser og stavmodeller. Målet ved denne oppgaven er å sammenligne disse to metodene anvendt på en D-region av betong.

Store betongkonstruksjoner vil typisk ha mange D-regioner som kan være utsatt for et stort antall lastkombinasjoner. Med dette i tankene, har modelleringen med stavmodeller blitt løst med en Matlabkode [1] i stand til å generere og beregne modeller for mange lastsituasjoner på kort tid. Koden regner gjennom flere mulige stavmodeller for hver lastsituasjon og velger tilslutt den mest optimale modellen basert på minste tøyningsenergi. De resulterende stavmodellene for hver lastsituasjon blir sammenlignet med ikkelineære elementanalyser i to forskjellige programvarer: DIANA [2] og IDEA StatiCa [3].

D-regionen som har blitt undersøkt i denne oppgaven er et T-knutepunkt mellom to vegger. Tre lastsituasjoner har blitt testet og beregningstiden brukt av Matlabkoden for alle tre lastsituasjonene er 0.1-0.2 sekunder totalt. For de ikkelineære elementanalysene har basismodeller blitt lagd i begge programvarene. Dette gir seks analyser. Med ønske om å sjekke effekten av valgt strekkmodell i betong-materialmodellen, har en ekstra analyse i DIANA blitt utført for lastsituasjonen som utsetter D-regionen for en dominerende strekkraft i den ene veggen. Dermed har det totalt blitt utført syv ikkelineære elementanalyser. Fem av disse viste en kapasitet større enn hva som ble funnet i stavmodellene. Én av de syv nådde brudd ved lastfaktor 1.00. Den siste analysen nådde en maksimal lastfaktor lik 0.631. Noe uforventet opprissing ble observert ved lastpåføringen i denne analysen. Det har blitt argumentert for at dette er forårsaket av at buelengdeprosedyren leder til for tidlig avlastning siden hverken knusing av betong eller armeringsbrudd er observert ved den maksimale lastfaktoren. Det faktum at denne lastsituasjonen viste størst forskjell ($\Delta_3 = 0.449$) i lastfaktor mellom de to programvarene underbygger dette argumentet. Forskjellen observert for de to andre lastsituasjonene var betydelig mindre ($\Delta_1 = 0.08$ & $\Delta_2 = 0.02$).

De forskjellige tilnærmingene til reduksjon av betongtrykkfastheten forårsaket av transversale strekktøyninger er blitt vurdert for både de ikkelineære elementanalysene og stavmodellene. En sammenligning av resultatene viser at reduksjonene i de mest kritiske trykkfeltene i stavmodellene er på den konservative siden av hva som er sett i de ikkelineære elementanalysene. Derimot, i områder med lite trykkspenninger viser sistnevnte større reduksjoner enn hva som er anbefalt av Eurokode 2 [4] for nodene i stavmodellene. Med alt tatt i betraktning, antyder resultatene at stavmodeller gir konservative resultater sammenlignet med ikkelineære elementanalyser.

Table of Contents

Abbreviations and Nomenclatures

Abbreviations

DOF Degree of freedom

FEM Finite element method

NLFEA Nonlinear finite element analysis

STM Strut-and-tie model

ULS Ultimate limit state

Nomenclatures

α_{lat} Lateral tensile strain

$\Delta\mathbf{u}$ Displacement increment

$\delta\mathbf{u}$ Total iterative displacement increment

ϵ_E Tolerance of energy convergence criterion

ϵ_F Tolerance of force convergence criterion

η_{f_c} Reduction factor due to brittle behavior of concrete (fib Model Code 2010 [5])

λ_i Load factor in arc-length procedure

$[\mathbf{K}]$ Global stiffness matrix

$\hat{\mathbf{f}}$ Unit load in arc-length procedure

$\{\mathbf{D}\}$ Global displacement vector

$\{\mathbf{R}\}$ Global load vector

$\mathbf{f_{int}}$ Internal force vector

ν' Reduction factor due to brittle behavior of concrete (Eurocode 2 [4])

σ_1 Maximum principal stress

σ_2 Minimum principal stress

$\sigma_{Rd,max}$ Maximum allowable stress in nodes

θ Shear angle

ε_0 Compressive peak strain

ε_1 Maximum principal strain

ε_2 Minimum principal strain

ε_m Mean strain

ε_u Ultimate strain

ε_{c2} Compressive strain with maximum compressive stress reached (Eurocode 2 [4])

ε_{cu2} Ultimate compressive strain (Eurocode 2 [4])

a Distance from surface to longitudinal trusses in STM

A_s Cross-sectional area of reinforcement

b Width of cross section

c Concrete cover

E_{cm} Mean Young's modulus of concrete

E_{edge} Young's modulus of beam elements for loading in DIANA analyses

E_{sm} Mean Young's modulus of reinforcement steel

F Force

f_c Compressive strength of concrete

f_t Tensile strength of concrete

f_{cd} Design compressive strength

f_{ck} Characteristic cylinder compressive strength

f_{cm} Mean compressive strength

f_{ctm} Mean tensile strength

f_{yd} Design yield strength

f_{yk} Characteristic yield strength

G_C Compressive fracture energy

G_F Fracture energy

h	Height of cross section
h_{eq}	Crack band width
k_c	Compressive reduction factor (IDEA StatiCa)
k_{c2}	Compression softening factor due to transverse tensile strains (IDEA StatiCa)
l	Length of truss
M	Moment
N	Axial force
t_{edge}	Thickness of beam elements for loading in DIANA analyses
V	Shear force
w	Width of compression field represented by strut
x	Length from center of D-region to edge
$\emptyset$	Reinforcement bar diameter

List of Figures

List of Tables

Chapter 1

Introduction

In concrete structures, one will find regions experiencing sudden changes in loads or geometry. These sudden changes result in a nonlinear response of the region typically called a D-region. Because of these effects, a linear analysis is no longer sufficient and a nonlinear modeling approach has to be utilized in order to model the behavior of the region. Two modeling approaches which may be used to model the nonlinear behavior of D-regions are NLFEA and strut-and-tie modeling.

In this thesis, a comparison between these two modeling approaches is carried out. This is done by applying the two modeling approaches to a T-connection between two concrete walls exposed to three different load cases. The strut-and-tie modeling has in this thesis been executed by making a Matlab code able to generate and calculate STMs at a rapid speed. The motivation for this is to find an effective approach for dealing with a large number of D-regions and/or load cases. This is relevant for large concrete structures, as they typically may have many D-regions possibly exposed to a large number of load cases. The objective of this thesis is to compare the two modeling approaches applied to a D-region with focus on the different aspects of the respective modeling choices. Also, an attempt to demonstrate that NLFEA produces mean estimates while strut-and-tie modeling provides lower-bound estimates is made.

In order to answer the problem description, the D-region is tested for three different load cases. First, the Matlab code calculates through the three load cases and gives the three respective STMs as output. Then, the NLFEAs are made using the reinforcement, loads, and geometry calculated by the Matlab code for the STMs. In that way, the two modeling approaches can be compared more accurately. Finally, comparisons of the results are made. The discussion focuses on utilized material models and the numerical modeling of the NLFEAs and the approach used for the strut-and-tie modeling, and in addition the accuracy of the results obtained from these two modeling approaches.

First, the theoretical background of NLFEA and strut-and-tie modeling will be covered in chapter 2 and chapter 3, respectively. In chapter 4, the solution method for the two modeling approaches will be presented. An explanation of assumptions and the process of the Matlab code are provided. Also, the approaches for the NLFEAs in DIANA and IDEA StatiCa will be presented. In chapter 5, the results from both modeling approaches are presented. For the strut-and-tie modeling, the resulting STM accompanied by the truss forces, necessary reinforcement,

and resulting compression fields with the respective compressive reductions are provided. Results from the FEM-analyses will be provided from two softwares: DIANA and IDEA StatiCa. In chapter 6, the results are discussed with respect to the objective set for the thesis. Conclusions are drawn in chapter 7, followed by some suggestions for future work in chapter 8.

Chapter 2

Nonlinear Finite Element Analysis for Concrete Structures

2.1 Numerical solution

A time independent NLFEA problem can be described by

$$[\mathbf{K}]\{\mathbf{D}\} = \{\mathbf{R}\} \tag{2.1}$$

where the stiffness, $[\mathbf{K}]$, and the load, $\{\mathbf{R}\}]$, may be dependent on the displacement history $\{\mathbf{D}\}]$. This means that in most cases, an iterative process is needed in order to find the displacement.

2.1.1 Iterative Scheme

A popular choice for NLFEA problems is the Newton-Raphson method. The full Newton-Raphson method updates the tangent stiffness at each iteration. This reduces the number of iterations needed in order to find a solution which satisfies the convergence criterion. While the full Newton-Raphson method updates the tangent stiffness at every iteration, the modified Newton-Raphson method only updates it occasionally. Thus, the computational time of each iteration is reduced. In exchange, the modified Newton-Raphson method requires more iterations in order to achieve convergence. An increased number of iterations means a slower convergence rate. According to Cook [13], the overall computational time is typically reduced when using the Modified Newton-Raphson method compared to the full Newton-Raphson method.

2.1.2 Arc-Length Method

A load-displacement curve may include both points with zero tangent stiffness and infinite tangent stiffness. These points are called limit points and turning points, respectively. When using load control, failure is experienced at the limit points. Meanwhile, if displacement control is utilized, it is the turning points which cause failure of the numerical scheme [14]. In order for the numerical scheme to get past the critical points, the arc-length method may be applied. The total iterative increment can be described by ([8])

$$\delta\mathbf{u_i} = \delta\mathbf{u_i^I} + \Delta\lambda_i\delta\mathbf{u_i^{II}} \tag{2.2}$$

where

$$\delta \mathbf{u_i^I} = \mathbf{K_i^{-1}}(\mathbf{f_{int}} - \mathbf{f_{int,i}}) \text{ and } \mathbf{u_i^I} = \mathbf{K_i^{-1}}\hat{\mathbf{f}} \tag{2.3}$$

One way of finding the load factor $\Delta\lambda$ is to use the updated normal plane method where a linearized constraint is applied. This results in the following load factor ([8])

$$\lambda_i = -\frac{(\mathbf{\Delta u_{i-1}})^\mathbf{T}\delta \mathbf{u_i^I}}{(\mathbf{\Delta u_{i-1}})^\mathbf{T}\delta \mathbf{u_i^{II}}} \tag{2.4}$$

2.1.3 Convergence Criteria

When using the Newton-Raphson method, a proper convergence criterion has to be in place in order to secure a satisfying solution to the problem at hand. The convergence criterion has to be chosen such that a sufficiently high accuracy of the solution is obtained while also ensuring that the iterative process is not unnecessarily slowed down by a too strict criterion. Convergence criteria can be both be based on displacement and force [13]. These may be formulated as:

$$\|\mathbf{\Delta D}\| < \epsilon_D \|\mathbf{\Delta D_0}\| \tag{2.5}$$

$$\|\mathbf{e_R}\| < \epsilon_R \|\mathbf{R}\| \tag{2.6}$$

A third convergence criterion is the energy criterion. According to Mathisen [14], using this combined with line search may in some cases be inadvisable. A line search algorithm is used to find the optimal incremental step, which is done by minimizing the residual force. Utilizing a line search algorithm can be useful when dealing with concrete because of the rapid changes in response due to cracking and reinforcement yield [14]. According to Mathisen, the line search algorithm may both increase the speed of the iteration process and in some cases obtain a solution where it would not have been possible without the line search. In DIANA, the problem of combining line search with an energy criterion is solved by using the internal force instead of the out-of-balance force. If using an energy norm based on the out-of-balance force combined with a line search, the line search could minimize the norm before actual convergence [8]. By using the internal force, the following energy criterion is obtained:

$$\left\|\delta \mathbf{u_i^T}(\mathbf{f_{int,i+1}} + \mathbf{f_{int,i}})\right\| < \epsilon_E \left\|\mathbf{\Delta u_0^T}(\mathbf{f_{int,1}} + \mathbf{f_{int,0}})\right\| \tag{2.7}$$

When choosing a convergence criterion, it might for instance prove to be insufficient to only use a displacement criterion. If the solution lies in an area with a large tangent stiffness (a small change in displacement gives a large change in force), a displacement criterion may indicate convergence while there still is a significant force imbalance [13]. Dutch guidelines [7] recommends using a combination of the force and energy criteria, and that a convergence criterion based solely on the displacement should be avoided. The recommended values for the force

and energy norm ratio are as follows:

$$\epsilon_R = 0.01$$

$$\epsilon_E = 0.001$$

2.2 Material Model - Concrete

A proper material model is necessary in order to represent the behavior of the concrete satisfyingly. Concrete crack models can be divided into two main groups: Discrete crack models and smeared crack models. These two different types of crack models are illustrated in Figure 2.1.

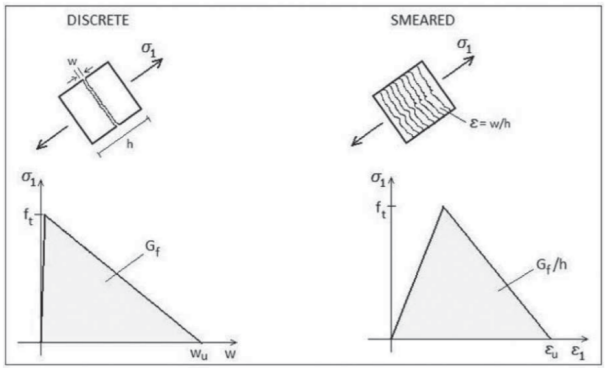

Figure 2.1: Discrete and smeared crack models [6].

There are several smeared crack models to choose between and some examples are [15]:

- Decomposed-strain based smeared crack models
- Total-strain based models
- Plasticity based crack models

Dutch Guidelines suggest using the total-strain based crack model. From here, only this will presented further.

2.2.1 Total Strain Crack Model

The total strain crack model can be formulated with either a fixed or a rotating set of axes. When using a fixed crack model, it is necessary to define shear retention parameters. This is used in order to find the shear stresses resulting from the rotation of principal stresses and strains relative to the fixed cracks. Dutch guidelines recommends using a variable shear retention model [7]. According to Rots [15], a fixed crack model may experience stress-locking when there are large rotations of stresses after the crack initiation. The stress-locking results in an overestimation of the capacity. In a rotating crack model, the axes rotate with the principal strain direction.

A rotating crack model will usually experience less shear-locking compared to a fixed crack model and thus give a more conservative capacity.

It is necessary to define the linear-elastic properties of the concrete and the two parameters needed for this are the Poisson ratio and Young's modulus. Dutch guidelines proposes an initial Poisson ratio of 0.20 [7]. This should be reduced during progressive cracking. A reduction in Young's modulus is also recommended.

It is necessary to have a proper representation of both the tensile and the compressive behavior of the concrete. For the representation of the tensile behavior, a mesh dependent exponential-type softening curve is favored [7]. One example of such a curve is the tensile softening curve proposed by Hordijk [16]. This is shown in Figure 2.2, where the tensile behavior consists of a linear stress-strain relationship up to the tensile strength f_t followed by an exponential softening of the stresses. Other parameters necessary to provide values for are the tensile fracture energy, G_f, and the crack band width, h_{eq}. The area below the curve is defined as the tensile fracture energy divided by the crack band width. This means that the curve is mesh dependent and reduces the results dependency on the used mesh. The crack band width is related to the dimensions of the used elements in the finite element model. An automatic procedure is recommended by Dutch guidelines for the calculation of the crack band width.

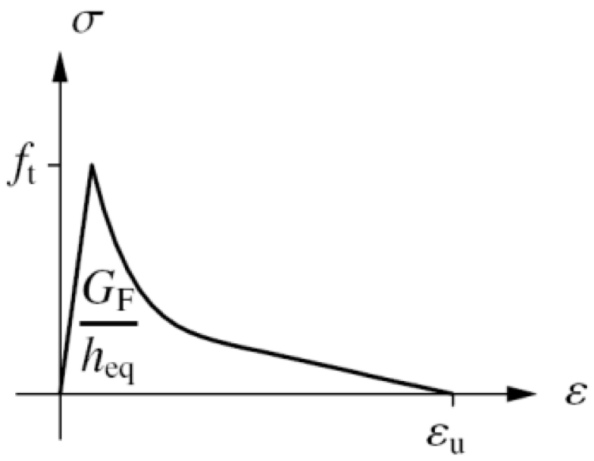

Figure 2.2: Hordijk softening [7].

When using this softening curve, the concrete contribution to tensile stiffness vanishes at the ultimate strain ε_u:

$$\varepsilon_u = 5.136 \frac{G_F}{h_{eq} f_t} \tag{2.8}$$

For the compressive behavior of the concrete, Dutch guidelines [7] recommends using the parabolic stress-strain diagram with softening. Necessary input parameters are the compres-

sive fracture energy, G_c, the crack band width, h_{eq}, and the compressive strength, f_c, of the concrete. The parabolic compression curve according to Feenstra [17] is shown in Figure 2.3.

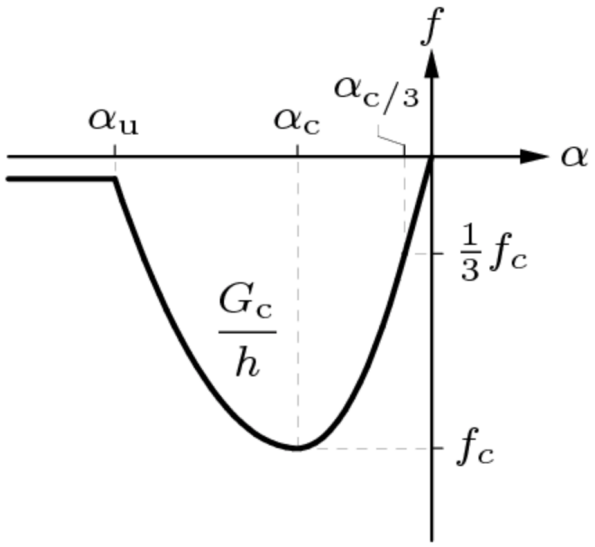

Figure 2.3: Parabolic compression curve [8].

The strains $\alpha_{c/3}$ and α_c are calculated independent of the element size:

$$\alpha_c = -\frac{5}{3}\frac{f_c}{E} = 5\alpha_{c/3} \tag{2.9}$$

In contrast, the ultimate strain, α_u, is mesh dependent as the crack band width, h_{eq}, is included in the equation:

$$\alpha_u = -\frac{3}{2}\frac{G_c}{h_{eq} f_c} \tag{2.10}$$

Another compression curve is proposed in Eurocode 2, where a parabola-rectangular compression curve is used. This is shown in Figure 2.4. The parabola-rectangular compression curve only limits the compressive strength of the concrete. Thus, it is necessary to do a post-analysis check of the strains [7]. Concrete failure can be assumed if the ultimate compressive strain of the concrete, ε_{cu2}, is reached. For concrete classes C50/60 and lower, the Eurocode 2 gives the following ultimate compressive strain [4]:

$$\varepsilon_{cu2} = -3.5 \cdot 10^{-3} \tag{2.11}$$

It is also necessary to consider any interaction between tension and compression in the concrete. As cracking of the concrete increases, the compressive strength decreases. Thus, the material model should include a reduction in compressive strength when the concrete experiences lateral cracking. This may be provided by using the strength reduction curve proposed by Vecchio and Collins (1993) [18]. The reduction curve is shown in Figure 2.5.

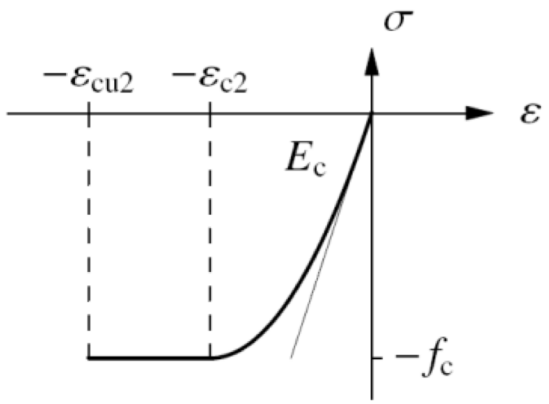

Figure 2.4: The parabolic-rectangular compression curve used in Eurocode 2 [7].

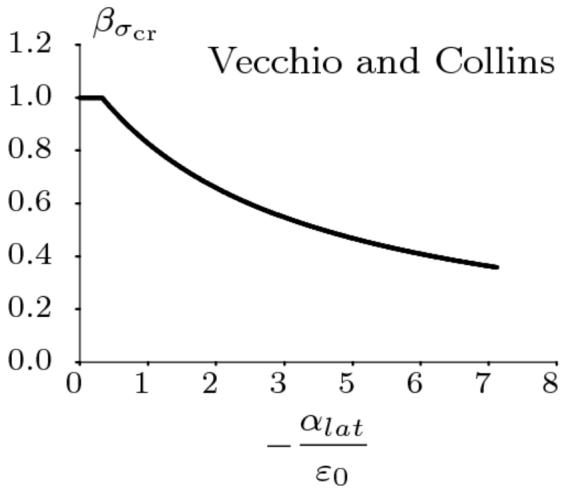

Figure 2.5: Reduction of compressive strength according to Vecchio and Collins [7].

The concrete compressive strength is reduced by a factor $\beta_{\sigma_{cr}}$:

$$\beta_{\sigma_{cr}} = \frac{1}{1 + K_c} \tag{2.12}$$

where

$$K_c = 0.27(\frac{\alpha_{lat}}{\varepsilon_0} - 0.37) \tag{2.13}$$

In order to not reduce the compressive strength excessively, Dutch guidelines recommends using a lower limit of $\beta_{\sigma_{cr}} > \beta_{min} = 0.4$ [7].

2.3 Material Model - Reinforcement

One way to add reinforcement into the NLFEA model is to use embedded reinforcement. This is the preferred method of modeling the reinforcement according to Dutch guidelines [7]. Embedded reinforcement is placed in the structural elements without independent DOFs [8]. The

reinforcement strains are calculated from the displacement field of the structural elements.

In the software IDEA StatiCa Detail, the reinforcement is modeled using the tension chord model [9, 19]. Figure 2.6 shows reinforcement stresses and change in concrete stresses along with the considered stress-strain relationship of the reinforcement using the tension chord model. The reinforcement stresses experiences the lowest stresses in the middle of the concrete elements in the figure. Here, the contribution from the tension stiffening effect is at its largest. At the crack openings, the reinforcement does not experience any tension stiffening. Thus the stresses here are equal to what is obtained with naked steel.

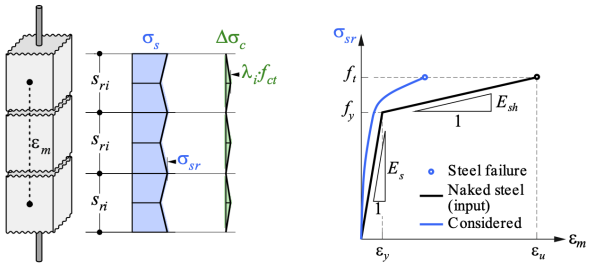

Figure 2.6: Tension stiffening when using the tension chord model [9].

Chapter 3

The Concept of the Strut-and-Tie-Model

3.1 General

The idea of STMs is that the forces through the assessed region are carried by an imaginary truss system. Further, it is assumed that the concrete represents the trusses in compression (struts), while the reinforcement is placed where trusses in tension (ties) are located. Also, the tensile strength contribution from the concrete is conservatively neglected.

3.2 B- and D-Regions

A structure may be divided into two different types of regions: B-regions and D-regions. A region may be defined as a B-region if the Bernoulli hypothesis is valid in it. This means that plane sections has to remain plane during bending [10]. If that is the case, classic beam theory is still possible to use in these regions, given that the deformations are assumed to be small. A D-region appears because of a discontinuity in the structure. This discontinuity may be an abrupt change in geometry, a concentrated load, or a support. The discontinuity causes nonlinear effects to appear in the D-region, which means that the Bernoulli hypothesis is no longer valid [12]. Therefore, the solution method used in the B-regions can not be applied here. In order to divide a structure into the two different types of regions, St. Venant's principle may be used. This states that the area of a D-region usually extends to a distance equal the cross section height from the discontinuity [12]. Some examples of D-regions defined according to this principle are shown in Figure 3.1. Outside the area of the D-region, the nonlinear effects from the discontinuity can be assumed as negligible. The disturbed stress field occurring in the D-regions can be assessed by the method of strut-and-tie modeling. Although the disturbance in the stress field can be assumed gone in the B-regions, strut-and-tie modeling can also be used in these regions if desired [12].

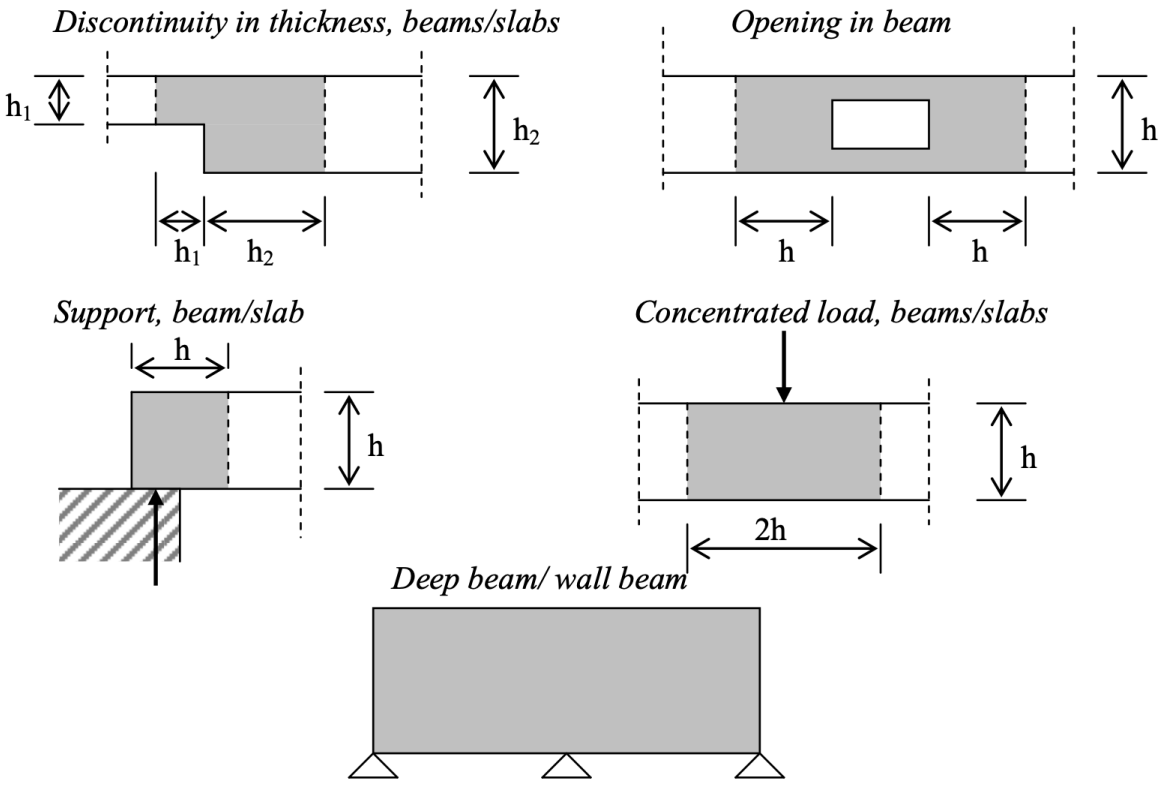

Figure 3.1: Examples of different types of D-regions [10].

3.3 Design Rules and Optimization

As stated by Schlaich et al. [12], a strut-and-tie model is designed according the the lower bound theorem of plasticity if the model is developed in an appropriate manner. They further state that it is important to limit the expected deformation of the struts as concrete only allows for limited plastic deformation.

By using the Load path method, the STM will often result in being kinematic [12]. In the load path method, an STM is made in the D-region by predicting the path the loads follows through the region and placing the trusses in this path. The motivation of this method is the fact that forces will often choose the shortest way through the D-region. By running a elastic FEM-analysis, the load path through the D-region may be easier to find.

There are many possible configurations of the STM in a D-region. In order to find the optimal configuration, the following optimization criterion can be used [12]:

$$\Sigma F_i l_i \varepsilon_{mi} = Minimum \tag{3.1}$$

In this equation, the product of the truss force, F_i, truss length, l_i, and mean strain, ε_{mi}, is summed over every truss member i to find the total strain energy of the considered STM. When multiple STMs are considered, the model with the minimum strain energy is chosen. As the strain obtained in the ties are often expected to dominate, it may be sufficient to optimize for the reinforcement strain only [12].

3.4 Sectional Forces

For many D-regions, it is necessary to find the sectional forces acting on the edges of the D-region. Further, the sectional forces effects has to be converted to point loads which satisfies both moment equilibrium and force equilibrium. These point loads are applied to the truss system at the edge of the D-region where the sectional forces are acting.

3.5 Dimensioning of Strut-and-Tie Models

3.5.1 Capacity Control of Struts

The struts are a simplification of compression fields in the D-region. There are mainly three types of compression fields: The fan, the bottle and the prism [12]. Dependent on the type of compression field located in a strut, transverse tensile forces may appear. To account for these tensile forces, reinforcement can be placed according to 6.5.3 in Eurocode 2 [4]. Another possibility is to reduce the maximum allowable stress in the strut by 6.5.2 in the Eurocode. For a compression field experiencing transverse tension, as in "the bottle"-type, the maximum allowable stress is as follows:

$$\sigma_{Rd,max} = 0.6\nu' f_{cd} \tag{3.2}$$

where

$$\nu' = 1 - \frac{f_{ck}}{250} \tag{3.3}$$

The reduction factor ν' takes into account the reduction in concrete strength of cracked concrete due to the brittle behavior [4]. If no transverse tension occurs in the compression field, no reduction of the dimensioning concrete strength is needed:

$$\sigma_{Rd,max} = f_{cd} \tag{3.4}$$

3.5.2 Capacity Control of Ties

The ties are dimensioned such that yield is reached for the acting tensile forces. No work-hardening is conservatively assumed. The necessary reinforcement can be calculated as.

$$A_s = \frac{F}{f_{yd}} \tag{3.5}$$

where F is the tensile forces in the tie while f_{yd} is the design yield stress of the reinforcement. The center of gravity of the reinforcement is placed at the location of the tie. This means that both the diameter of the rebar, the number of layers, and the concrete cover has to be known before the truss forces are calculated. If the placement of the tie is changed by for example adding another layer of reinforcement, the forces has to be recalculated.

3.5.3 Capacity Control of Nodes

In Eurocode 2 [4], the capacity control of the nodes are carried out by the use of clause 6.5.4. The governing maximum allowable nodal stress, $\sigma_{Rd,max}$, depends on the number of ties anchored in the node. $\sigma_{Rd,max}$ is reduced when the number of anchored ties in the node increases. If there are no ties anchored in the node, 6.5.4(4)a gives the following maximum allowable nodal stress:

$$\sigma_{Rd,max} = 1.0\nu' f_{cd} \tag{3.6}$$

With one anchored tie, $\sigma_{Rd,max}$ is given by 6.5.4(4)b:

$$\sigma_{Rd,max} = 0.85\nu' f_{cd} \tag{3.7}$$

Lastly, if there are two or more ties anchored in the node, 6.5.4(4)c gives the following governing maximum stress:

$$\sigma_{Rd,max} = 0.75\nu' f_{cd} \tag{3.8}$$

Further, 6.5.4(5) states that the capacity of the node can be increased with up to 10% if at least one of the following conditions are fulfilled [4]:

- triaxial compression is present
- all angles between struts and ties are $\geq 55°$
- stresses applied at supports or in point loads are evenly distributed and the node is confined of stirrups
- the reinforcement is placed in more than one layer
- the node is sufficiently confined with the help of the support or friction

In clause 6.5.4(6), Eurocode 2 opens up for a node in triaxial compression to be dimensioned with an upper limit of

$$\sigma_{Rd,max} \leq 3.0\nu' f_{cd} \tag{3.9}$$

if the distribution of the compression in all three directions is known.

Schlaich et al. [12] present another method of determining the maximum allowable compressive stress, f^*_{cd}, which is used for both struts and nodes. If the concrete experiences a uniaxial compressive state, the limit value for the stress can be assumed as equal to the design strength f_{cd}. The different limit compressive stresses are summarized in Table 3.1.

Table 3.1: Reduction in compressive stress according to Schlaich et al. [12]

f^*_{cd}	Description
$1.0 \cdot f_{cd}$	Uniaxial compressive stress state
$0.8 \cdot f_{cd}$	Transverse tensile strains or transverse reinforcement. Cracking parallel to the strut.
$0.6 \cdot f_{cd}$	Skew cracking or reinforcement.
$0.4 \cdot f_{cd}$	Skew cracks width significant width.

Chapter 4

Solution Methods

In this chapter the solution methods for both the strut-and-tie modeling and the FEM-analyses are presented. First, the solution method behind the calculation and optimization of the STMs is explained. Following this, the approaches in the two FEM-softwares will be presented.

4.1 D-Region

The D-region assessed in this thesis is based on Example 14 in the fib Bulletin 61 [20]. This includes geometry, materials, and load cases. The D-region is a T-connection between two walls. The height of the two walls are shown in Figure 4.1.

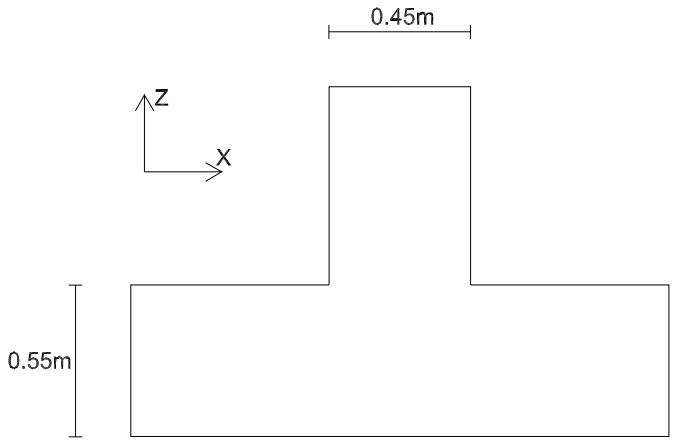

Figure 4.1: Height of the two cross sections in the D-region.

As the D-region is made of two intersecting walls, the values of the loads are given per meter. Thus, the width of the cross sections is considered as $1\mathrm{m}/\mathrm{m}$. The range of the D-region varies between the D-regions and is calculated as a part of the STM optimization. The code allows for a region larger than the D-region defined by St. Venants principle, which means parts of the analyzed region may be B-regions. According to Schlaich et al. [12], STMs may be used for B-regions as well. From here and for the rest of the chapters, the assessed regions will be named ”D-regions” although the regions may include B-regions. The concrete class used is C50/60 while the reinforcement used is B500NC. Relevant material properties are listed in Table 4.1 and Table 4.2, respectively. For the longitudinal reinforcement, a bar diameter of Ø25 is used. Bundles of two bars is allowed in a layer. With the assumed centering distance of c200, this results in a maximum number of 10 bars per meter allowed in each layer. The concrete cover

used is 50mm

Table 4.1: Concrete material data for C50/60 [4]

Material Data - Concrete	
Parameter	Value
f_{ck}	50MPa
f_{cm}	58MPa
f_{ctm}	4.1MPa
E_{cm}	37GPa

Table 4.2: Reinforcement material data for B500NC [4]

Material Data - Reinforcement	
Parameter	Value
f_{yk}	500MPa
E_{sm}	200GPa

The D-region is tested for three different load cases. These are shown in Table 4.3 and are acting at the center of the intersection. The directions of the forces and moments in the different load cases are shown in Figure 4.2. The axial force is defined as positive in tension and negative in compression, while the positive direction of the shear force is according to the defined coordinate system shown in the figure. Finally, the moment is positive when clockwise. The effect of external forces are not assessed in this thesis. Thus, only the moments acting at the edges of the D-region have to be recalculated from the values given in Table 4.3. This will be treated in subsection 4.2.1.

Table 4.3: Load cases tested.

		Axial force $[\frac{\text{kN}}{\text{m}}]$	Shear force $[[\frac{\text{kN}}{\text{m}}]$	Moment $[\frac{\text{kNm}}{\text{m}}]$
Load case 1	Left edge	-3424	695	683
	Right edge	-2753	47	6
	Top edge	-742	-671	-689
Load case 2	Left edge	-1701	-452	-467
	Right edge	-1699	-498	480
	Top edge	950	-2	-13
Load case 3	Left edge	-2735	-894	-498
	Right edge	-3603	257	-141
	Top edge	637	868	639

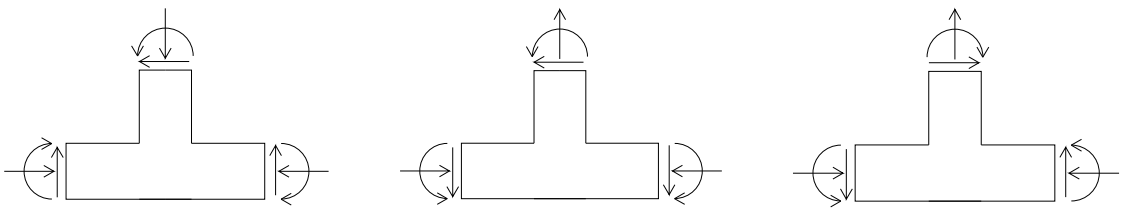

(a) Load case 1. **(b)** Load case 2. **(c)** Load case 3.

Figure 4.2: Directions of forces and moments in the three load cases.

4.2 Strut-and-Tie Models

In order to calculate the STMs for the three load cases, a Matlab code is made (see Appendix B). The Matlab code is made such that it can take an arbitrary load case (axial force, shear force, and moment) and give the user a resulting STM.

When considering a multiple number of load cases, most likely a multiple number of different load paths has to be taken into account. In order to be able to model any kind of load path, it is necessary to be able to place trusses in various directions in the STM. For instance, the direction of the shear forces determines the direction of the resulting diagonal compression fields. Thus, both possible directions of the shear force has to be represented in the pool of possible trusses. Then, by checking the direction of the shear force when choosing a set of trusses in the considered STM, the trusses not representing the correct direction of these compression fields can be omitted for the given load case. In that way, a large number of unnecessary analyses testing STMs providing invalid results may be avoided.

When modeling an STM for a given D-region and load case, there are may possible configurations which give sufficient capacity. Thus, by testing mulitple STMs and optimizing each one, a more economical reinforcement layout may be calculated. In the Matlab code, an orthogonal reinforcement layout is assumed. This limits the STM optimization as models with inclined reinforcement will be discarded even if they prove to be more efficient when using the minimum strain energy criterion in Equation 3.1.

The concrete cover will only be considered for the longitudinal reinforcement in this thesis. This is to be able to test STMs with compression fields where the compressive stress is close to the maximum allowable stress. By removing the restriction of the concrete cover for the shear reinforcement, any present longitudinal struts may be placed in a distance determined by the resulting compression field from the surface. This is achieved by a geometric optimization procedure. Dependent on the signs of the forces in the longitudinal trusses, chosen nodes are moved such that compression fields utilize their available space to produce the maximum allowable stress. By moving the nodes in this manner, the moment lever arm is maximized and the contribution from the moment minimized. The geometric optimization procedure will be explained further as a part subsection 4.2.4.

4.2.1 Application of Sectional Forces

In order to calculate the forces in the D-region, the sectional forces acting at the ends of the region has to be applied appropriately. The sectional forces obtained at the intersection of the walls is used as input in the calculations. This means that the sectional forces has to be cal-

culated to their correct values at the edge of the D-region. With no external loads, only the moment changes from the middle of the intersection where the loads in Table 4.3 are extracted from.

The definition of positive directions of forces and moments results in two different equations for calculating the moment at the end of the D-region. By using the moment ($\mathrm{M_i}$) and shear force ($\mathrm{V_i}$) obtained at the intersection combined with the distance ($\mathrm{x_i}$) from the intersection to the edges, the moment at the edge ($\mathrm{M_i(x_i)}$) is calculated. For the left side and the top side of the D-region, the following equation is used:

$$M_i(x_i) = M_i - V_i \cdot x_i \tag{4.1}$$

For the right side of the D-region, the moment can be calculated as following:

$$M_i(x_i) = M_i + V_i \cdot x_i \tag{4.2}$$

Figure 4.3 shows the sectional forces at one end of the D-region and the point loads which represents them in the strut-and-tie-model. All three sectional forces make up a pair of forces where the two forces are applied at opposite sides of the model.

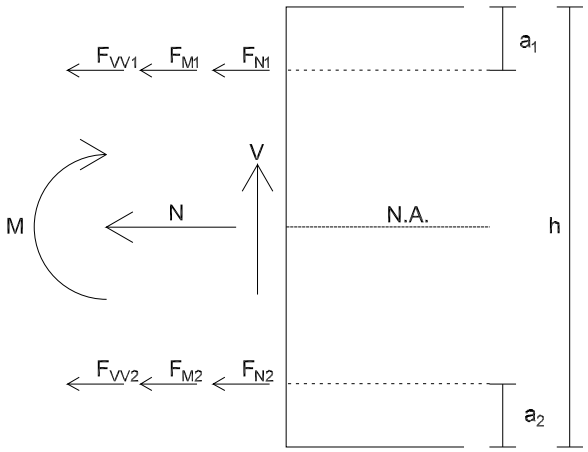

Figure 4.3: Sectional forces represented by corresponding pairs of forces.

For all three force pairs, both a force equilibrium and a moment equilibrium have to be satisfied in order to correctly represent the sectional forces. When adding the contributions from all sectional forces, the point loads F_1 and F_2 are obtained. These point loads are placed in the nodes at the ends of the D-region, placed in a distance of a_1 and a_2 from the surface, respectively. The point loads F_1 and F_2 are found as:

$$F_1 = F_{N1} + F_{VV1} + F_{M1} \tag{4.3}$$

$$F_2 = F_{N2} + F_{VV2} + F_{M2} \tag{4.4}$$

Axial Force

First, the force equilibrium is satisfied:

$$F_{N_1} + F_{N_2} = N \tag{4.5}$$

The axial force does not contribute to any moment. Thus, the two forces representing the axial force should also not contribute to any moment:

$$-F_{N_1} \cdot (\frac{h}{2} - a_1) + F_{N_2} \cdot (\frac{h}{2} - a_2) = 0 \tag{4.6}$$

By combining Equation 4.5 and Equation 4.6, the following two expressions for the truss forces are obtained:

$$F_{N_2} = N \cdot \frac{\frac{h}{2}}{h - a_1 - a_2} \qquad F_{N_1} = N - F_{N_2} \tag{4.7}$$

Shear Force

In order to apply the shear force to the strut-and-tie-model, it can be decomposed as shown in Figure 4.4a.

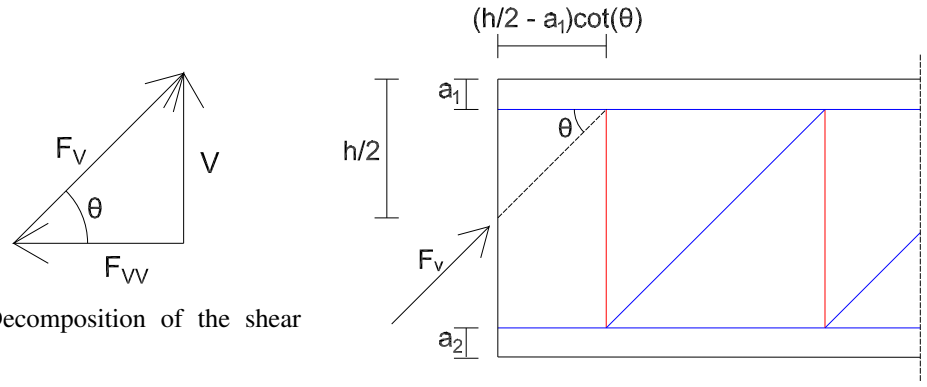

(a) Decomposition of the shear force.

(b) Line of attack.

Figure 4.4: Application of F_v due to the shear force.

The force F_{vv} can be converted to truss forces in the same manner as the axial force, while the force F_v can be applied directly in the node lying in its line of attack. It is important that the shear force is obtained at a distance from the wall intersection such that this diagonal force has a line of attack through the node it is applied to. If not, an additional moment caused by the eccentricity occurs and the moment equilibrium of the model is destroyed. The line of attack is shown in Figure 4.4b Both F_{vv} and F_v are calculated from the shear force V and the assumed angle θ. According to Eurocode 2 clause 6.2.3(2), the angle may be chosen in the interval

$1 \leq \cot\theta \leq 2.5$. From here, an angle of $\theta = 45^o$ ($\cot\theta = 1$) is used.

$$F_{VV} = \frac{V}{tan(\theta)} \qquad F_V = \frac{V}{sin(\theta)} \tag{4.8}$$

$$F_{VV_2} = F_{VV} \cdot \frac{\frac{h}{2}}{h - a_1 - a_2} \qquad F_{VV_1} = F_{VV} - F_{VV_2} \tag{4.9}$$

Moment

The force pair representing the moment should not contribute to additional forces in the model:

$$F_{M_1} + F_{M_2} = 0 \tag{4.10}$$

Also, the force pair has to represent the moment M correctly:

$$-F_{M_1} \cdot (\frac{h}{2} - a_1) + F_{M_2} \cdot (\frac{h}{2} - a_2) = M \tag{4.11}$$

When combining Equation 4.10 and Equation 4.11, the following expressions for the force pair is obtained:

$$F_{M_2} = \frac{M}{h - a_1 - a_2} \qquad F_{M_1} = -F_{M_2} \tag{4.12}$$

Placement of Trusses

The placement of the struts and ties which the sectional forces are applied to are governed by the variables a_1 and a_2. For a tie, the corresponding a_i equals the distance from the surface to the center of the reinforcement. In the case of a strut, the value of a_i can be chosen more freely. The strut has to be placed such that the necessary width of its compression field is not greater than the available width.

As the ties are placed in the center of gravity of the reinforcement, the number of bars needed for the longitudinal reinforcement has to be calculated. As already mentioned, bundles of two bars is allowed in a layer, which results in 10 bars in each layer with the centering distance of c200.

4.2.2 The Geometry of the Strut-and-Tie Models

The calculation of the length from the intersection to the ends of the D-region is illustrated in Figure 4.5 for the left side. The length of truss 2, 4, 6, and 8 in x-direction is the same as the length of truss 1. This is done in order to make sure that the angle of truss 3 and 7 is as close as possible to 45 degrees. With this angle, the contribution from the shear forces to the longitudinal trusses are reduced. The calculation of the distance from truss 1 to the left side of the

D-region is shown in Figure 4.4b.

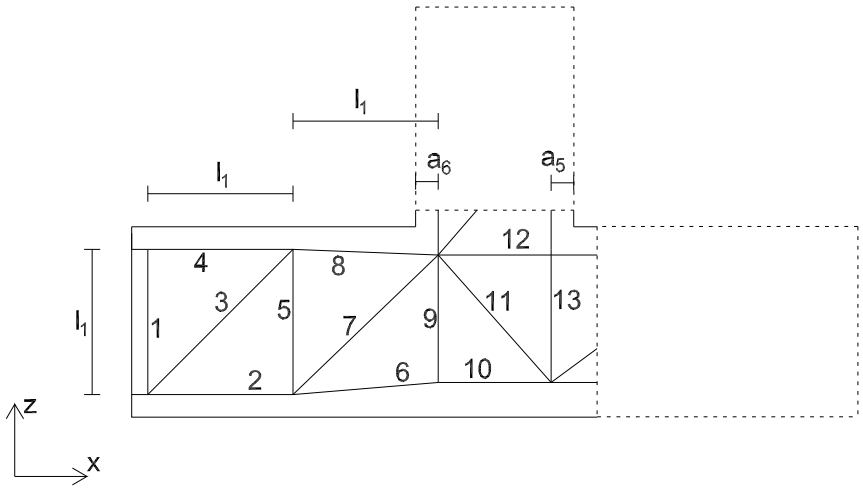

Figure 4.5: Range of D-region.

The longitudinal trusses are initially placed as if one layer of the chosen reinforcement is needed. This placement may however be changed in the geometric optimization procedure. With the concrete cover $c = 50\text{mm}$ and the bar diameter of $\emptyset = 25\text{mm}$, the distance from the surface to the truss is as follows:

$$a = c + \frac{\emptyset}{2} = 62.5\text{mm} \tag{4.13}$$

4.2.3 Node Check

Maximum Allowable Stress in Nodes

The maximum allowable stress in each node is found according to 6.5.4(4) in the Eurocode 2 [4]. In the Matlab Code, this is executed by counting the number of ties in each node and then assigning the correct $\sigma_{Rd,max}$ to the nodes.

Nodal Zones

In order to check the capacity of the nodes, the D-region is divided into nodal zones where each node is assigned an individual area. An illustration of these nodal zones in the D-region is found in Figure 4.6. The area of a nodal zone ends at half the distance to certain neighboring nodes. For instance, node 12 is limited by half the distance to node 5, 13, and 14. The limits of all nodal zones may be found in Appendix A.

The D-region is made up of 16 nodal zones. For each node, a maximum possible width of each

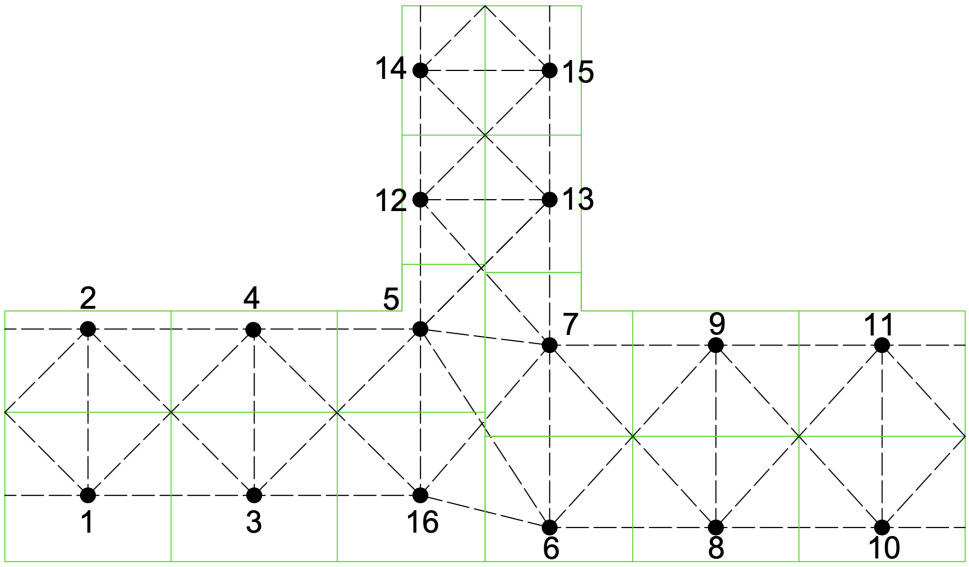

Figure 4.6: Example of nodal zones in the D-region.

strut is calculated. This is done by finding the shortest distance, measured normal to the strut, to either the end of the zone or to a neighboring truss. If a neighboring truss is a strut, the distance is measured from the truss in focus to the end of the compression field of this neighboring strut. The stress in the compression field of a neighboring strut is assumed to be equal to the maximum allowable stress in the nodal zone at hand. Figure 4.7 shows how the maximum width of a strut may be found. The shortest distance from the strut in focus to the neighboring strut (blue) or tie (red) is used as the half of the maximum allowed width:

$$0.5 \cdot w_{max} = \min\{\frac{w_1}{2}, \frac{w_2}{2}\}$$

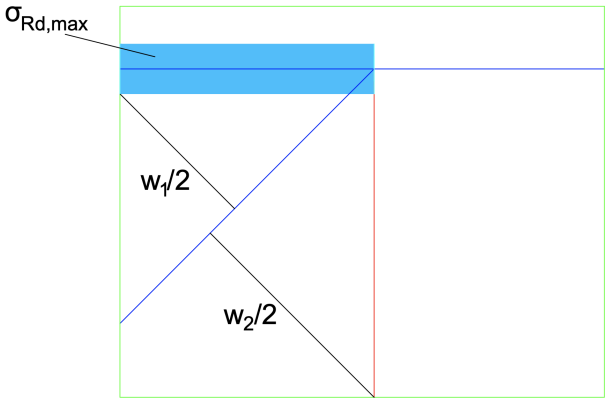

Figure 4.7: Finding maximum allowed width.

The capacity check is carried out by checking this maximum width of each strut in every node and comparing it to the necessary width. This is done in the following:

$$w_{nec.} = \frac{F}{b \cdot \sigma_{Rd,max}} \tag{4.14}$$

$$w_{nec.} \leqslant w_{max} \implies \text{OK capacity} \tag{4.15}$$

A maximum width of a strut has to be calculated in both of its nodes. It is chosen to use the minimum value from the two nodes for the entire strut. This is done in order to ensure that compression fields from two different nodal zones do not overlap. The full calculations of the maximum widths are included in Appendix A.

4.2.4 Process

The process of finding and calculating STMs for the load cases can be divided into seven steps. The first step is the only one which requires any action from the user.

Step 1 - Initialization

First, geometry, material data, and load case(s) have to be defined. In regards of the geometry, the height (and width) of the two intersecting walls have to be provided. Additionally, the concrete cover on both sides of all three ends of the D-region (1-6 in Figure 4.8) has to be defined. If desired, it is possible to give different covers for all of the six sides. The necessary material parameters are shown in Table 4.4.

Table 4.4: Necessary material input.

Necessary Material Data	
Concrete	Reinforcement
f_{ck}	f_{yk}
f_{cm}	E_{sm}
f_{ctm}	

For the reinforcement, it is also necessary to provide the spacing of the longitudinal reinforcement and the rebar diameter. As for the concrete cover, a value has to be given for both sides of all three ends of the D-region.

Step 2 - Choose STM

For each load case, eight possible sets of trusses will be tested. These different sets is made up of different combinations of the four green trusses in Figure 4.8. The two green diagonal trusses

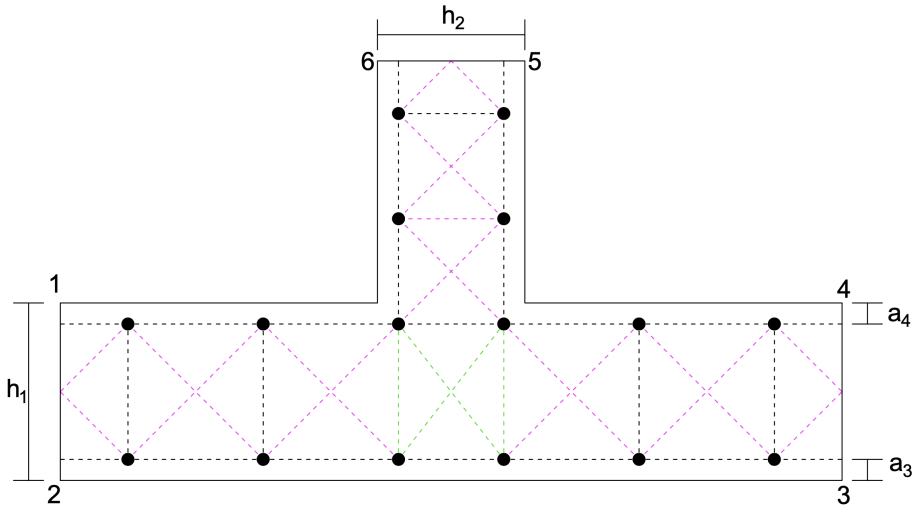

Figure 4.8: Available trusses to include in the STM.

is not used in the same sets, thus resulting in $2^3 = 8$ combinations. The two diagonal trusses are limited to compression. This limitation ensures that no diagonal reinforcement is necessary, which gives an easier reinforcement layout in terms of the construction process. However, if the possibility of inclined reinforcement is desired, this is easily included by removing the limitation. The direction of the shear forces determines which of the purple diagonal trusses are used. Thus, none of the purple trusses overlap in the chosen STM. Lastly, the black trusses are used in every STM. Figure 4.9a shows a possible load case, where the D-region experiences a closing moment on the left side. This will be used as an example throughout the steps. A possible STM for this load case is shown in Figure 4.9b.

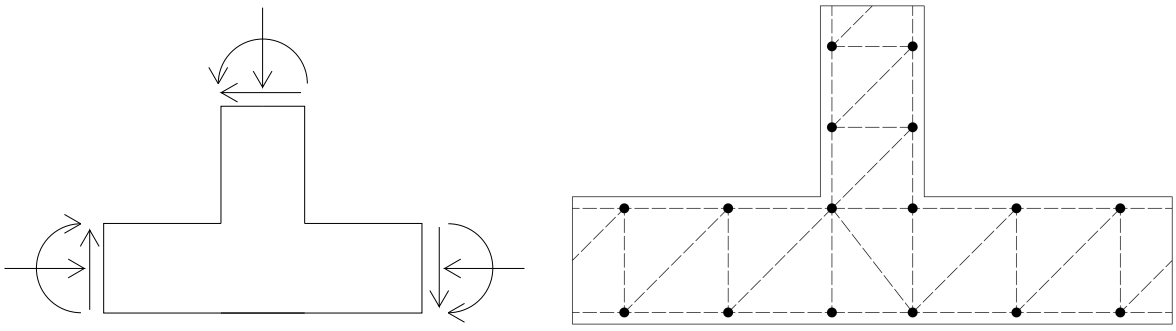

(a) **(b)**

Figure 4.9: Possible load case and STM for the D-region.

Step 3 - Application of Sectional Forces

Sectional forces are calculated and applied according to subsection 4.2.1, and the forces in the STM are calculated. If the code is in its first iteration, the calculation of the STM will be done in two stages. First, an initial calculation is carried out. This calculation uses the STM in Figure 4.9b where the longitudinal trusses placed according to Equation 4.13, and is only done

in the first iteration. Stage two of the calculation uses the signs of the truss forces in the previous STM calculation in order to alter the orientations of the longitudinal trusses if needed, and then do the updated calculations. This stage is performed in every iteration.

Step 4 - Repositioning of Trusses

Trusses are moved such that they satisfy the needed reinforcement and strut widths of the configuration in step 3. A change in the truss placements will change the force distribution in the STM and thus also the necessary reinforcement and strut widths.

The configuration of the STM in the continuous wall depends on the force distribution. As the longitudinal reinforcement is restricted to be placed parallel to its corresponding surface, any tie representing this reinforcement can not be placed diagonal. Figure 4.10 shows one possible configuration of the bottom trusses. The following may also be applied to the top trusses.

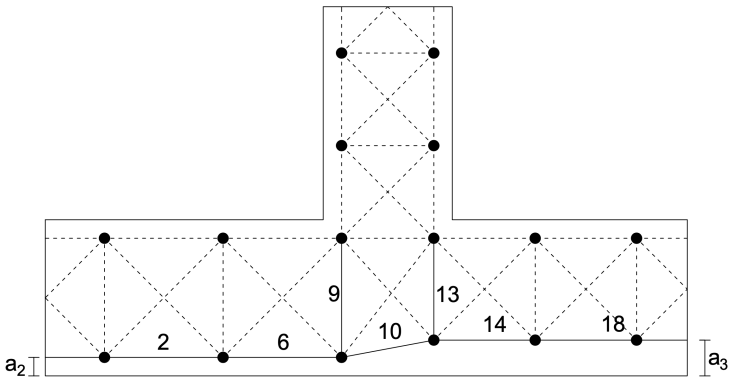

Figure 4.10: One possible configuration of the trusses at the bottom of the D-region.

Truss 2 & 18 has been restricted to be horizontal in the Matlab Code. These two struts are placed in a distance a_2 and a_3, respectively, from the surface. If $a_2 \neq a_3$, at least one of the three other trusses has to be diagonal in order to connect the two sides. Which one(s) that has to be diagonal depends on whether they are struts or ties. As the three other trusses (6, 10, and 14) either will be in tension or compression, there are eight possible force combinations. In seven of these, only one of the three trusses is allowed to be diagonal. The last case, where truss 10 is in tension while truss 6 & 14 are in compression, it may be necessary for both 6 & 10 to be diagonal. The eight cases with the corresponding configurations are given in Table 4.5.

The combinations in Table 4.5 are based on the assumption that both truss 9 & 13 are active. If for instance truss 9 is excluded from the STM, both truss 6 & 10 have to be either horizontal or diagonal with the same inclination if none of the two diagonal trusses in this node is used. This is required in order to secure the equilibrium in the node connecting the two trusses.

When the geometry of the STM is changed, the reinforcement check of the ties and the node check of the struts has to be done again. As the geometry of the STM configuration in this step is based on the capacity needs of the STM in the previous step, the new configuration may give insufficient results in regards to the convergence criteria. If this is the case, a new iteration is needed. This happens in step 5.

Table 4.5: Finding the diagonal truss.

Strut	Tie	Diagonal
6 & 10 & 14	-	10
6 & 10	14	10
10 & 14	6	10
6	10 & 14	6
10	6 & 14	6
14	6 & 10	14
-	6 & 10 & 14	-
6 & 14	10	6 & 14

Step 5 - Iteration

Step 3 and 4 are repeated until satisfied convergence is achieved.

Step 6 - Check

After step 5 is finished, the D-region has been checked for one possible set of trusses. As there may be other sets which may give more efficient results, these should also be checked. This is done by repeating step 2 to 5 for all relevant STMs.

Step 7 - Final STM

When all sets of trusses have been tested, the most efficient STM is chosen out of the valid ones. This is found by utilizing the minimum strain energy criterion in Equation 3.1.

4.3 Nonlinear Finite Element Analysis with DIANA

4.3.1 Material Models

Concrete

The concrete material model is to a great extent made according to recommendations of Dutch guidelines [7]. A total strain rotating crack model is applied. For material parameters, the

mean values are used. The Hordijk softening curve is used for the modeling of the tensile behavior. In addition, load case 2 has been tested with a linear-ultimate crack strain tensile softening. The ultimate strain used for this analysis is $\varepsilon_u = \frac{f_{yk}}{E_{sm}} = 0.0025$. A parabolic curve is used for the compressive behavior. Compression-tension interaction is taken into account by a reduction in compression strength according to Vecchio and Collins (1993) [18]. A lower limit of $\beta_{\sigma_{cr}} = 0.6$ is used, thus reducing the concrete compressive strength with 40% at most. In addition, a reduction in the Poisson ratio due to lateral cracking is applied. Where possible, material parameters are found in Eurocode 2 [4]. The initial Poisson ratio used is 0.20.

Reinforcement

An elastic perfectly plastic material model is used. The two material parameters used to model the reinforcement behavior are the characteristic yield stress and the Young's modulus:

$$f_{yk} = 500 \frac{\mathrm{N}}{\mathrm{mm}^2}$$

$$E_{sm} = 2 \cdot 10^5 \frac{\mathrm{N}}{\mathrm{mm}^2}$$

Embedded reinforcement is used.

4.3.2 Loading

The sectional forces acting on the ends of the D-region are calculated as in subsection 4.2.1. The sectional forces acting on the right and top side of the D-region are applied to the respective edges, while the left side edge is constrained from both displacement and rotation. The two loaded edges are enforced to be straight by adding beam elements along these edges. A large value of the thickness combined with a small Young's modulus is used:

$$t_{edge} = 10^6 \mathrm{mm}$$

$$E_{edge} = 10 \frac{\mathrm{N}}{\mathrm{mm}^2}$$

This is done in order to keep the line elements stiff in bending while keeping a relatively low axial stiffness. The axial force is calculated to an evenly distributed force and applied to the edge, while the shear force is loaded directly into the middle node of the edge. As the beam elements have rotational degrees of freedom, the moment is added directly to the middle node of both edges. Figure 4.11 shows how the axial force, shear force, and moment are applied to the finite element model. The loaded edge and middle node are marked as red.

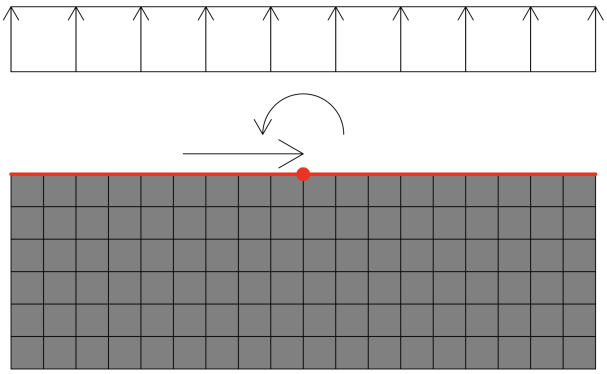

Figure 4.11: An illustration of the application of loads in the DIANA analyses.

4.3.3 Geometry and Reinforcement

The geometry of the D-region is extracted from the STMs such that the results from the STMs and the NLFEAs depict the same load situation. This also applies for the reinforcement, as the reinforcement is placed in the same locations as in the STMs. The cross-sectional area of the reinforcement is as calculated in the STMs.

4.3.4 Analysis

The Regular Newton-Raphson method is the chosen method for the equilibrium iteration. The arc-length method is applied, where the updated normal plane method is used. As the D-region is tested for ULS, there is an increased possibility of critical points in the equilibrium path. In order to find the optimal next load increment, a line search algorithm is applied. Default settings in DIANA [2] is used for both the arc-length method and the line search algorithm.

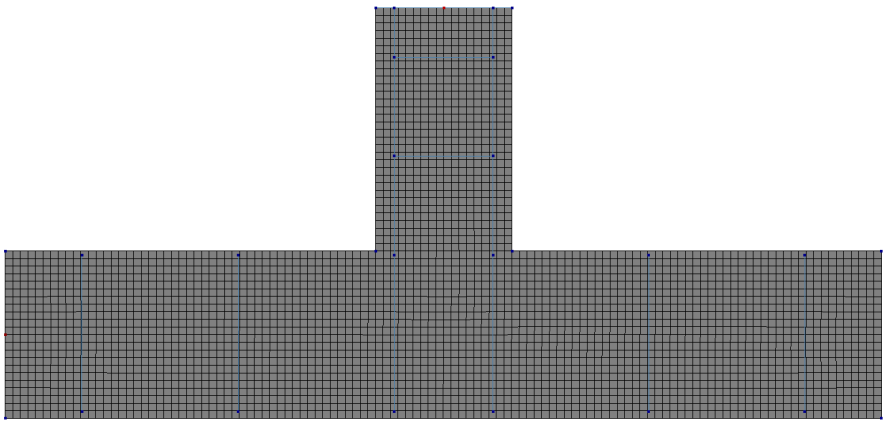

Figure 4.12: The mesh used for Load Case 2. The same approximate element size is used for all three load cases.

The D-region is meshed with quadrilateral plane stress elements of quadratic order. An approximate size of $25 \times 25\text{mm}$ is used. The resulting mesh for load case 2 is shown in Figure 4.12. The mesh has a similar layout for the two other load cases as only the range of the D-region varies between the cases.

A combined convergence criterion of both energy and force is chosen. The convergence criteria for the energy and force are as follows:

$$\epsilon_E = 0.001$$

$$\epsilon_F = 0.01$$

A maximum number of 100 iterations is calculated for each load increment. Convergence is assumed to be satisfied when both criteria are satisfied. If convergence is not achieved in the 100 iterations, the analysis is continued.

A summary of the modeling choices in the numerical analysis is shown in Table 4.6. Table 4.7 shows a summary of the material models used in DIANA.

Table 4.6: Summary of numerical analysis in DIANA.

Property	Value
Iterative procedure	Regular Newton-Raphson
Line search	Default
Arc-length method	Updated normal plane
Maximum number of iterations per step	100
Load step size	0.05
Convergence criterion	Force $< 10^{-2}$ **and** Energy $< 10^{-3}$
No convergence	Continue

Table 4.7: Summary of material model in DIANA.

Property	Value
Concrete class	C50/60 [4]
Crack model	Total strain rotating crack
Crack band width	Govindjee [21]
Poisson ratio	Variable, Initial=0.20
Fracture energy	$0.7 \cdot 0.073 f_{cm}^{0.18}$ [7]
Compressive fracture energy	$250 \cdot \frac{f_{ck}}{f_{cm}} \cdot 0.073 f_{cm}^{0.18}$ [7, 22]
Reinforcement	Embedded
Tension softening	Hordijk (and one with Linear ultimate crack strain)
Compression softening	Parabolic
Stress reduction	Vecchio and Collins (1993)

4.4 Nonlinear Finite Element Analysis with IDEA StatiCa

4.4.1 Material

Mean values are used for both reinforcement and concrete in order to describe the material behavior. All necessary material parameters are found in Eurocode 2 [4]. The reinforcement is modeled with no work hardening.

The concrete compression curve implemented in the software is the parabolic-rectangular curve shown in Figure 2.4. The curve is modified with a factor η_{f_c} for brittle behavior [5]:

$$\eta_{f_c} = \left(\frac{30}{f_{ck}}\right)^{\frac{1}{3}} \tag{4.16}$$

This results in the curve reaching its maximum compressive stress $\eta_{f_c} \cdot f_c$ at the strain $\eta_{f_c} \cdot \varepsilon_{c2}$. The reduction is included to account for the analysis being allowed to exceed the ultimate strain found in Eurocode 2 ($\varepsilon_{cu2} = 0.0035$) [11]. The reduction factor is $\eta = 0.80$ for concrete class C50/60 when using two digits of precision. This results in the same reduction as ν' used in the STMs. Compression softening due to transverse tensile strains is dealt with by the factor k_{c2} shown in Figure 4.13. When compression softening is necessary, the new resulting compressive strength becomes $k_c \cdot f_c$ where $k_c = \eta_{f_c} k_{c2}$. This new compressive strength is reached at the strain $k_c \cdot \varepsilon_{c2}$

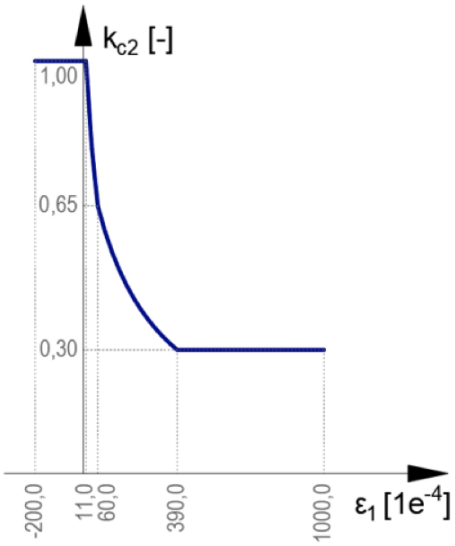

Figure 4.13: The reduction factor for compression softening in IDEA StatiCa [11]

No concrete contribution to tensile strength is assumed, apart from the tension stiffening

effect on the reinforcement [9]. The reinforcement is modeled using the tension chord model [19].

4.4.2 Loading

The loads in Table 4.3 are inserted in the analysis. The software then calculates the moments at the edges of the D-region, as done in subsection 4.2.1 for the STMs. The loads are applied to the model through a St.Venant transfer zone [11]. This is to ensure a realistic stress flow resulting from the load application. The software does not assess the concrete behavior in the transfer zone. Edges are constrained to remain straight, while still being able to rotate.

4.4.3 Geometry and Reinforcement

The geometry used for the D-region is identical to what is obtained in the calculation of the STM. For the reinforcement, IDEA StatiCa takes the bar diameter, number of bars and number of layers as input. Thus, identical reinforcement amounts as in the STM is not possible. The number of reinforcement bars and stirrups, in addition to the bar diameters, are chosen such that the bar area is as close as possible to what was calculated for the STM. Reinforcement amounts on the conservative side is preferred. The cross-section areas of the reinforcement is provided in the results.

4.4.4 Analysis

The Regular Newton-Raphson method is used for the numerical analysis. The D-region is meshed with the smallest elements possible in the software, where quadrilateral shell elements are applied. IDEA StatiCa stops the analysis of the D-region either when load factor=1.00 is reached or the capacity is found to be insufficient. In order to find the maximum capacity of the D-region, other analyses are run for every load case where the loads are scaled up with a factor larger than the ultimate load factor.

Chapter 5

Results

In this chapter, the results from the three different load cases are presented in order. For every load case, the results from the STM optimization will be presented first. This includes the truss forces in the STM, the necessary reinforcement in the ties, and the resulting stress field in the D-region based on the necessary widths of the struts. A compressive stress equal to the maximum allowable stress, $\sigma_{Rd,max}$ is used for these calculations. The STMs are made of blue struts and red ties. The Matlab code uses in total 0.1-0.2 seconds for all three load cases. Next, the results from the NLFEA are presented. First the analyses from DIANA and then from IDEA StatiCa. Lastly, the results are compared.

5.1 Load Case 1: Closing Moment

5.1.1 Strut-and-Tie Model

The STM found for load case 1 is shown in Figure 5.1. The STM gives no longitudinal reinforcement in the left side and right side wall.

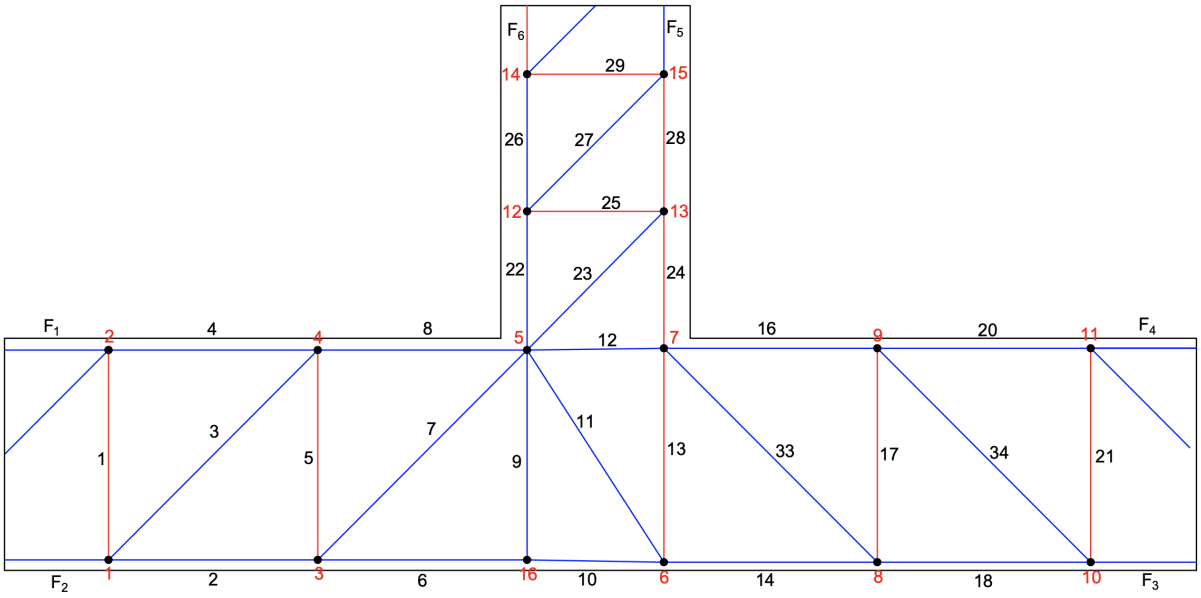

Figure 5.1: Resulting STM for load case 1.

Forces

The acting forces in the STM are shown in Table 5.1. The largest tension force is located in truss 13 while the largest compression force is obtained in truss 8.

Table 5.1: Acting forces in the STM calculated for load case 1

Truss Number	Force $[\frac{\text{kN}}{\text{m}}]$	Truss Number	Force $[\frac{\text{kN}}{\text{m}}]$
1	695.0	21	47.0
2	−1249.8	22	−1301.4
3	−982.9	23	−955.0
4	−1479.2	24	1238.9
5	695.0	25	671.0
6	−554.8	26	−630.4
7	−982.9	27	−948.9
8	−2174.2	28	559.4
9	−9.7	29	671.0
10	−554.8	33	−66.5
11	−1540.2	34	−66.5
12	−1362.4	F_1	−784.2
13	1303.2	F_2	−1944.8
14	−1390.7	F_3	−1484.7
16	−1315.3	F_4	−1221.3
17	47.0	F_5	−111.6
18	−1437.7	F_6	40.6
20	−1268.3		

Nodes

The necessary widths of the struts are shown in Figure 5.2. The figure shows that several struts are placed with virtually no extra space for the compression field. This applied to truss 8 which also is shown to be the strut with the largest compression force. Table 5.2 shows the maximum allowable stress, $\sigma_{Rd,max}$, in the nodes. As there are no ties anchored in node 5 and 16, these two nodes have the highest allowable stress. In comparison, nodes 7, 13, and 15 have more than two ties anchored in the nodes and thus experience the lowest $\sigma_{Rd,max}$.

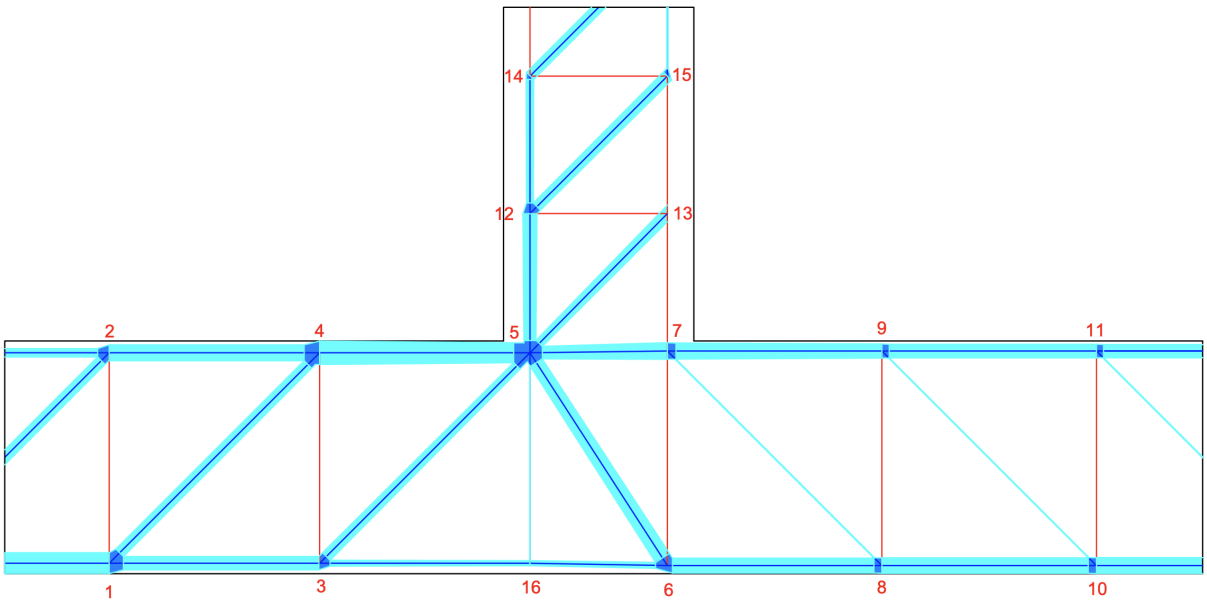

Figure 5.2: Necessary widths of struts for load case 1.

Table 5.2: Maximum allowable stress, $\sigma_{Rd,max}$, in the nodes for load case 1.

	k_{red}	$\sigma_{Rd,max}[\frac{\mathrm{N}}{\mathrm{mm}^2}]$
Node 1	0.68	39.44
Node 2	0.68	39.44
Node 3	0.68	39.44
Node 4	0.68	39.44
Node 5	0.8	46.40
Node 6	0.68	39.44
Node 7	0.6	34.80
Node 8	0.68	39.44
Node 9	0.68	39.44
Node 10	0.68	39.44
Node 11	0.68	39.44
Node 12	0.68	39.44
Node 13	0.6	34.80
Node 14	0.6	34.80
Node 15	0.6	34.80
Node 16	0.8	46.40

Reinforcement

The necessary reinforcement in the ties are shown in Table 5.3. The calculation of the amounts assumes yield in the reinforcement. The need for shear reinforcement is significantly lower on the right side than the left side of the D-region.

Table 5.3: Necessary reinforcement in ties for load case 1.

Truss Number	Reinforcement $\left[\frac{\text{mm}^2}{\text{m}}\right]$
1	1390
5	1390
13	2606
17	94.0
21	94.0
24	2478
25	1342
28	1119
29	1342

5.1.2 Nonlinear Finite Element Analysis

DIANA

Figure 5.3 shows the load-displacement curve obtained for load case 1. The horizontal displacement of the middle node of the top edge is used. The maximum obtained load factor is 1.18. It is observed that the failure is induced by concrete compression softening in the area most exposed to compressive stresses, namely the corner between the top wall and the left side wall.

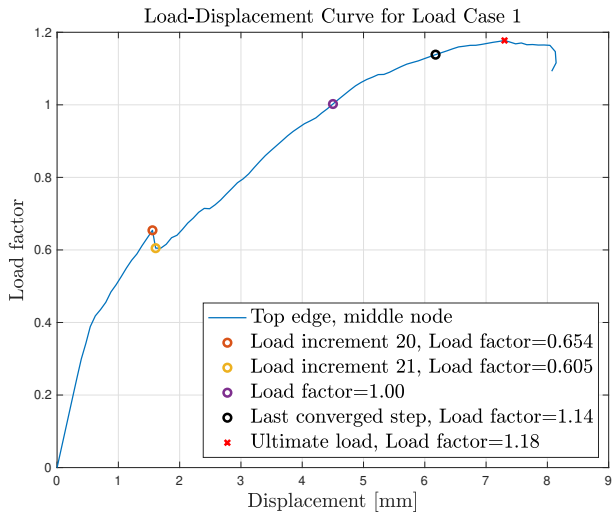

Figure 5.3: Load-displacement curve for load case 1 with limit points and ultimate load.

Two limit points occur at load step 20 and 21, where the load factors are 0.654 and 0.605, respectively. The vertical crack widths obtained in both load increments are shown in Figure 5.4. A developing crack pattern is observed between the two limit points, both along the longitudinal reinforcement and through the top wall. Furthermore, it is seen that the deformation mode at the cracked part of the top wall changes between the two limit points.

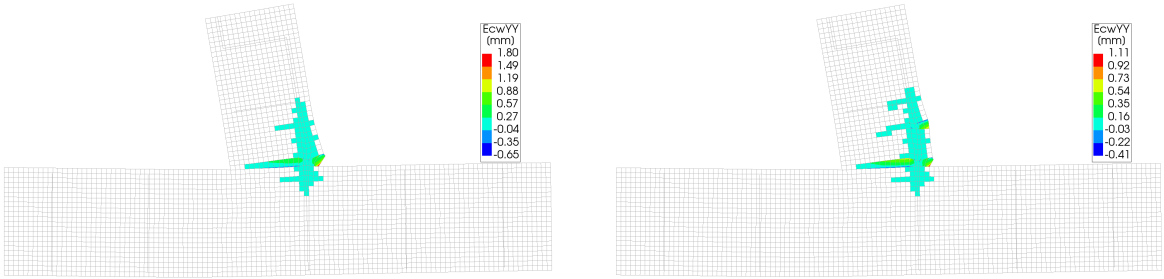

(a) Load increment 20 **(b)** Load increment 21

Figure 5.4: Vertical crack widths for the two highlighted limits points at load case 1.

Figure 5.5 shows the reinforcement stresses obtained at load step 1.00. Yield is reached for parts of the longitudinal reinforcement on the right side of the top wall. Moreover, the shear reinforcement also reaches the largest utilization in the top wall. In contrast, the shear reinforcement in the bottom wall is at most 16% utilized with respect to the yield stress at load factor 1.00.

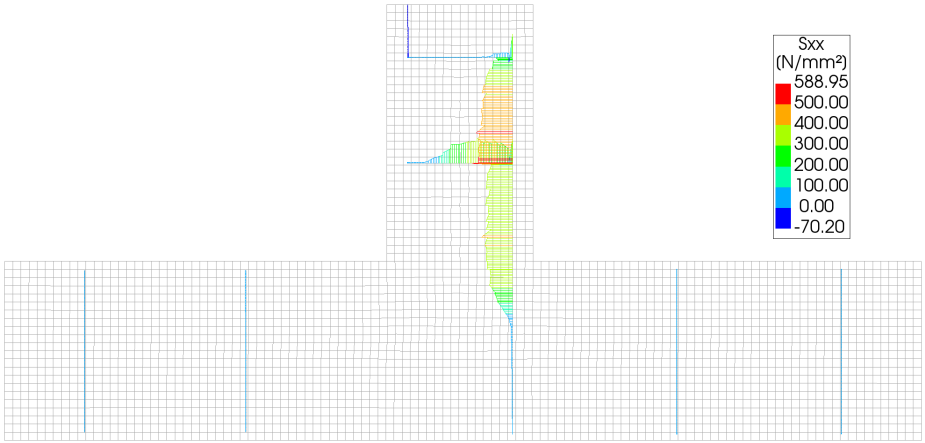

Figure 5.5: The reinforcement stress for load case 1 with a load factor=1.00.

The principal strains ε_1 are shown in Figure 5.6. It is observed that large parts of the D-region experience maximum principal strains in the elastic area of the tension curve. The maximum principal strain in the corner between the top wall and the left hand side wall is observed to be negative. Also, maximum principal strains larger than the ultimate strain $\varepsilon_u = 0.00546$ is observed along the longitudinal reinforcement at the right hand side of the top wall.

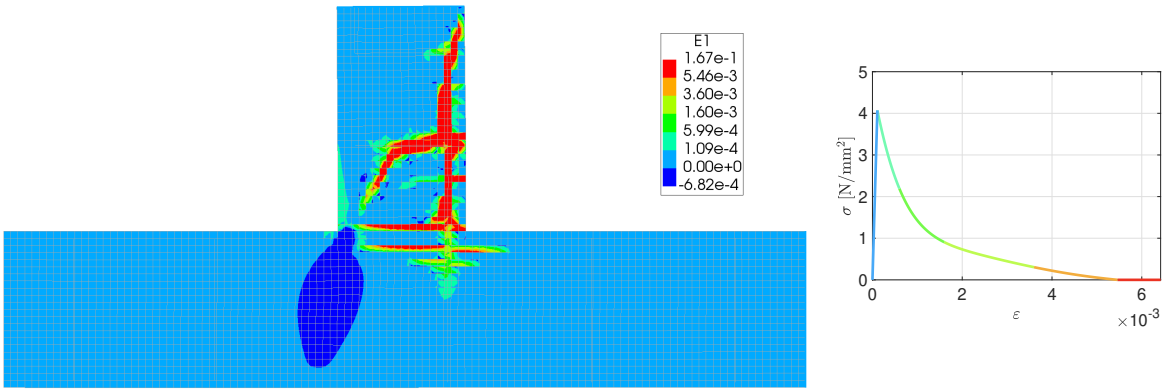

Figure 5.6: The maximum principal strain, ε_1, for load case 1 with a load factor=1.00

Figure 5.7 shows the in-plane principal stress components in the D-region. The largest compressive stresses are obtained at the corner between the left wall and the top wall, where both σ_1 and σ_2 are in compression. Here, the compressive stress is observed to be $\sigma_2 = -45.8 \frac{\text{N}}{\text{mm}^2}$.

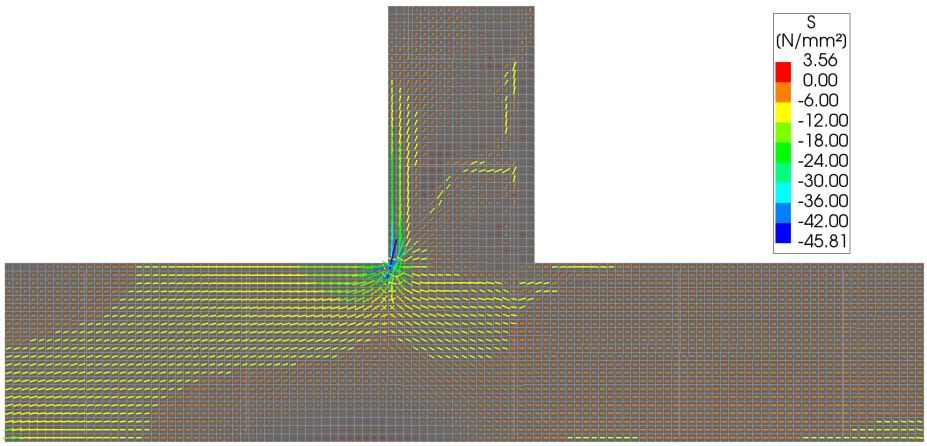

Figure 5.7: The in-plane principal stress components, for load case 1 with a load factor=1.00.

Figure 5.8 shows the development of vertical cracks in the D-region. At load factor 1.00, the vertical cracks have developed far through the top wall, leaving a small compression zone of uncracked elements on the left hand side. Moreover, the development of a diagonal crack is evident in the top wall. No diagonal cracks are observed in the bottom wall. This is in line with the observed utilization of the shear reinforcement. Finally, it is observed that cracks have developed along the entire right side of the top wall.

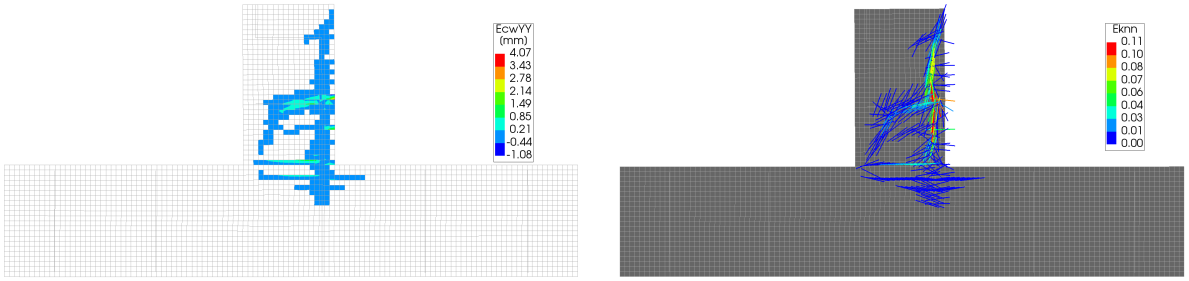

(a) Vertical crack widths **(b)** Crack strains

Figure 5.8: Cracking for load case 1 at load factor=1.00.

IDEA StatiCa

Figure 5.9 shows the concrete principal stresses and reinforcement stresses obtained. The minimum concrete principal stress, located at the corner between the left and top wall, is $\sigma_2 = -46.3\frac{\mathrm{N}}{\mathrm{mm}^2}$. A check of the concrete principal strains shows a minimum strain value of $\varepsilon_2 = -2.7 \cdot 10^{-3}$ is reached at load factor 1.00. It is observed that parts of the reinforcement at the right side of the top wall is fully utilized. The D-region reaches $\varepsilon_{cu2} = -0.0035$ at the load factor of 1.10. When the analysis is run past this load factor, failure is obtained at load factor 1.26, where a strain of $\varepsilon_2 = -0.00891$ is observed. The insufficient concrete strength at the corner between the top and left wall proved to be the reason for failure.

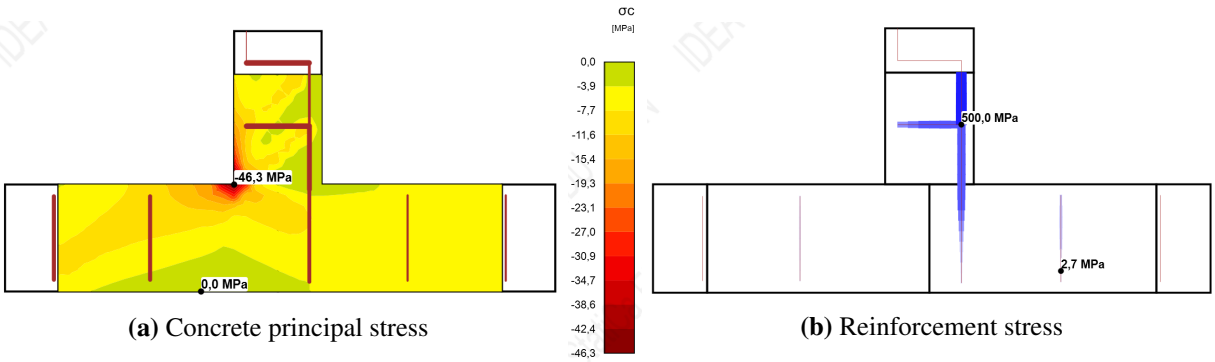

(a) Concrete principal stress **(b)** Reinforcement stress

Figure 5.9: Concrete and reinforcement stress obtained for load case 1 at load factor=1.00.

In Figure 5.10, the resulting reductions of the concrete compressive strength due to transverse tensile strains are shown by the governing $\mathrm{k_{c2}}$-factors. The most significant reductions are observed at the right side of the top wall. At most, the compressive strength is reduced with a $\mathrm{k_{c2}}$-factor of 0.59. This, combined with the reduction factor $\eta_{f_c} = 0.80$ for brittle behavior, gives a total reduction factor of $k_c = 0.47$.

Table 5.4: Reinforcement amounts for load case 1 in IDEA StatiCa.

	Reinforcement amount $[\frac{mm^2}{m}]$	Fraction of calculated reinforcement in STM
Truss 1	1385	0.996
Truss 5	1385	0.996
Truss 13	2513	0.964
Truss 17	95	1.01
Truss 21	95	1.01
Truss 24	2454	0.990
Truss 25	1321	0.984
Truss 28	1078	0.963
Truss 29	1321	0.984
F6	75	0.924

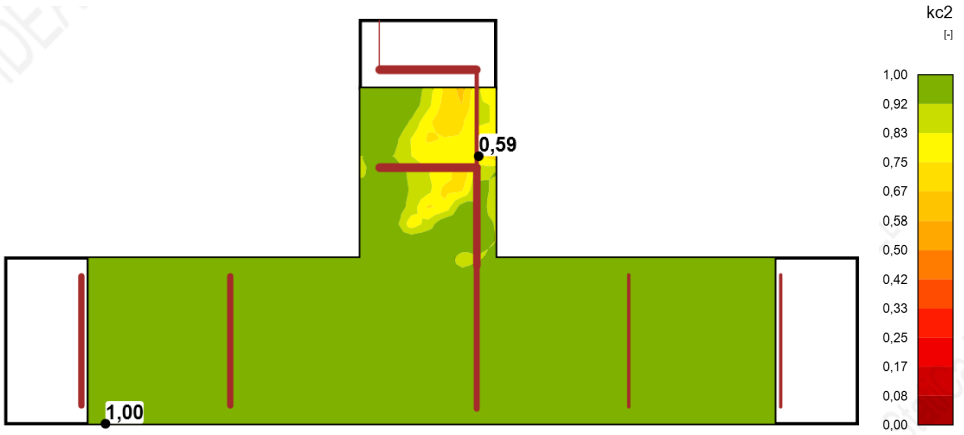

Figure 5.10: Reduction factor k_{c2} for load case 1 at load factor=1.00.

5.1.3 Comparison

Both FEM-analyses show a capacity larger than what was calculated in the STM, where the analysis from IDEA StatiCa shows highest capacity. Concrete failure was the source of failure in both NLFEAs.

The two NLFEAs show similar results when considering the principal stress σ_2. Both analyses show a minimum value of the stress at virtually the same location, namely the corner between the top and left wall. Furthermore, the obtained values of the minimum principal stress in this area are very close, where the analysis run in IDEA StatiCa shows a stress which is 0.94% lower than what was obtained in DIANA.

The reinforcement stresses show a similar utilization between the the two NLFEAs. In both analyses, the reinforcement corresponding to truss 28 is most utilized. Compared to the STM, this is the truss with the least reinforcement of the three trusses along right surface of the top

wall. Meanwhile, the truss (nr. 13) that gave the largest reinforcement amount in the STM is the least utilized of these three.

When comparing the reductions in compressive strength in Table 5.2 with Figure 5.10, it is observed that the reductions are in general more conservative in the STM. However, this is not the case in node 13 in the STM. While the calculation from the Eurocode 2 gives a reduction factor of 0.6, the compressive strength is reduced by a factor of $k_c = 0.8 \cdot 0.59 = 0.47$ in the NLFEA. Furthermore, the comparison shows that the NLFEA obtains the same reduction factors as the STM in node 5 and 16. Equation 3.6 shows the calculation of $\sigma_{Rd,max}$ in a node where there are no anchored ties. By using Equation 3.3, a reduction factor of $\nu' = 0.8$ is obtained for such nodes.

5.2 Load Case 2: Dominating Tension

5.2.1 Strut-and-Tie Model

Then STM found for load case 2 is shown in Table 5.5. According to the STM found, no longitudinal reinforcement is necessary in the left side and right side wall.

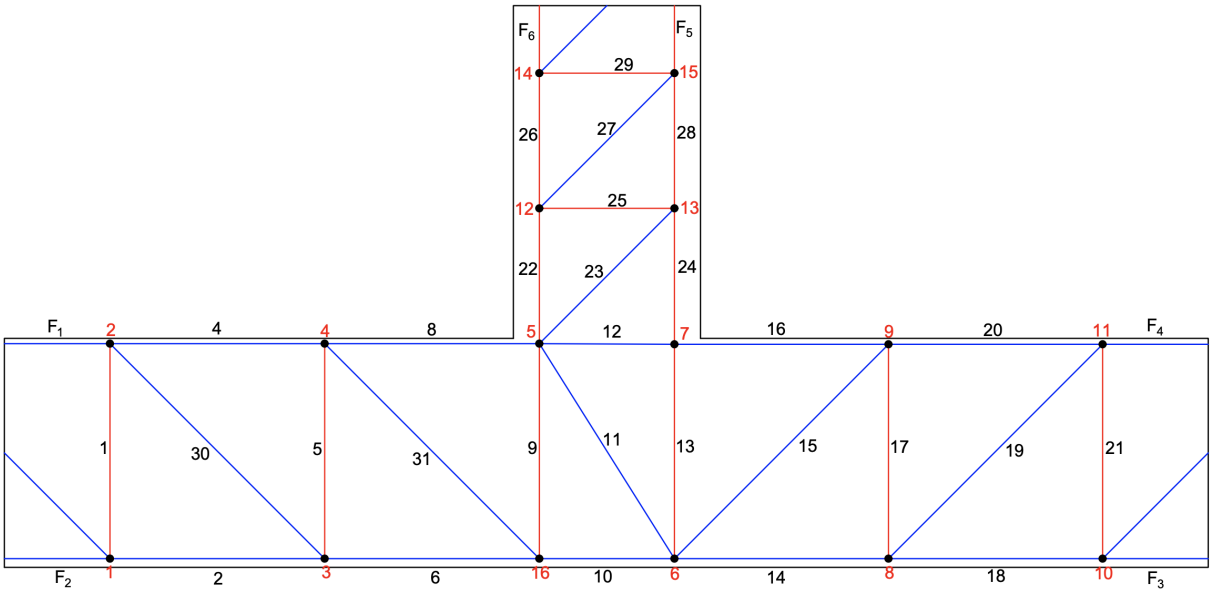

Figure 5.11: Resulting STM for load case 2.

Forces

The forces acting in the STM are shown in Table 5.5. The largest tensile force is located in truss 24 while the largest compression force is located in truss 10.

Table 5.5: Truss forces for load case 2.

Truss Number	Force $[\frac{\text{kN}}{\text{m}}]$	Truss Number	Force $[\frac{\text{kN}}{\text{m}}]$
1	452.0	21	498.0
2	−721.9	22	438.6
4	−527.1	23	−2.8
5	452.0	24	513.4
6	−1173.9	25	2.0
8	−75.1	26	440.6
9	452	27	−2.8
10	−1625.9	28	511.4
11	−17.9	29	2.0
12	−63.6	30	−639.2
13	513.1	31	−639.2
14	−1137.4	F_1	−979.1
15	−704.3	F_2	−269.9
16	63.6	F_3	−141.4
17	498.0	F_4	−1059.6
18	−639.4	F_5	509.4
19	−704.3	F_6	442.6
20	−561.6		

Nodes

The necessary widths and the resulting compression fields are shown in Figure 5.12. It is observed that the widest compression field is located in truss 10 at the bottom of the intersection, which also experiences the largest compression force. The maximum allowable stress in the nodes of the STM are shown in Table 5.6. It is observed that every node have at least one anchored tie, which reduces the allowable stress in the nodes.

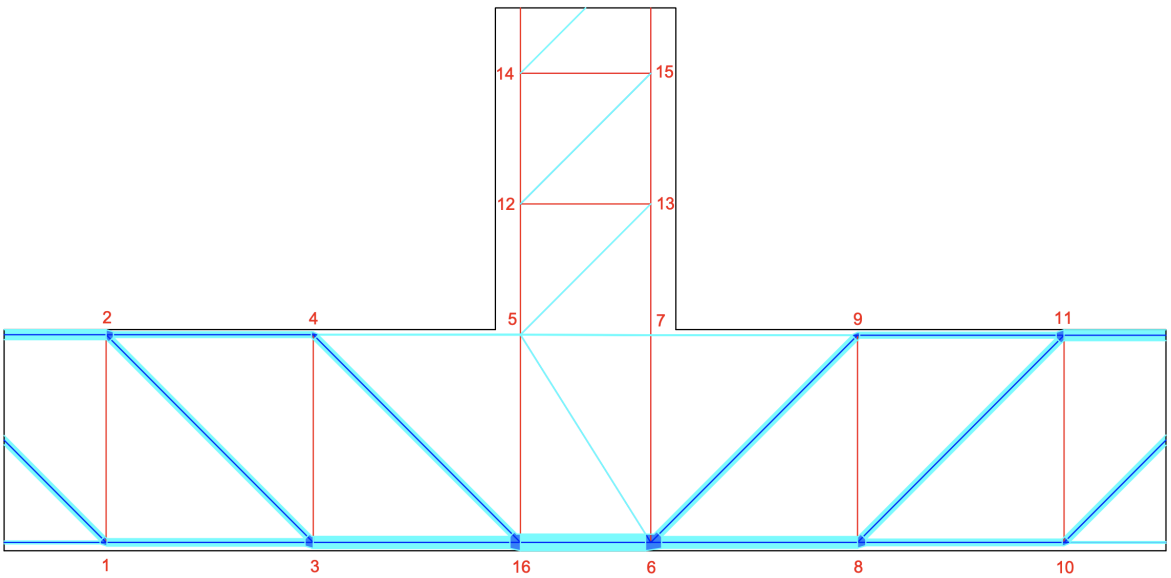

Figure 5.12: Necessary widths of struts for load case 2.

Table 5.6: Maximum allowable stress, $\sigma_{Rd,max}$, in the nodes for load case 2.

	k_{red}	$\sigma_{Rd,max}[\frac{\mathrm{N}}{\mathrm{mm}^2}]$
Node 1	0.68	39.44
Node 2	0.68	39.44
Node 3	0.68	39.44
Node 4	0.68	39.44
Node 5	0.6	34.80
Node 6	0.68	39.44
Node 7	0.6	34.80
Node 8	0.68	39.44
Node 9	0.68	39.44
Node 10	0.68	39.44
Node 11	0.68	39.44
Node 12	0.6	34.80
Node 13	0.6	34.80
Node 14	0.6	34.80
Node 15	0.6	34.80
Node 16	0.68	39.44

Reinforcement

The necessary reinforcement for the ties are shown in Table 5.7. The largest demand of longitudinal reinforcement is located along the right side surface of the top wall. The area of the shear reinforcement (truss 25 & 29) in the top side wall is virtually zero.

Table 5.7: Necessary reinforcement in ties for load case 2.

	Reinforcement amount $[\frac{\mathrm{mm}^2}{\mathrm{m}}]$
Truss 1	904
Truss 5	904
Truss 9	904
Truss 13	1026
Truss 17	996
Truss 21	996
Truss 22	877
Truss 24	1027
Truss 25	4.0
Truss 26	881
Truss 28	1023
Truss 29	4.0
F5	1005
F6	1019

5.2.2 Nonlinear Finite Element Analysis

DIANA - Hordijk Softening

Figure 5.13 shows the load-displacement curve obtained for load case 2. The vertical displacement of the middle node of the right side wall is used. The maximum obtained load factor is 1.00. At this load factor, a crack snaps horizontally through the top wall close to shear reinforcement representing truss 29. The last converged step occurs at a load factor of 0.999, which is one load step before 1.00 is reached and two steps before the ultimate load factor of 1.00.

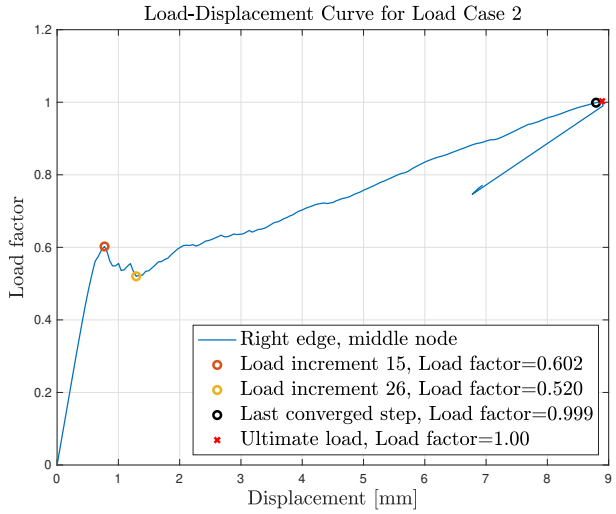

Figure 5.13: Load-displacement curve for load case 2 with limit points and ultimate load.

The two marked limit points (before ultimate load) happen at load increment 15 and 26, with load factors 0.602 and 0.520, respectively. The crack development at these two limit points are shown in Figure 5.14. The propagation of a diagonal crack is observed in the center of the intersection.

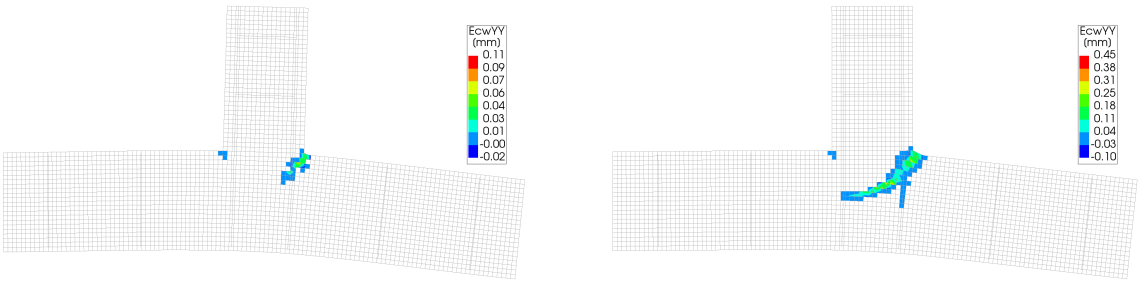

(a) Load increment 15 **(b)** Load increment 26

Figure 5.14: Vertical crack widths for the two highlighted limits points at load case 2.

Figure 5.15 shows the reinforcement stresses obtained with a load factor of 1.00. Yield is reached in parts of the longitudinal reinforcement on the right hand side of the top wall. The

utilization of the shear reinforcement is observed to be low.

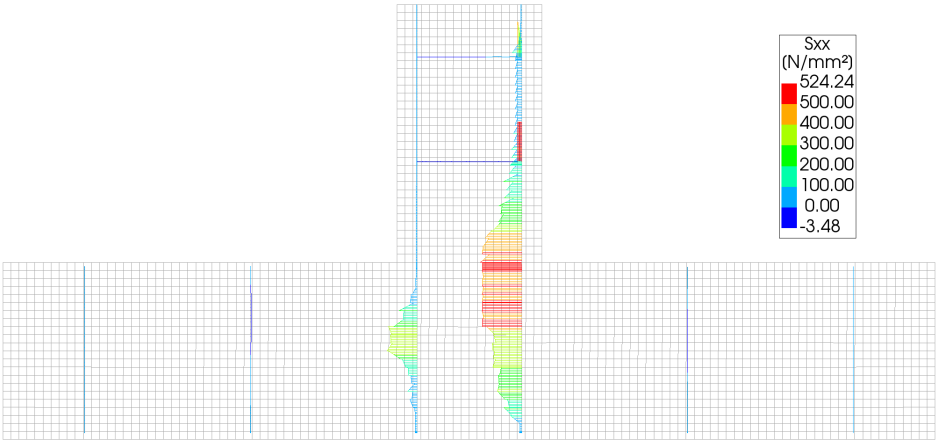

Figure 5.15: The reinforcement stress for load case 2 with Hordijk softening. Load factor=1.00.

The maximum principal strains, ε_1, are shown in Figure 5.16. Substantial tension softening is observed along the major part of the longitudinal reinforcement on the right side of the top wall. Large parts of the D-region are observed to experience maximum principal strains in the elastic area, resulting in no tension softening in these parts.

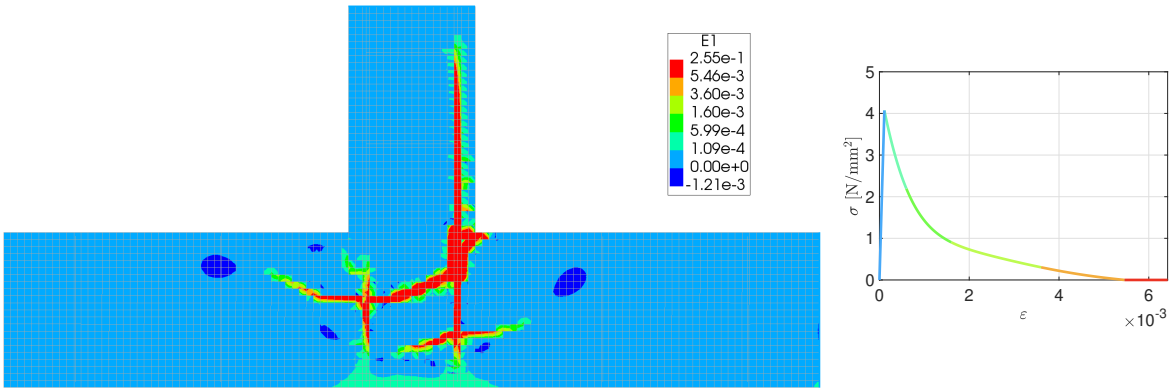

Figure 5.16: The maximum principal strain, ε_1, for load case 2 using Hordijk softening. Load factor=1.00.

Figure 5.17 shows the in-plane principal stress components. The largest compression stresses are obtained at the bottom middle of the D-region, where the value is $\sigma_2 = -33.4\frac{\mathrm{N}}{\mathrm{mm}^2}$. The corresponding minimum strain is found to be $\varepsilon_2 = -9.4 \cdot 10^{-4}$.

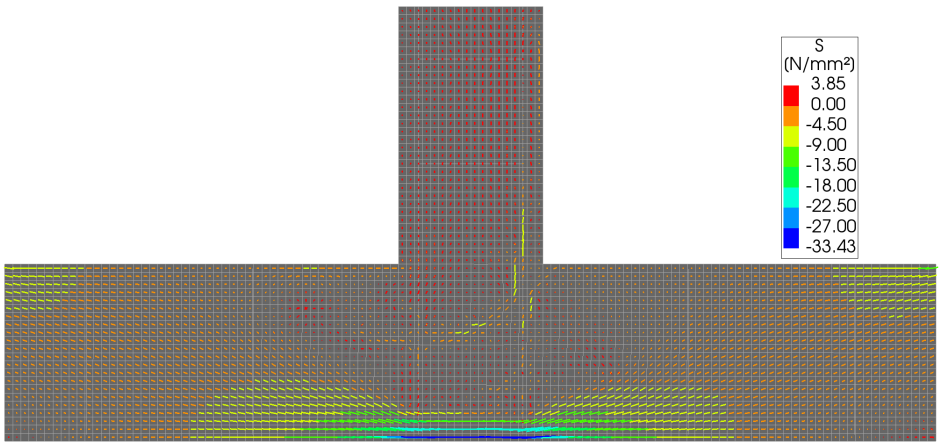

Figure 5.17: The in-plane principal stress components for load case 2 using Hordijk softening. Load factor=1.00.

Figure 5.18a shows the development of vertical cracks in the D-region. The crack strains at load factor 1.00 are shown in Figure 5.18b. Cracks have developed along large parts of the longitudinal reinforcement at the right hand side of the top wall. The beginning of a diagonal shear crack is observed in the wall to the left.

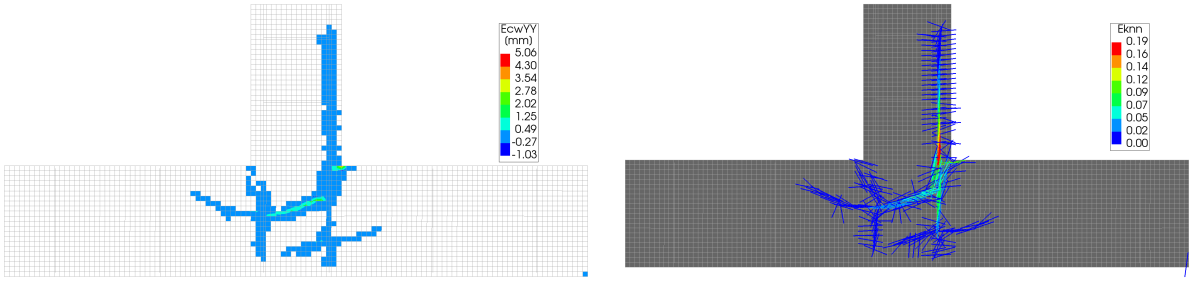

(a) Vertical crack widths

(b) Crack strains

Figure 5.18: Cracking for load factor 2 with Hordijk softening at load factor=1.00.

DIANA - Linear Tensile Softening

An analysis with a tensile behavior using linear-ultimate crack strain softening has also been run. The load-displacement curve for the analysis, using an ultimate strain $\varepsilon_u = f_{yk}/E_{sm}$=0.0025, is shown in Figure 5.19. It is observed that a load factor of 1.15 is obtained using this tensile behavior. The failure is caused by a crack snapping horizontally through the top wall just below the shear reinforcement corresponding to truss 29.

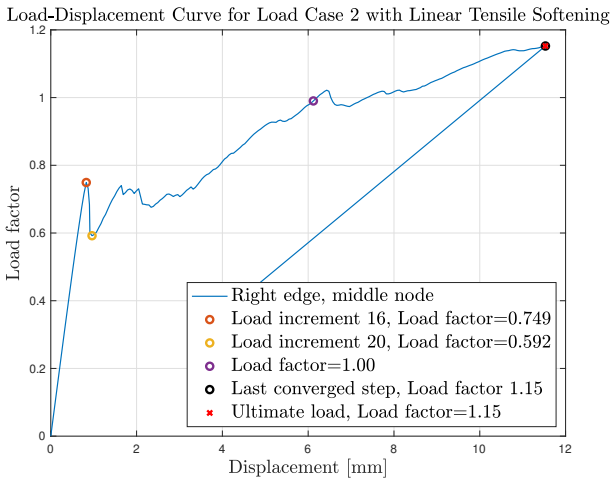

Figure 5.19: Load-displacement curve for load case 2 with limit points and ultimate load.

Two limit points are observed at load increment 16 and 20, with load factors of 0.749 and 0.592 (respectively). The vertical crack patterns for these two load steps are shown in Figure 5.20. Between the two limit points, vertical cracks develop along the longitudinal reinforcement at the right hand side of the top wall.

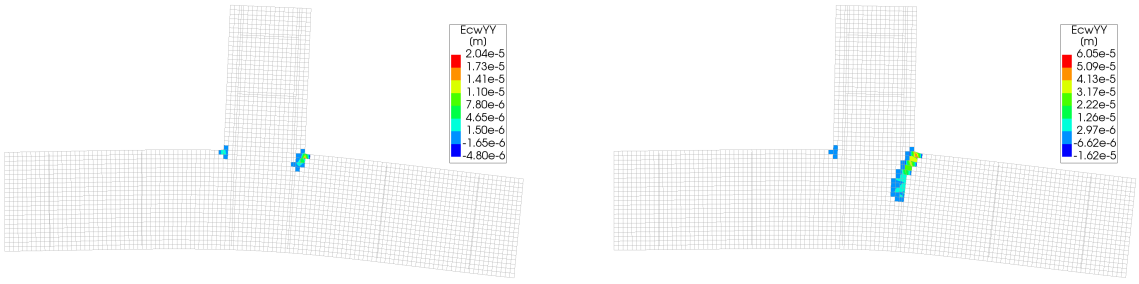

(a) Load increment 16 **(b)** Load increment 20

Figure 5.20: Vertical crack widths for the two limits points at load case 2 using a linear tensile softening.

Figure 5.21 shows the stresses obtained in the reinforcement at load factor 1.00. It is noted that the reinforcement is in general far from being fully utilized. The shear reinforcement in the top wall experiences compressive stress.

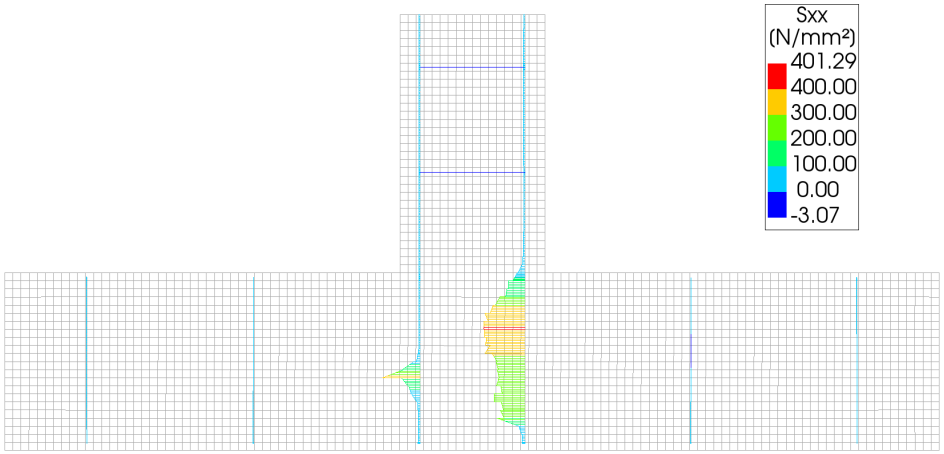

Figure 5.21: The reinforcement stress for load case 2 using linear tensile softening. Load factor=1.00.

The maximum principal strains, ε_1, are shown in Figure 5.22. Large parts of the D-region does not experience maximum principal strains past the elastic area of the tension curve. The tension softening observed is located in the middle of the D-region, below the top wall. In this area, strains past the ultimate strain $\varepsilon_u = 0.0025$ is observed.

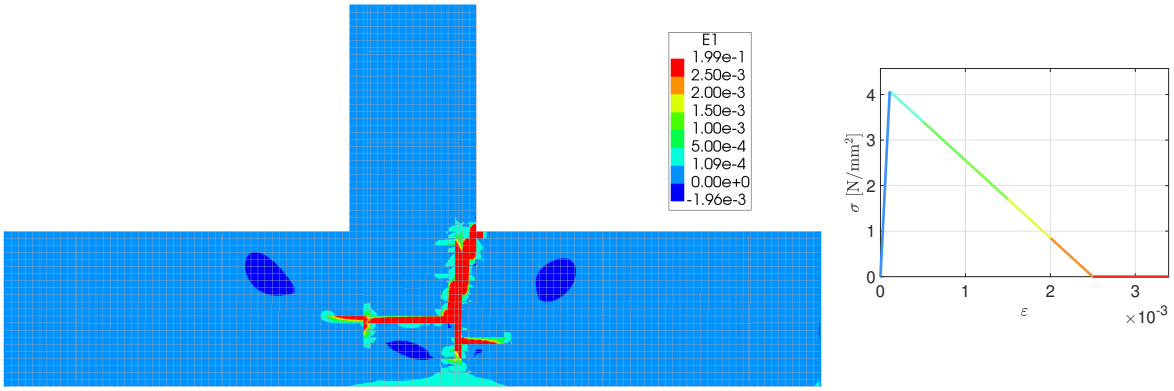

Figure 5.22: The maximum principal strain, ε_1 for load case 2 using linear tensile softening. Load factor=1.00.

Figure 5.23 shows the in-plane principal stress components obtained in the D-region. The largest compressive stress, located at the bottom middle, is $\sigma_2 = -31.50 \frac{\text{N}}{\text{mm}^2}$. The corresponding minimum principal strain is $\varepsilon_2 = -8.8 \cdot 10^{-4}$.

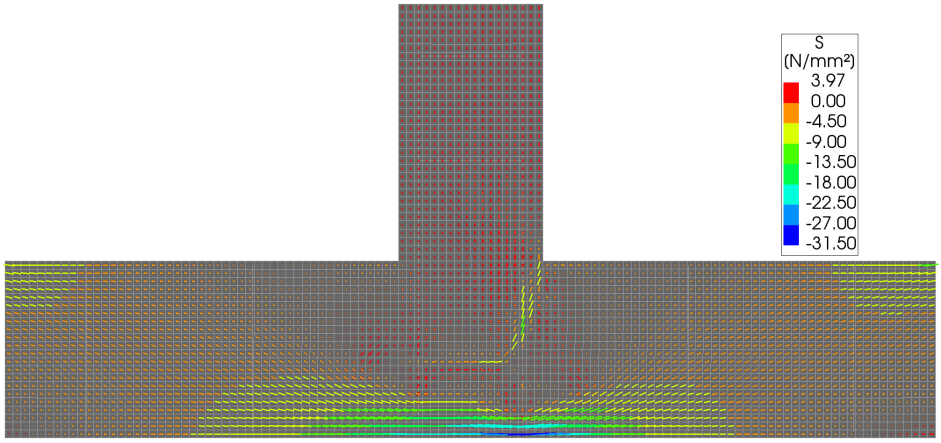

Figure 5.23: The in-plane principal stress components for load case 2 using linear tensile softening. Load factor=1.00.

Figure 5.24a shows the resulting vertical crack pattern at load factor=1.00. The major part of the cracking is located in the intersection between the three ends of the D-region.

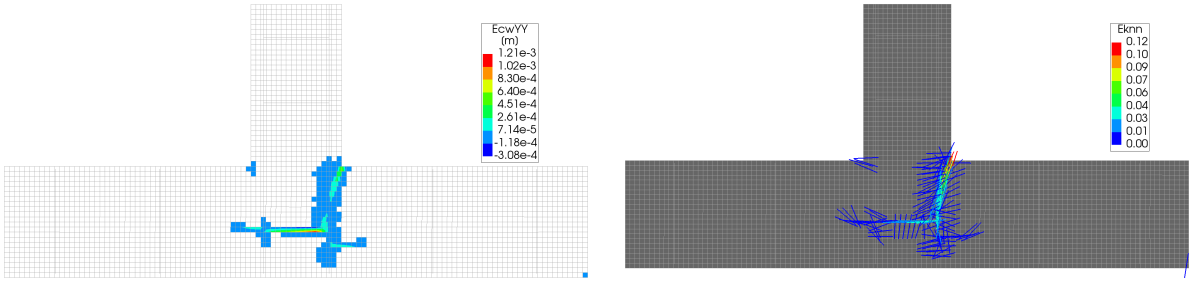

(a) Vertical crack widths **(b)** Crack strains

Figure 5.24: Cracking for load case 2 with linear tensile softening at load factor=1.00.

IDEA StatiCa

Figure 5.25a and Figure 5.25b show the concrete principal stress and reinforcement stress at load factor 1.00. A check of the concrete principal strains shows that the minimum value reached for the compressive strains is $\varepsilon_2 = -5.5 \cdot 10^{-4}$. The largest obtained minimum principal stress is $\sigma_2 = -26.5 \frac{\mathrm{N}}{\mathrm{mm}^2}$. It is observed that the reinforcement in truss 13, 22, 24, and 26 is fully utilized, but the largest strain is obtained in truss 13. The concrete is most utilized at the bottom middle of the D-region. Failure is reached at a load factor of 1.02. The reinforcement depicting truss 24 shows to be the critical part of the D-region.

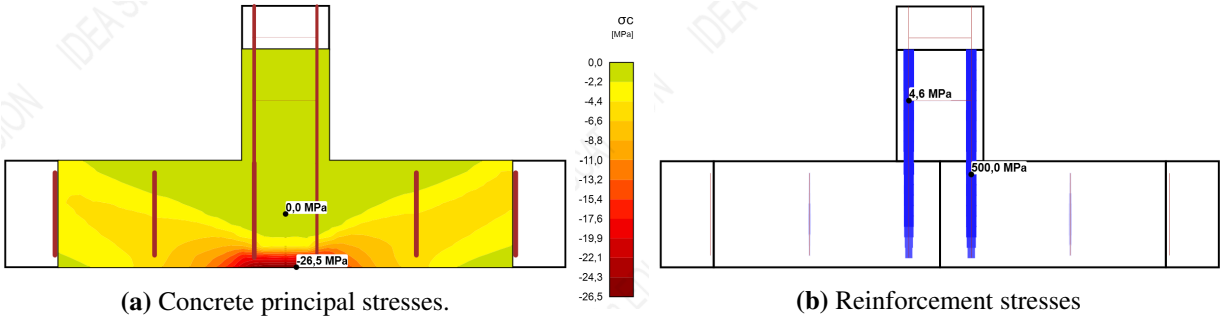

(a) Concrete principal stresses.

(b) Reinforcement stresses

Figure 5.25: Concrete and reinforcement stresses obtained for load case 2 at load factor=1.00.

Table 5.8: Reinforcement amounts for load case 2 in IDEA StatiCa.

	Reinforcement amount $[\frac{mm^2}{m}]$	Fraction of calculated reinforcement in STM
Truss 1	905	1.00
Truss 5	905	1.00
Truss 9	905	1.00
Truss 13	1005	0.979
Truss 17	982	0.986
Truss 21	982	0.986
Truss 22	851	0.970
Truss 24	1005	0.979
Truss 25	3.9	0.975
Truss 26	851	0.966
Truss 28	1005	0.983
Truss 29	3.9	0.975
F5	1005	0.986
F6	851	0.961

The reductions in the concrete compressive strength due to transverse tensile strains are shown in Figure 5.26. It is observed that the compressive softening due to compression-tension interaction is located in the top wall and along the longitudinal reinforcement. The largest reductions are found in the corners where the walls intersect.

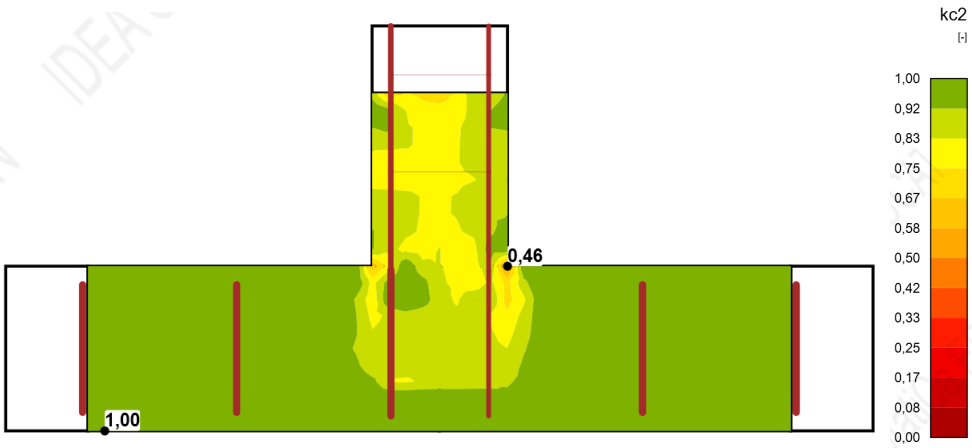

Figure 5.26: Reduction factor k_{c2} for load case 2 at load factor=1.00.

5.2.3 Comparison

All three analyses reach at least load factor of 1.00, where the analysis with linear tension softening obtained the largest capacity while the analysis with Hordijk softening obtained the smallest. Failure was located in the top wall for all three analyses.

Differences are observed between the two analyses from DIANA testing the tensile softening branch. When using a linear tensile softening based on ultimate crack strain, a higher load factor is reached. Differences also occur in the crack patterns. The crack pattern in the analysis using Hordijk softening (Figure 5.14) propagated more diagonally than in the analysis using linear-ultimate crack strain softening (Figure 5.20). Moreover, wider cracks are in general observed at load factor 1.00 when using the Hordijk softening. Lastly, the vertical cracks have developed further along the longitudinal reinforcement in the model using Hordijk softening.

Both FEM-analyses give the highest utilization of the reinforcement between truss 13 and 24. The analysis from IDEA StatiCa shows in general higher reinforcement stresses in the longitudinal reinforcement.

Table 5.6 and Figure 5.26 show the difference in the reduction of the compressive strength between the STM and the NLFEA, respectively. The largest reduction of compressive strength in the NLFEA is obtained in the area of node 7 in the STM. Here, the NLFEA results in a larger reduction of the compressive strength than the STM. Furthermore, the NLFEA gives a reduction factor k_{c2} between $0.92 - 1.0$ in the area around node 6 and 16. Multiplied with $\eta_{f_c} = 0.80$, this gives a total reduction factor of $k_{c2} = 0.74 - 0.80$. As these two nodes have one anchored tie each, a reduction factor of 0.68 is used in the STM.

5.3 Load Case 3: Opening Moment

5.3.1 Strut-and-Tie Model

The calculated STM for load case 3 is shown in Figure 5.27. In the bottom wall, reinforcement is found to be necessary at the bottom left corner. Only two trusses are found in node 6, which enforces them to be parallel and equal in force.

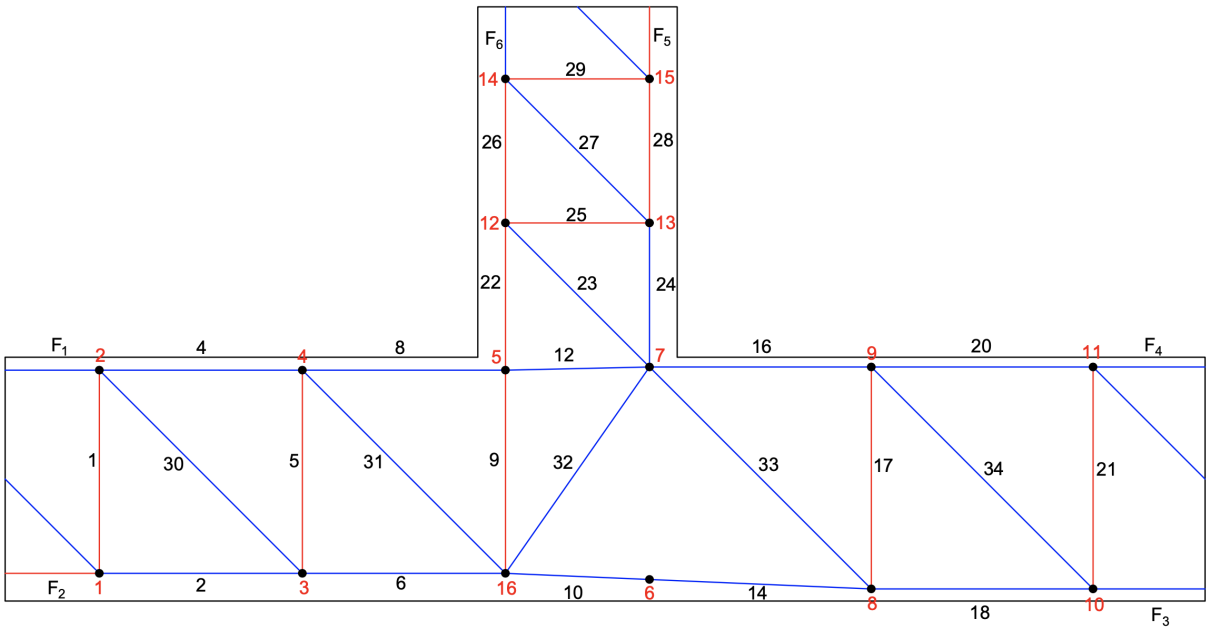

Figure 5.27: Resulting STM for load case 3.

Forces

The acting forces in the STM are given in Table 5.9. The largest tension force is found in truss F_5 while the largest compression force is located in truss F_1. Thus, both the largest tension force and compression force are found in the point loads representing the sectional forces.

Table 5.9: Truss forces for load case 3.

Truss Number	Force $[\frac{\text{kN}}{\text{m}}]$	Truss Number	Force $[\frac{\text{kN}}{\text{m}}]$
1	894.0	25	868.0
2	−448.4	26	741.5
4	−1392.6	28	763.5
5	894.0	29	868.0
6	−1342.4	30	−1264.3
8	−498.6	31	−1264.3
9	1598.7	32	−947.7
10	−1695.3	33	−261.4
12	−498.7	34	−363.5
14	−1695.3	35	−1227.5
16	−1724.4	36	−1227.5
17	257.0	F_1	−2286.6
18	−1878.6	F_2	445.6
20	−1467.4	F_3	−2135.6
21	257	F_4	−1210.4
22	1609.5	F_5	1631.5
24	−104.5	F_6	−126.5

Nodes

The necessary widths of the struts are shown in Figure 5.28. The figure shows that several struts are placed such that their compression fields cover most of the available space. It is noted that the struts along the top surface of the right hand side wall have very little space left for the compression fields. The maximum allowable stresses in the nodes are shown in Table 5.10. It is seen that node 6 and 7 have the largest allowable maximum concrete compressive strength.

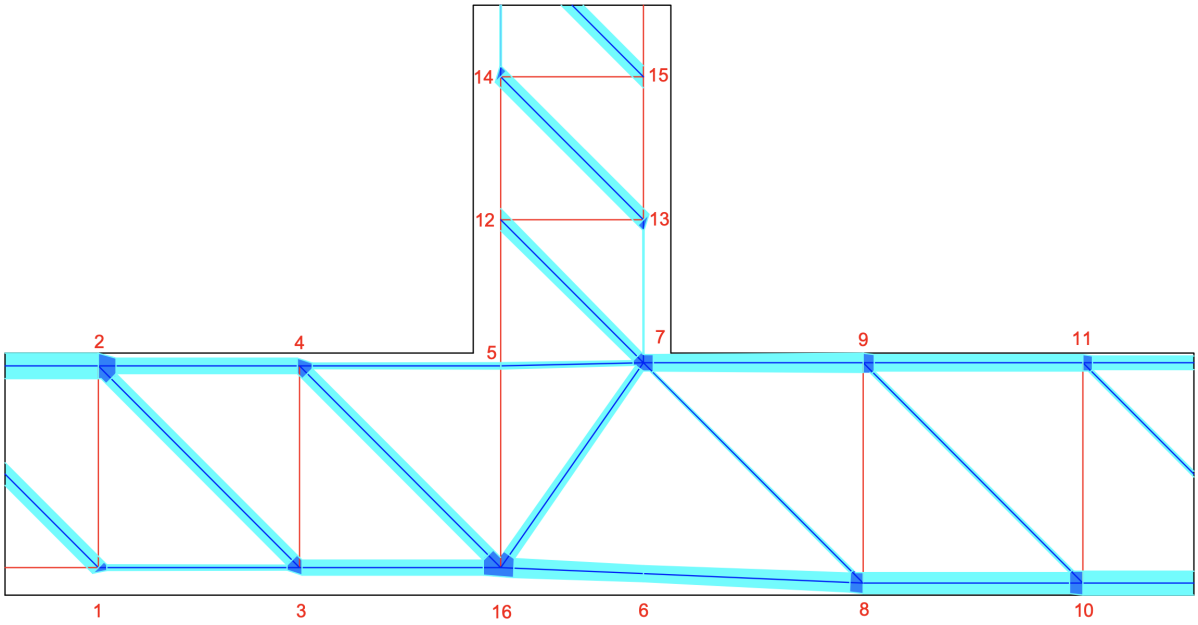

Figure 5.28: Necessary widths of struts for load case 3.

Table 5.10: Maximum allowable stress, $\sigma_{Rd,max}$, in the nodes for load case 3.

	k_{red}	$\sigma_{Rd,max}[\frac{\mathrm{N}}{\mathrm{mm}^2}]$
Node 1	0.6	34.80
Node 2	0.68	39.44
Node 3	0.68	39.44
Node 4	0.68	39.44
Node 5	0.6	34.80
Node 6	0.8	46.40
Node 7	0.8	46.40
Node 8	0.68	39.44
Node 9	0.68	39.44
Node 10	0.68	39.44
Node 11	0.68	39.44
Node 12	0.6	34.80
Node 13	0.6	34.80
Node 14	0.6	34.80
Node 15	0.6	34.80
Node 16	0.68	39.44

Reinforcement

The necessary reinforcement for the ties are shown in Table 5.11. Significantly larger amounts of shear reinforcement is needed for the top and left walls compared to the right hand side wall.

Table 5.11: Necessary reinforcement in ties for load case 3.

	Reinforcement amount $[\frac{\mathrm{mm}^2}{\mathrm{m}}]$
Truss 1	1788
Truss 5	1788
Truss 9	3197
Truss 17	514
Truss 21	514
Truss 22	3219
Truss 25	1736
Truss 26	1483
Truss 28	1527
Truss 29	1736
F2	891
F5	3263

5.3.2 Nonlinear Finite Element Analysis

DIANA

Figure 5.29 shows the load-displacement curve obtained for load case 3. The horizontal displacement of the middle node of the top edge is used. The maximum obtained load factor is 0.631. The two limit points reached at load increment 18 and 19 are highlighted, where the load factors are 0.540 and 0.494 (respectively). The vertical cracks at these two increments are shown in Figure 5.30a and Figure 5.30b. An increased cracked area along the longitudinal reinforcement along the left surface of the top wall is observed. Also, the cracking along the top loading edge is observed at these two limit points. Finally, the figures show a developing diagonal crack in the top wall between the two limit points.

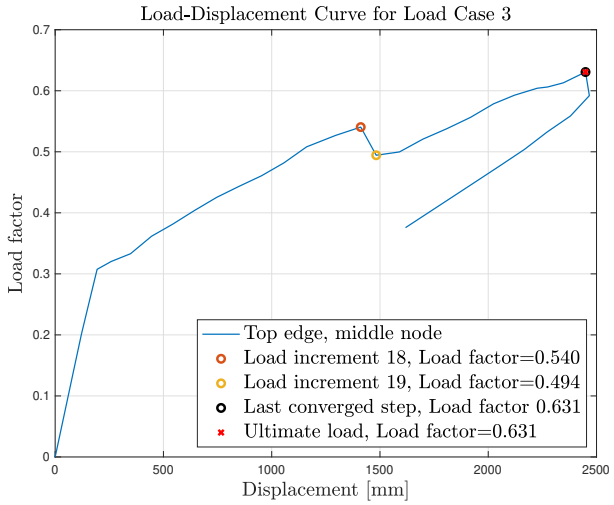

Figure 5.29: Load-displacement curve for load case 3 with limit points and ultimate load.

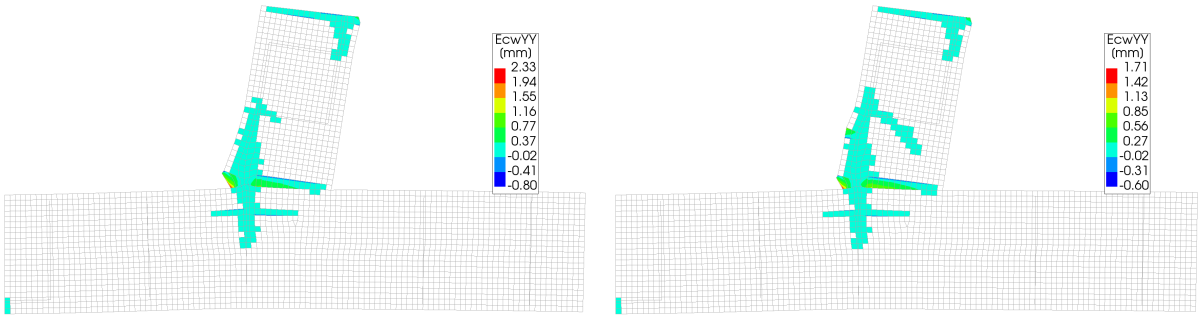

(a) Load increment 18 **(b)** Load increment 19

Figure 5.30: Vertical crack widths for the two highlighted limits points at load case 3.

Figure 5.31 shows the reinforcement stresses obtained at at load factor=0.631. The reinforcement is in general observed to be far from fully utilized. The highest utilization of the shear reinforcement is found in the top wall.

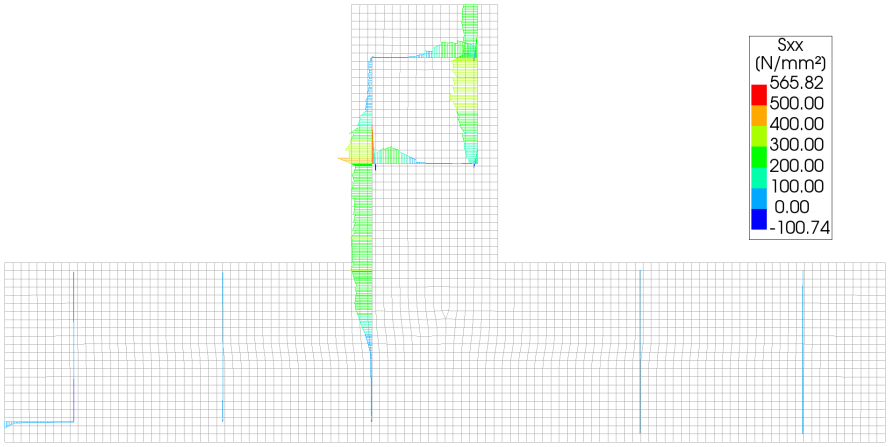

Figure 5.31: The reinforcement stress for load case 3. Load factor=0.631.

The maximal principal strains, ε_1 at failure are shown in Figure 5.32. The majority of the tension softening is located in the top wall, where strains past the ultimate strain $\varepsilon_u = 0.00546$ is observed. The bottom wall experiences in general maximum principal strains in the elastic area of the tension curve. An area with negative maximum principal strains are observed below the corner between the top wall and right hand side wall.

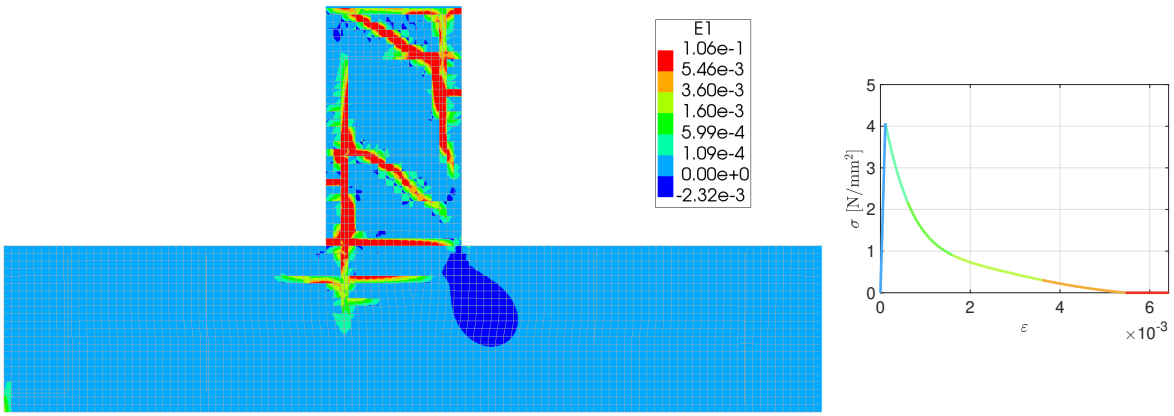

Figure 5.32: The maximum principal strain, ε_1, for load case 3. Load factor=0.631.

The in-plane principal stress components are shown in Figure 5.33. Here, the largest compressive stress is observed in the corner between the top wall and the right wall with a value of $\sigma_2 = -21.7\frac{\mathrm{N}}{\mathrm{mm}^2}$. The corresponding minimum compressive strain in this area is $\varepsilon_2 = -6.03 \cdot 10^{-4}$.

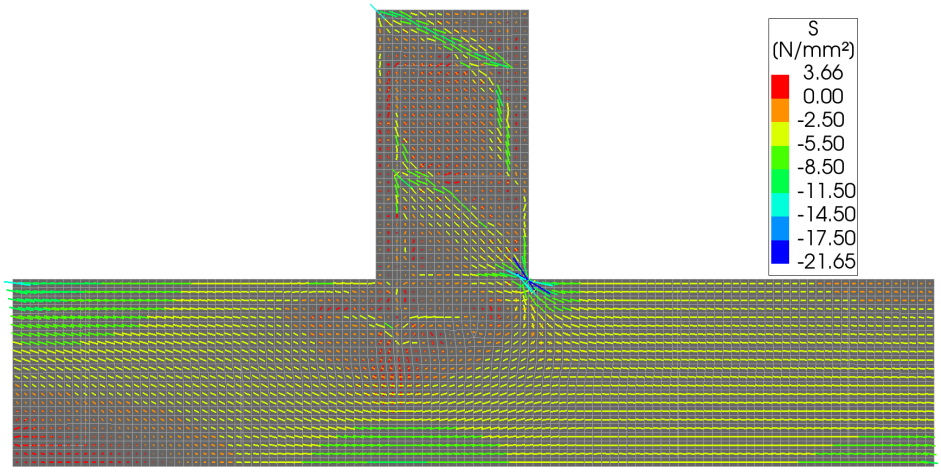

Figure 5.33: The in-plane principal stress components, for load case 3. Load factor=0.631.

Figure 5.34a shows the development of cracks in the D-region. The figure shows substantial cracking in the top wall, with both diagonal cracks and cracking along the major length of the longitudinal reinforcement. Also, the cross section is cracked along the top edge where loads are applied. This is also observed along the left edge, but not as extensive.

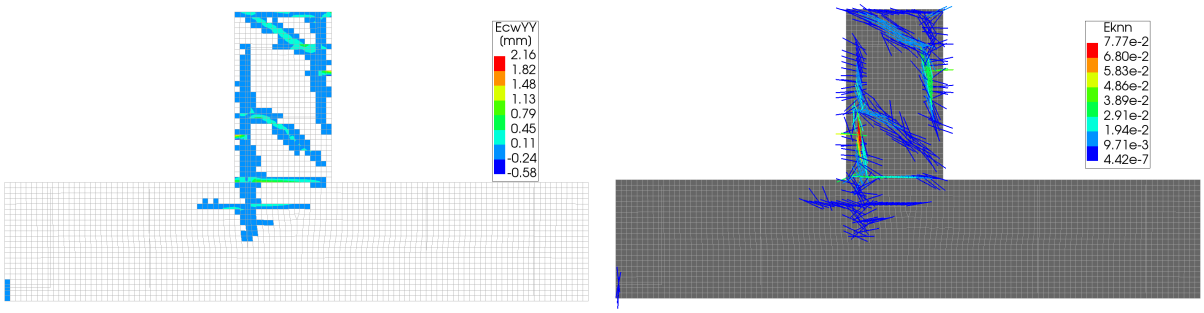

(a) Vertical crack widths **(b)** Crack strains

Figure 5.34: Cracking for load case 3 at load factor=0.631.

IDEA StatiCa

Figure 5.35a and Figure 5.35b show the stresses obtained in the concrete and reinforcement, respectively. A check of the compressive strains show a maximum value of $\varepsilon_2 = -9.5 \cdot 10^{-4}$ is reached, which is less than the ultimate compression strain ε_{cu2} defined by Eurocode 2 [4]. The ultimate load factor obtained is 1.08. It is observed that the reinforcement replicating truss 26 is the source of failure.

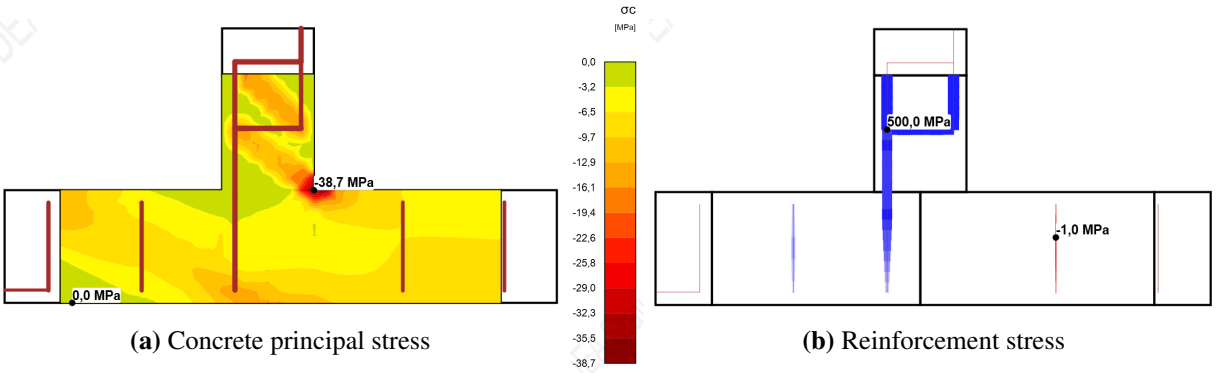

(a) Concrete principal stress

(b) Reinforcement stress

Figure 5.35: Concrete and reinforcement stresses obtained for load case 3 at load factor=1.00.

Table 5.12: Reinforcement amounts for load case 3 in IDEA StatiCa.

	Reinforcement amount $[\frac{\text{mm}^2}{\text{m}}]$	Fraction of calculated reinforcement in STM
Truss 1	1732	0.969
Truss 5	1732	0.969
Truss 9	3186	1.00
Truss 17	509	1.01
Truss 21	509	1.01
Truss 22	3186	0.990
Truss 25	1718	0.990
Truss 26	1473	1.01
Truss 28	1521	1.00
Truss 29	1718	0.990
F2	884	0.992
F5	3186	0.976

Figure 5.36 shows the reduction factors k_{c2} for the concrete compressive strength. The most significant reductions are observed in the top wall, where the concrete compressive strength is at most reduced by 65.6% $(1 - 0.8 \cdot 0.43)$.

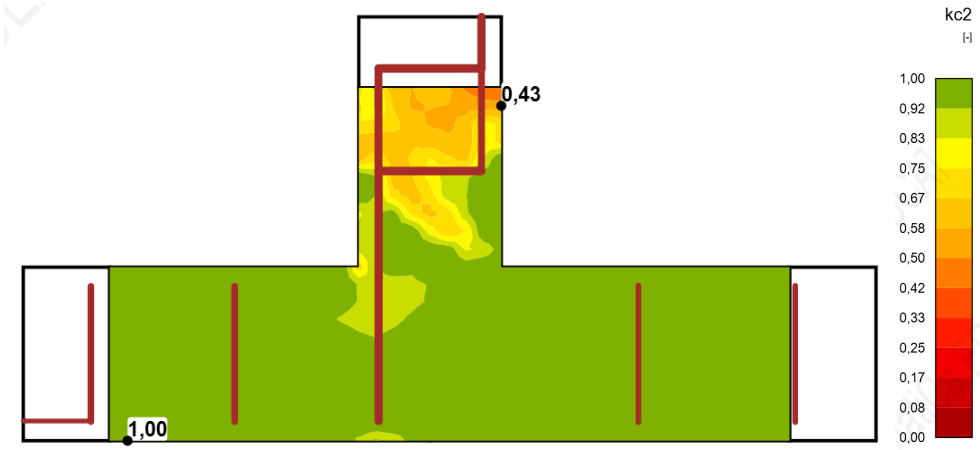

Figure 5.36: Reduction factor k_{c2} for load case 3 at load factor=1.00.

5.3.3 Comparison

The highest capacity was obtained in IDEA StatiCa with a load factor 1.08. In contrast, the analysis run in DIANA resulted in a load factor $0.631 << 1.00$. Thus, the two analyses give a capacity on each side of the capacity obtained with the STM. A comparison of the two analyses show a substantially higher utilization of both concrete strength and reinforcement in the IDEA StatiCa analysis (at load factor 1.00). The analysis in IDEA Statica also showed the largest compressive strain ($\varepsilon_2 = -9.50 \cdot 10^{-4}$ vs. $\varepsilon_2 = -6.03 \cdot 10^{-4}$). Both these strains are located in the corner between the top wall and the right hands side wall.

The reduction factors obtained from the STM and NLFEA are shown in Table 5.10 and Figure 5.36, respectively. In the top wall, a larger reduction is observed in the NLFEA. For instance, the largest reduction in the NLFEA is located around node 15 of the STM, where the stress is reduced by a factor of 0.60.

Chapter 6

Discussion

6.1 Discussion of Results

6.1.1 Numerical Model

As the analyses in DIANA have been allowed to continue if convergence is not satisfied after 100 iterations, the convergence history should be assessed. This is necessary as a poorly satisfied convergence criterion might lead to an inaccurate solution. When studying the three presented load-displacement curves with capacity ≥ 1.00 obtained from the DIANA analyses, it is observed that apart from load case 2 with Hordijk softening, converged steps are reached at load factors > 1.00. In the analysis of load case 2 with Hordijk softening, the last converged step is one step before load factor 1.00 is reached and two before the ultimate load. At both these steps, the energy criterion is closest to convergence with relative energy variations of $1.894 \cdot 10^{-3}$ and $1.506 \cdot 10^{-3}$. The analyses were run with a combined criterion of force and energy, where the analyses consider the steps as converged if both are satisfied. However, in the post-processing, any step where at least one criterion was satisfied has been considered converged. This is done as it was observed several times that the energy criterion was satisfied at an iteration where the force criterion still was significantly far from being converged. According to Cook [13], the force criterion may in some cases be difficult to satisfy because of local force imbalances not affecting the structural response significantly. By running the analyses past a satisfied energy criterion, a reduction of the imbalance in forces may be achieved.

When studying the load-displacement curves of the executed analyses, it is evident that the use of an arc-length method is necessary. In all four load-displacement curves presented, the D-region experiences snap-throughs. After the snap-throughs highlighted (by the limit points) in each load-displacement curve, the tangent stiffness of the response changes. This effect is most visible for load case 2 with Hordijk tensile softening, shown in Figure 5.13. The snap-through is followed by a significant drop in the tangent stiffness, where the post-peak tangent stiffness is found to be $K_{T,post} \approx \frac{K_{T,pre}}{18}$. Crack development and a redistribution of stresses are also observed between the two limit points.

An important part of the analyses is the application of the loads to the edges of the D-region. In the analyses executed in DIANA, the axial force was applied as a distributed force, while the shear force and moment were applied as concentrated loads in the middle nodes. When using

concentrated loads for application of loads, one may experience notable stresses concentrated around the loaded node. This may result in numerical failure before the analysis reaches the ultimate load [7]. When studying the principal stress plots from the three load cases, no such concentrations of stresses are observed at the loaded nodes. Thus, this should not be the reason for the early failure of the DIANA analysis of load case 3.

Another key aspect of the load application is the response of the edges where the loads are applied. While IDEA StatiCa has a built-in possibility of adding sectional forces to the D-region by the use of a St.Venant transfer zone, this had to be done manually in DIANA by enforcing the edges to remain straight. The normalized deformation plots of the load cases suggest that the bending stiffness is sufficiently high in order to fulfill this constraint. In addition, a relatively small axial stiffness is desired in order to not excessively constrain the transverse displacement along the edges. The normalized displacement for load case 3 in Figure 5.30 may indicate that the top edge is to certain degree constrained transversely.

A point of interest concerning the load application is the observed cracking along the edges. This is present in both load cases 2 and 3 at the ultimate load factor, although most significant in the latter load case. In addition, this is also observed at the highlighted limit points for load case 3 (Figure 5.34), where the load factor is around 0.5. This cracking along the edges at the observed load factors may influence the response of the D-region and possibly be coupled to the early failure.

6.1.2 Concrete Material Model

The compressive behavior of the concrete is a crucial aspect of the material model. The two different compression curves tested in this report are shown in Figure 6.1 along with the difference in stress in the domain $\varepsilon \in [0, -0.00891]$. This domain is based on the observed compression strains in the IDEA StatiCa analysis of load case 1, as it experienced the largest compressive strains. The parabola-rectangular compression curve from Eurocode 2 [4], which is implemented in IDEA StatiCa, shows a slightly steeper curve towards its compressive strength $\eta_{f_c} \cdot f_c = -46.4 \frac{\mathrm{N}}{\mathrm{mm}^2}$. Where the parabola-rectangular curve reaches its maximum compressive strength at a strain of $\eta_{f_c} \cdot \varepsilon_{c2} = -0.0016$, the extrema of the parabolic curve is located at a strain of $\alpha_c = -0.0026$. At most, the difference between the two curves in favor of the parabola-rectangular curve is $\Delta f_c = -6.0 \frac{\mathrm{N}}{\mathrm{mm}}$. Isolated, this difference in concrete strength may allow for a stiffer response. However, the comparison of the two compression curves shows that after a strain of $\varepsilon = -0.0014$, the parabolic curve results in a larger compressive strength. Thus, which of the two compression curves that gives the stiffest response, depends on what magnitude of compressive strains is present in the concrete.

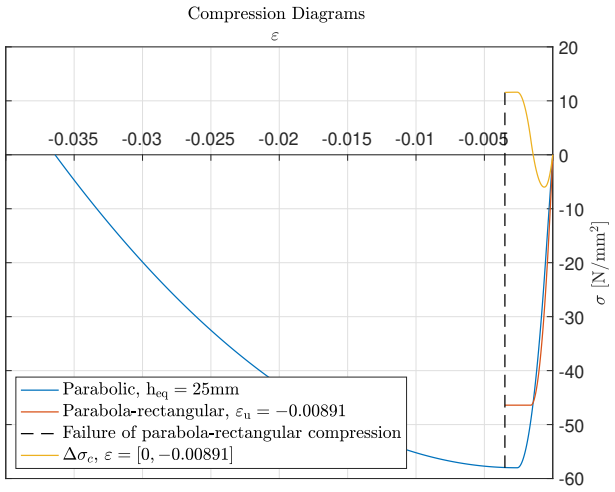

Figure 6.1: Parabolic and parabola-rectangular compression diagrams. Both calculated for concrete class C50/60.

The three NLFEAs of load case 2 show three different values of the largest compressive strains obtained. Where the DIANA analyses with Hordijk and linear tension softening obtained compressive strains of $\varepsilon_2 = -9.4 \cdot 10^{-4}$ and $\varepsilon_2 = -8.8 \cdot 10^{-4}$, respectively, the analysis in IDEA StatiCa only reached a compressive strain of $\varepsilon_2 = -5.5 \cdot 10^{-4}$. These strains are found in the domain where the compressive strength of the parabolic-rectangular curve is larger than what is obtained with the parabolic curve. Of the three compressive strains assessed, the one obtained from IDEA StatiCa is located at the largest difference between the two curves. For this strain, the parabolic-rectangular curve results in a stress which is $\Delta f_c = -5.9 \frac{\text{N}}{\text{mm}^2}$ larger. This may be one of the reasons for smaller compression strains obtained in the IDEA StatiCa analysis. However, because of the differences in compressive strains observed in the two DIANA analyses, the difference in the two compression curves can not be the only reason for the differences in the observed compressive strains.

Another, more obvious difference between the two compressive curves is the softening branch. While the parabolic curve assumes a softening of the compressive behavior after the compressive strength, f_{cm}, is reached, no softening is included in the parabola-rectangular curve. This is taken into account in IDEA StatiCa by reducing the compressive strength, which for concrete class C50/60 is done with a reduction factor of $\eta_{f_c} = 0.80$. Thus, as observed in Figure 6.1, the softening branch of the parabolic curve produces stresses above the parabola-rectangular curve for the compressive strains observed in all three load cases.

The NLFEAs of load case 1 are the only two analyses which shows compressive strains beyond what is needed for the maximum compressive strength. As already stated, failure was reached before maximum compressive strength in the two other load cases. In the analysis of load case 1 in IDEA StatiCa, failure was observed to be caused by concrete failure in the corner

between the top and left wall where a compressive strain of $\varepsilon_2 = -0.00891$ was observed. In the DIANA analysis of the same load case, a compressive strain of $\varepsilon_2 = -3.93 \cdot 10^{-3}$ was obtained in the same area of the D-region. This peak compressive strain was obtained after the ultimate load factor was reached. With these results, the analysis run in IDEA StatiCa reaches a higher load factor despite the fact that it uses a compression curve with a lower compressive stress for large parts of the observed compressive strain domain.

When attempting to model the concrete behavior, it is critical to assess the interaction between tension and compression. As compressive capacity of concrete is reduced when it experiences lateral cracking, it is important to include this effect in a numerical model. The analyses run in IDEA StatiCa show significant reductions in compressive strength for parts of the D-region in all three load cases. For instance, the analysis of load case 3 results in a minimum reduction factor of $k_{c2} = 0.43$. Although this reduction is not observed at a location with considerable compressive stresses, significant reductions are also observed in the middle of the top wall where the shear forces produce compressive stresses of notable size. Load case 1, which was the only analysis (from IDEA StatiCa) where concrete failure was observed, shows no reduction in concrete strength due to transverse tension at the location of failure.

The two DIANA analyses of load case 2 show the importance of the modeling of the tensile behavior. By using a linear tensile softening curve with an ultimate strain of $\varepsilon_u = 0.0025$, a load factor of 1.15 is obtained compared to 1.00 with Hordijk softening. Furthermore, the effects of the tensile behavior are also observed in the utilization of reinforcement and the crack patterns. While yielding is reached with Hordijk softening, a reinforcement utilization above 80% is barely observed with the linear tensile softening at load factor 1.00. In contrast, a notable amount of the reinforcement is utilized above 80% with the Hordijk softening. In line with the differences in reinforcement utilization, a significantly more developed crack pattern is observed when using Hordijk softening (comparing at load factor 1.00). The two different approaches for the tensile softening are compared in Figure 6.2. For the Hordijk softening curve in the figure, an equivalent length of $25\mathrm{mm}$ is used.

While the linear tensile softening is defined such that it reaches fully open cracks (no concrete tensile contribution) at the yielding of the reinforcement ($\varepsilon_u = 0.0025$), the Hordijk softening shows a contribution to about double this strain ($\varepsilon_u = 0.00546$). However, when considering the area under the curves, the linear softening ($0.0049\frac{\mathrm{N}}{\mathrm{mm}^2}$) shows a larger contribution to the tensile strength than the Hordijk softening ($0.0042\frac{\mathrm{N}}{\mathrm{mm}^2}$). As a smeared crack model has been used, the area under a mesh dependent softening branch changes with the crack band width. With only the Hordijk softening being mesh dependent, the difference between the two softening branches will vary along with the crack band width.

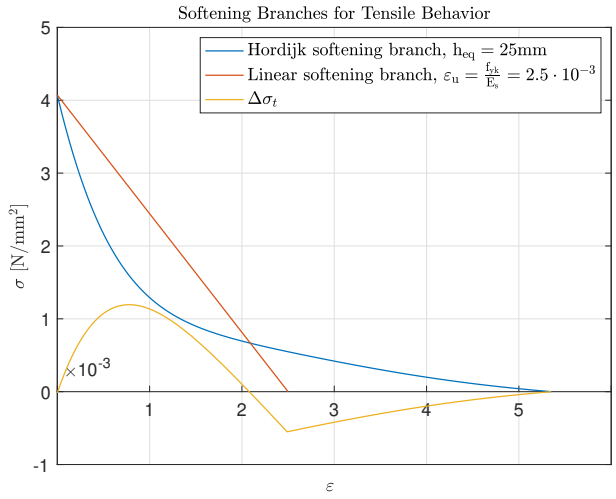

Figure 6.2: Hordijk and linear ultimate crack strain tensile softening.

Another difference between the two tensile softening curves is the initial curvature of the softening curves. With an equivalent length of $h_{eq} = 25\text{mm}$, the Hordijk softening shows an initial slope which is ≈ 3.3 times as steep as the linear softening. According to Dutch guidelines [7], exponential-type softening curves are a preferred choice as they will give more localized cracks [7]. An indication of this may be seen when comparing the model with Hordijk softening in Figure 5.18a to the model with linear softening in Figure 5.24a.

When comparing the maximum strain plots for the two DIANA analyses of load case 2, it is observed that large parts of the D-region experiences maximum principal strains in the linear-elastic area of the tension curve for both of the analyses. That being said, the model using Hordijk softening experiences significantly more tension softening compared to the model using linear tensile softening. This difference is especially located along the longitudinal reinforcement at the right side of the top wall and is consistent with the difference observed in the crack width plots. The linear softening also results in less softening than the Hordijk softening at the bottom middle of the D-region, although this difference is not as significant. These strains are located in the area where both analyses show the largest compression forces. The positive maximum principal strains may result in a strength reduction when using the tension-compression relationship by Vecchio and Collins (1993) [18]. Equation 2.12 and Equation 2.13 show that a reduction of the compressive strength is obtained when $\frac{\alpha_{lat}}{\varepsilon_0} > 0.37$. As the maximum principal strains observed in the area of maximum compression is below $\varepsilon_1 = 10^{-3}$, no reduction in compressive strength appears at the locations of the largest compressive strains.

A difference in reinforcement utilization is observed for load case 2 when comparing the two analyses from DIANA with the analysis from IDEA StatiCa. The latter analysis shows a much higher utilization of the reinforcement. This can be expected as in this analysis, concrete tensile strength is neglected apart from its stiffening effect on the reinforcement [9]. The higher ultiliza-

tion of reinforcement in the analysis from IDEA StatiCa suggests that the tension stiffening in this analysis contributes less than the tension curves used in DIANA. With less contribution from the concrete, the reinforcement has to carry more of the load.

An important aspect of the material model is the determination of the crack band width. In all Diana-analyses, an automatic determination of the crack band width has been used by applying Govindjees projection method [21]. As quadratic elements ($25 \times 25\text{mm}$) has been used, an estimation of the crack band width of a cracked element may vary between the length of the sides, h, and the length of the diagonal, $\sqrt{2} \cdot h$. For both the tensile and compressive behavior, mesh dependent softening branches have been used in the base models for the DIANA analyses. In other words, the curves depend on the crack band width as a smeared crack model has been applied. Figure 6.3a shows the Hordijk softening curves for the tensile behavior for the two values of the crack band width. The effect of the crack band width on the compressive behavior, using a parabolic compression curve, is shown in Figure 6.3b.

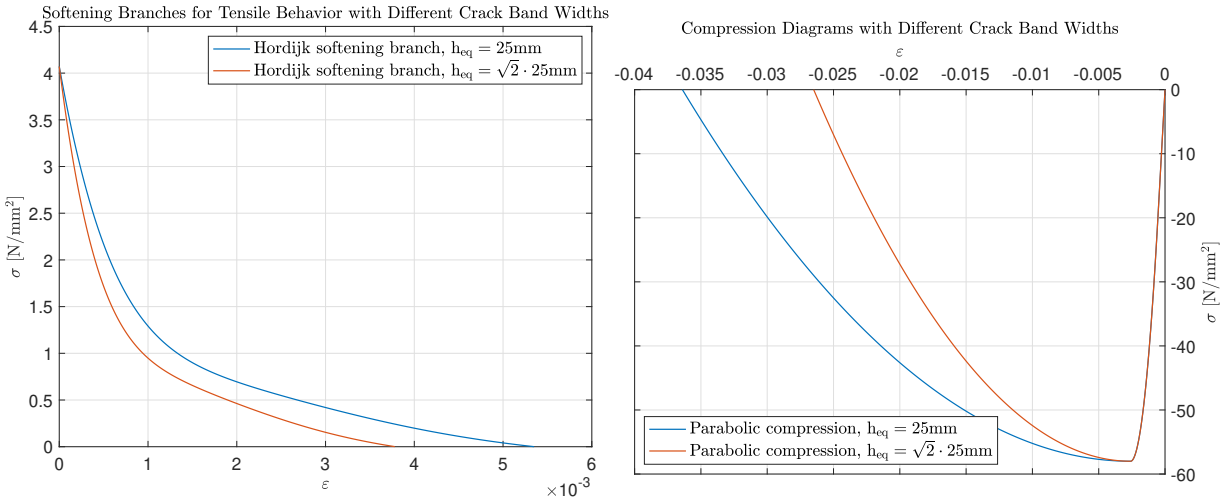

(a) Tensile behavior

(b) Compressive behavior

Figure 6.3: Effect of crack band width on softening branches

As the area under the softening branches are defined as G/h_{eq}, a crack band width of $h_{eq} = 25\text{mm}$ will result in an area which is $(\sqrt{2}-1) \cdot 100\% = 41\%$ larger. This underlines the importance of an accurate calculation of the crack band width. If automatic evaluation of the crack band width is not possible, a conservative approach would be to use $h_{eq} = \sqrt{2} \cdot h$ [7]. However, if the goal is to obtain a mean estimate of the concrete capacity, an automatic evaluation is preferred as crack directions will vary throughout the D-region. The variation of crack directions is evident in for instance Figure 5.34b.

Comparing the linear tensile softening used in load case 2 with the two Hordijk softening branches in Figure 6.3a, shows that the difference between the two types of softening increases

with the crack band width. This may be one of the reasons for the different crack patterns resulting from the two tension softening branches. Cracks are observed to form more diagonally in the model using Hordijk softening, producing a larger value of the crack band width.

The choice between using a rotating or fixed total strain crack model may influence the response of the numerical model. As stated in subsection 2.2.1, a fixed crack model may overestimate the capacity if significant rotation of stresses from their initial directions is present in the model. Such rotations of stresses are observed in the model from load case 2. The vertical crack strain tensors along the longitudinal reinforcement in Figure 5.18b are observed to appear as horizontal at earlier load increments, which means that they experience significant rotation. Thus, if a fixed crack model had been applied instead of the rotating model, this area may have experienced stress locking resulting in an overestimation of the capacity.

6.1.3 Strut-and-Tie Models

A crucial aspect of Strut-and-tie modeling is the maximum allowable stress, $\sigma_{Rd,max}$, in the compression fields represented by the struts. As already stated, the compressive behavior of concrete is reduced when lateral cracking is present. The presence of lateral cracking may vary along the length of a strut, which means that in order to remain conservative, a sufficient reduction has to be made for the entire strut. For instance, if a compression field is formed as "the bottle"-type mentioned in subsection 3.5.1, transverse reinforcement across the compression field should be unnecessary when using Equation 3.2 for $\sigma_{Rd,max}$. The capacity control of the nodes according to Eurocode 2 clause 6.5.4(4) also takes the presence of tensile stresses into account. Here, the reductions are determined by the number of ties anchored in the considered node.

In order to find an explanation of the early failure of the DIANA analysis of load case 3, the possibility of insufficient reductions of the compressive stresses has to be taken into account. When looking at the compression fields in Figure 5.28 loaded with the maximum allowable stresses, it is seen that several of these have very little space left in the case of an insufficient strength reduction. However, when comparing the maximum allowable stresses in the nodes (Table 5.10) to the in-plane principal stress components from the NLFEA, it is seen that $\sigma_{Rd,max}$ in the STM is far from being exceeded at the ultimate load factor. In addition, no compression fields depicting the "bottle"-field are observed.

It is also interesting to study this area of the D-region for load case 3 in the plot of the maximum principal strain in Figure 5.32. The compressive strength reduction applied in the DIANA analysis (Vecchio and Collins, 1993 [18]) uses the relationship between the lateral tensile strain

α_{lat} and the peak compressive strain ε_0 in order to calculate the necessary strength reduction. Comparing the maximum principal strain plot with the compression fields of the STM in Figure 5.28 shows that principal strains > 0 in the elastic area are present along most of the struts in the bottom wall. However, the most critical struts, in terms of utilization of the available space, are observed to be located in the most stressed areas of Figure 5.33, resulting in small or none reductions. As the strength in all compression fields of the STM are at least reduced with $\nu = 0.8$ (for brittle behavior), the NLFEA should not suffer from insufficient strength reductions in these areas.

When studying the compressive stresses in the NLFEAs of load case 1 with the struts in the corresponding STM, it is observed that the largest compressive stresses obtained are very close to what the STM allows in this area. The DIANA and IDEA StatiCa analyses show stresses of $-45.8\frac{\mathrm{N}}{\mathrm{mm}}$ and $-46.3\frac{\mathrm{N}}{\mathrm{mm}}$, respectively, which is just below what is used as $\sigma_{Rd,max}$ in node 5 in the STM ($\sigma_{Rd,max} = 46.4\frac{\mathrm{N}}{\mathrm{mm}}$). These small differences are interesting as the two struts (truss 8 & 22) which are placed in this area have enough space to produce compressive stresses lower than what is observed. Although truss 8 only have enough space to produce a stress equal to the $\sigma_{Rd,max}$ found in node 4 ($\sigma_{Rd,max} = -39.44\frac{\mathrm{N}}{\mathrm{mm}}$), truss 22 should be able to produce stresses far below what is observed. A possible explanation for this may be that the forces have found another load path than what is proposed by the STM. If so, an STM representing this load path would have produced a lower strain energy in Equation 3.1. As the lengths of the trusses are included in the strain energy equation, an STM assuming a short load path through the D-region is preferred. This is in line with Schlaich et al. [12] who states that the forces will typically find the shortest way through the D-region. This is also one of the principles of the load path method. When comparing the STM in Figure 5.1 with the stress flow in Figure 5.7, resemblance is found to a certain extent. This suggests that the STMs in general represent the load paths obtained in the NLFEAs although more optimal models most likely exist.

In the NLFEAs from load case 2, the area most exposed to compressive stresses is found to be on the bottom middle of the D-region. When comparing with the STM, it is found that the strut in this area (nr. 10) has a maximum allowable stress of $\sigma_{Rd,max} = -39.44$ and virtually no available space left beyond what is already covered by the compression field. The large compressive stresses obtained in this area of the NLFEAs are in line with what is predicted of the STM. However, as seen throughout the D-region, the NLFEAs produce compressive stresses which are below the maximum allowed stresses used in the STMs.

As stated in section 3.3, the expected deformation of the struts has to be limited in order for the STM to be dimensioned according to the lower bound theorem of plasticity. As already stated, the principal stress plots from the NLFEAs show stress flows resembling the directions of the compression fields in the STMs to a certain degree. This suggests that unrealistic STMs

and therefore also too high deformation capacities have not been assumed in the STMs.

6.2 Estimation of Actual Capacity

When comparing the two modeling approaches' ability to estimate the actual capacity of a D-region, it is important to look at their respective reductions in concrete strength due to transverse tension. As stated by Schlaich et al. [12], the compressive strength depends significantly on the stress state and the degree of disturbances from reinforcement and cracks. In the analyses from IDEA StatiCa, the reduction factors for the compression softening are given as output. Comparing these to the ones used in the nodes of the STMs shows that neither of the two consistently produces more conservative reductions than the other. In the analyses of load case 1, it is observed that IDEA StatiCa reduces the compressive strength less than in the STM. For instance, in node 7 of the STM, the compressive strength is reduced by the factor $0.75\nu'$ as it consists of two ties. Looking at the same area in the NLFEA, a reduction factor $\geq 0.83\eta_{f_c}$ is observed ($\nu' = \eta_{f_c} = 0.80$ for C50/60). Meanwhile, the largest reduction observed in the NLFEA is found to be $0.59\eta_{f_c}$, which is lower than what is recommended for any of the nodes when dimensioning according to Eurocode 2.

Whereas the NLFEAs can use compressive strength reduction models based on the degree of transverse tensile stresses, the nodal check in Eurocode 2 6.5.4(4) uses the number of anchored ties in the nodes in order to determine the strength reduction. With the latter approach, the same reduction in stress will be used in two nodes with the same number of anchored ties, regardless of any difference in tension forces in the ties. For instance, the nodes containing the shear ties in the bottom wall of the STM from load case 1 are applied the same compressive strength reductions even though the acting shear forces the left hand side is much larger than what is applied on the right hand side. In terms of the ability to model a realistic reduction in stress, the approach used in the NLFEAs is more favorable. This is because it takes into account the magnitude the compressive and/or tensile strains in the concrete, whereas the reductions for the nodes in the STMs are determined solely on the number of ties. That being said, the latter approach is much more practical to apply in the used Matlab code. This also applies when comparing the reductions proposed by Eurocode 2 to the reductions presented by Schlaich et al [12] in Table 3.1. Using reductions only based on the number of ties is much easier implemented in an automated process, such as in the Matlab code, compared to reductions based on the degree of cracking in the concrete.

When looking at the maximum capacities obtained in the NLFEAs, it is seen that five out of the seven analyses showed a larger capacity, one reached a load factor of 1.00 while the last only reached 0.631. Thus, the STMs produce capacities which in general are on the conservative side compared to the FEM-analyses. Regarding the one NLFEA showing insufficient capacity,

several possible sources for the early failure have been discussed. The problems do not stem from the concrete or reinforcement strength as neither concrete crushing nor reinforcement rupture is observed at the ultimate load factor. Some cracking is observed at the top edge where loads are applied which may affect the response of the analysis. However, the early failure is be blamed on the arc-length procedure inducing a premature unloading. This argument is substantiated by the notable difference between the two NLFEAs of the considered load case. Here, a difference of 0.449 is observed between the load factors of the two analyses. In comparison, the differences between the NLFEAs of the two other load cases are 0.08 and 0.02.

The STMs in this thesis have been chosen with regards to a minimum strain energy criterion (Equation 3.1) from a pool of up to eight STMs (several discarded because of lack of equilibrium or need for inclined reinforcement). While the tension forces are more constrained to follow the reinforcement, the compression forces are more free to choose other load paths. As already stated, loads will typically find the shortest way through the structure. As a limited set of trusses has been considered for the STMs, the most optimal STM for the D-region has most likely not been taken into account. Looking at the obtained stress fields in the NLFEAs reveals a resemblance to the compression fields obtained in the STMs. This suggests that the STMs considered are able to predict the stress flow to a certain degree. Out of the three load cases, the most resemblance is observed in load case 2. This is also the load case which displays the smallest difference in ultimate capacity between the STM and the NLFEAs (ignoring the analysis with linear tension softening).

An aspect of the concrete behavior not assessed in the FEM-analyses is the compression-compression interaction. If accurate, rather than conservative, results is the goal of the NLFEA, this is important to include in the material model [7]. With a compression-compression interaction, the strength of the concrete will increase. The plots of the maximum principal strain, ε_1, for the three load cases show some areas with compression-compression interaction, although most of the D-regions experience $\varepsilon_1 > 0$. Load case 1, where failure was caused by insufficient concrete strength, experiences compression-compression interaction in the area most exposed to compressive stress. Thus, including confinement effects here may result in a higher capacity. This applies to load case 3 as well, as also here compression-compression interaction is observed in the area most exposed to compressive stresses.

The compression-compression interaction can also be taken into account in the strut-and-tie models. Clause 6.5.2(1) of Eurocode 2 [4] states that compression fields with transverse compression or without transverse tension can be allowed a stress of $\sigma_{Rd,max} = f_{cd}$. Further, 6.5.4(4) allows for an increase of up to 10% of the dimensioning compression strength if one or more of the stated criteria are fulfilled. One of these criteria is a triaxial compressive stress state. In the case of a three dimensional stress state, which has not been covered in this thesis, this is an

aspect which should be considered in order to increase the accuracy of the solution. However, ignoring the allowable strength increase is a conservative approach.

When aiming for mean estimates of the capacity of reinforced concrete, it is also important to model the steel behavior accurately. In the NLFEAs, the material behavior of the reinforcement steel has been modeled using an elastic ideal plastic material model. In reality, this is a conservative approach as steel will experience work-hardening after reaching the yield stress. An approach to model the work-hardening is to use a bi-linear diagram [7]. This is also provided in Eurocode 2, clause 3.2.7(2) [4].

Although the reinforcement contributes significantly more to the tensile strength of the reinforced concrete, it is observed in the NLFEAs that the modeling of tensile behavior of the concrete is important as well. For instance, the two DIANA analyses of load case 2 show a notable difference ($\Delta = 0.15$) in ultimate load factor when changing the tensile softening behavior. The importance of the tensile behavior of concrete can also be observed when comparing these two analyses with the one from IDEA StatiCa. In the latter, a much higher utilization of the reinforcement is observed, suggesting that the tension stiffening effect from the concrete in this analysis contributes less.

It is also relevant to assess the accuracy and the modeling choices of the Matlab codes in terms of the STMs. As already stated, the limited number of possible STMs results in the final STM most likely overestimating the necessary reinforcement. Another point which limits the load path of the STM is the restriction from rotation of some of the struts. If all were allowed to rotate freely through the iteration process, more optimal models may have been found. However, this requires a more complicated Matlab code in terms of calculations and restricting STMs exceeding the deformation limit of the struts. Also, this would result in a longer computational time for the code as larger differences in the force distribution would be expected between the geometric optimizations as more nodes are moved. Even though this difference in time would most likely be negligible for the three load cases, where the used time is 0.1-0.2 seconds, the effect could be significant for a large number of load cases.

Chapter 7

Conclusion

In this thesis, strut-and-tie modeling and NLFEA have been compared. Three load cases have been tested for both methods. The strut-and-tie models have been made and calculated in an attached Matlab code, while the NLFEA has been executed by the use of two softwares, namely DIANA and IDEA StatiCa.

The Matlab code generated STMs which utilized the height of the cross sections such that the moment arm between the trusses were maximized with respect to the limitations of the code. The total time used of the Matlab code for all three load cases was 0.1-0.2 seconds in total.

The three calculated STMs have been tested in both DIANA and IDEA StatiCa, with four analyses in the former software and three in the latter. The reason for the extra analysis in DIANA was the desire of testing additional tension softening curve to see the effect of the tension softening. Of these seven analyses, five reached a capacity larger than the STMs, one reached a capacity equal to its STM and the final only got to a load factor of 0.631. In the first load case, the load factors obtained were 1.18 for the DIANA analysis and 1.26 for the analysis from IDEA StatiCa. In both, failure was caused by lack of concrete strength. Reduction in compressive strength due to transverse tension in the location of failure showed to be equal to what was used in the STM. In addition, both NLFEAs gave compressive stresses about equal to the STM in this area. The largest reinforcement utilization was predicted in the same ties of the STM for both analyses, but the reinforcement in multiple ties still have a notable capacity left at load factor 1.00.

The second load case was tested with two different tension softening models in DIANA in addition to the IDEA StatiCa analysis. Out of the two DIANA analyses, the largest capacity was obtained with linear tension softening defined by ultimate strain. A load factor of 1.15 was reached with this tension softening. The analysis using Hordijk softening reached a load factor of 1.00. The two softening models produced different crack patterns and the latter analysis showed significantly more cracking along the longitudinal reinforcement when comparing the results at load factor=1.00. Both analyses experienced failure by the sudden propagation of a crack transverse to the length of the top wall. A load factor of 1.02 was obtained in the analysis from IDEA StatiCa. Failure was here observed to be caused by a lack of capacity in the longitudinal reinforcement in the top wall. The analysis from IDEA StatiCa showed a reinforcement utilization significantly larger than what was observed in the DIANA analyses.

The DIANA analysis of the third load case was the only FEM-analysis which did not reach a sufficient capacity with the reinforcement layout from the STM. A load factor of 0.631 was obtained. Unexpected cracks were observed along the entire top edge of the D-region where loads are applied. The NLFEA from IDEA StatiCa reached failure at load factor 1.08, where reinforcement rupture was reached. In the DIANA analysis, neither reinforcement rupture nor concrete crushing was observed. It was argued that the early failure of the analysis is caused by the arc-length procedure resulting in a premature unloading. This statement has been supported by the large difference in ultimate load factor between the two NLFEAs of the load case.

The importance of stress reductions due to transverse tensile strains has been discussed. A comparison of the STMs and the analyses from IDEA StatiCa shows that neither produces reductions which consistently are more conservative than the other. However, nodes with significant compressive forces in the STM show larger reductions in compressive strength than what was obtained in the analyses from IDEA StatiCa.

The results suggest that strut-and-tie modeling produces results on the conservative side of NLFEA. In terms of the NLFEA being able to produce mean estimates, the need for a correctly modeled concrete behavior has been emphasized. Accurate material models of the concrete and reinforcement combined with a good numerical model is necessary. With this in place, it is suggested that the NLFEA will produce the most accurate results. However, for a large number of load cases, running an NLFEA on all load cases might prove to be cumbersome. As the Matlab code produces models which are relatively close to the NLFEAs, the code could for instance be used in a preliminary analysis where governing load cases for the D-region are found.

Chapter 8

Further Work

Extend the code to include external loads

External loads are important to consider when present in the D-region. This could be solved by load lumping into the nodes. It is important that the resultant of any distributed load is unchanged when lumping the forces into the nodes.

Compare the two modeling approaches to more load cases

The strut-and-tie models produced by the Matlab code are shown to in general be on the conservative side of the nonlinear finite element analyses. Testing a large number of different load cases will of course give a better picture of the ability of the Matlab code, but the number of load cases had to be limited because of time.

Study the effect of including compression-compression interaction in the NLFEAs

As stated, a compression-compression interaction in the concrete would in reality result in a higher concrete strength in the affected area. Ignoring the effects is conservative, but in order to model the concrete behavior closest to reality, this should be considered. A study of these effects could be performed with a load case exposing the top wall to a dominating compression force.

Bibliography

[1] MathWorks. Matlab. URL https://se.mathworks.com/products/matlab.

[2] Apache Software Foundation. Diana fea. URL https://www.dianafea.com/.

[3] IDEA StatiCa. Idea statica detail. URL https://www.ideastatica.com/concrete/.

[4] Standard Norge. *NS-EN 1992-1-1:2004+NA:2008 Eurocode 2: Design of Concrete Structures - Part 1-1 : General Rules and Rules for Buildings*, 2008.

[5] Fédération internationale du béton. *fib Model Code 2010 for Concrete Structures*. Ernst & Sohn, 2013.

[6] Nerilli F., Rinaldi Z., Meda A., Cignitti F., and Sorge R. Numerical analysis of precast tunnel segmental lining supported by full-scale experimental tests. 05 2011.

[7] M.A.N. Hendriks and M.A. Roosen. *Guidelines for Nonlinear Finite Element Anlysis of Concrete Structures*. Rijkswaterstaat Centre for Infrastructure, Report RTD:1016-1:2019, 2019.

[8] Manie J. *DIANA User's Manual-10.0*, 2015.

[9] J. Mata-Falcón, D.T. Tran, W. Kaufmann, and J. Navrátil. Computer-aided stress field analysis of discontinuity concrete regions. 02 2018.

[10] Sørensen S.I. *Betongkonstruksjoner: Beregning og dimensjonering etter Eurocode 2*. Fagbokforlaget, second edition, 2013.

[11] Kaufmann W., Mata-Falcón J., Weber M., Galkovski T., Tran D.T., and Kabelac J. et.al. Idea statica detail 20 theoretical background. URL https://assets-us-01.kc-usercontent.com/1ca05609-4ad1-009e-bc40-2e1230b16a75/6abee761-8385-4454-8574-a29de5f94fa7/Theoretical%20Background%2020.pdf.

[12] J. Schlaich, K. Schäfer, and M. Jennewein. Toward a consistent design of structural concrete. *PCI Journal*, 32(3):74–146, 1987.

[13] Cook R.D., Malkus S.M., Plesha M.E., and Witt R.J. *Concepts and Applications of Finite Element Analysis*. Wiley, fourth edition, 2002.

[14] Mathisen K.M. Lecture notes. NTNU.

[15] J.G. Rots. Computer-aided stress field analysis of discontinuity concrete regions. 10 2002.

[16] Hordijk D.A. *Local Approach to Fatigue of Concrete*. PhD thesis, Delft University of Technology, 1991.

[17] Feenstra P.H. *Computational Aspects of Biaxial Stress in Plain and Reinforced Concrete*. PhD thesis, Delft University of Technology, 1993.

[18] Vecchio F.J. and Collins M.P. Compression response of cracked reinforced concrete. *Journal of Structural Engineering*, 119(12):3590–3610, 1993.

[19] Marti P., Alvarez M., Kaufmann W., and Sigrist V. Tension chord model for structural concrete. *Structural Engineering International*, 8:287–298, 11 1998. doi: 10.2749/101686698780488875.

[20] Fédération internationale du béton and K.H. Reineck. *Design Examples for Strut-and-tie Models: Technical Report*. Bulletin (fib Fédération internationale du béton). International Federation for Structural Concrete, 2011.

[21] Govindjee S., Kay G.J., and J.C. Simo. Anisotropic modelling and numerical simulation of brittle damage in concrete. *International Journal for Numerical Methods in Engineering*, 38:3611–3633, 1995.

[22] Nakamura H. and Higai T. Compressive fracture energy and fracture zone length of concrete. *Modeling of Inelastic Behavior of RC Structures Under Seismic Loads*, pages 471–487, 2001.

Appendices

Appendix A

Strut Width Calculations

In the following, the calculations behind the widths of the compression fields in the STMs are presented. The similarity of several nodes are utilized such that an individual calculation for every of the 16 nodes is not necessary. Instead, the calculation of each ”type” of node is presented followed by a table showing how to switch the parameters in order to obtain the equations for other nodes of the same type. The nodes presented with calculations are node 2, 4, 5, 12, and 16. In the figures, the nodal zones are marked with green lines, while the end of the compression fields of struts are drawn with blue lines. The trusses and the necessary widths are drawn with black lines. The numbering of the trusses are placed at the location where the trusses are exiting the nodal zones. For each truss, there may be more than one possible limit of the width of the compression field. Which of the limits that are used is decided by the necessary width of the neighboring compression fields. The notations for the widths are $w_{i,j}$, where subscript i is the truss number and subscript j distinguishes between the different possible limits of the maximum width.

Node 2

Figure A.1 shows the geometry of nodal zone 2 and the trusses within the node.

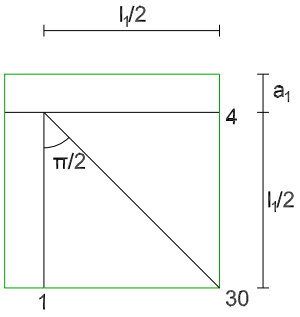

Figure A.1: Node 2.

Maximum allowed widths of struts

$$w_{F_1} = 2a_1 \tag{A.1}$$

$$w_{30,1} = \sin\frac{\pi}{4} \cdot \left(l_1 - \frac{w_1}{\tan\frac{\pi}{4}} \right) \tag{A.2}$$

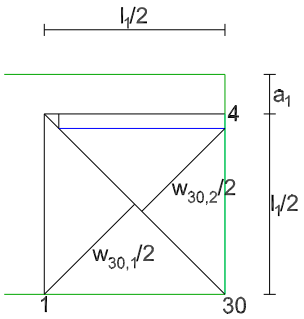

Figure A.2: Maximum width of truss 30

$$w_{30,2} = \sin\frac{\pi}{4} \cdot \left(l_1 - \frac{w_4}{\tan\frac{\pi}{4}} \right) \tag{A.3}$$

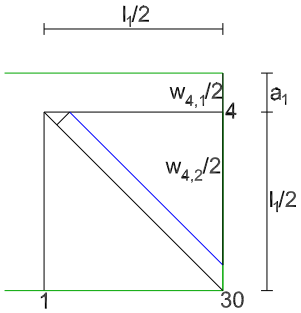

Figure A.3: Maximum width of truss 4

$$w_{4,1} = 2a_1 \tag{A.4}$$

$$w_{4,2} = \tan\frac{\pi}{4} \cdot \left(l_1 - \frac{w_{30}}{\sin\frac{\pi}{4}} \right) \tag{A.5}$$

Change to similar nodes

Node 2	Node 1	Node 10	Node 11	Node 14	Node 15
Truss 1	Truss 1	Truss 21	Truss 21	Truss 25	Truss 25
Truss 30	Truss 3	Truss 34	Truss 19	Truss 27	Truss 36
Truss 4	Truss 2	Truss 18	Truss 20	Truss 28	Truss 26
F_1	F_2	F_3	F_4	F_5	F_6
a_1	a_2	a_3	a_4	a_5	a_6

Node 4

The variables a_{ni} used in this node refers to the distance in z-direction from the surface to the node.

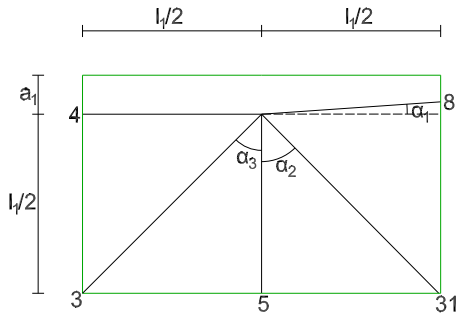

Figure A.4: Node 4.

Angles

$$\alpha_1 = \arccos \frac{l_1}{l_8} \tag{A.6}$$

$$\alpha_2 = \arctan \frac{l_1}{l_5 + a_{n16} - a_{n3}} \tag{A.7}$$

$$\alpha_3 = \arccos \frac{l_5}{l_3} = \frac{\pi}{4} \tag{A.8}$$

Maximum allowed widths of struts

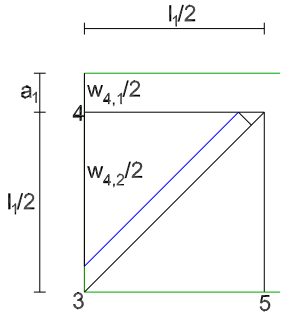

Figure A.5: Maximum width of truss 4

$$w_{4,1} = 2 \cdot a_1 \tag{A.9}$$

$$w_{4,2} = \sin\left(\frac{\pi}{2} - \alpha_3\right)\left(\frac{l_1}{\cos\left(\frac{\pi}{2} - \alpha_3\right)} - \frac{w_3}{\tan\left(\frac{\pi}{2} - \alpha_3\right)} - w_3 \cdot \tan\left(\frac{\pi}{2} - \alpha_3\right)\right) \tag{A.10}$$

$$w_{4,3} = l_5 \tag{A.11}$$

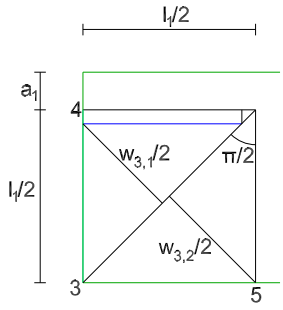

Figure A.6: Maximum width of truss 3

$$w_{3,1} = \sin\left(\frac{\pi}{2} - \alpha_3\right)\left(l_1 - \frac{w_4}{\tan\left(\frac{\pi}{2} - \alpha_3\right)}\right) \tag{A.12}$$

$$w_{3,2} = \sin\alpha_3\left(l_5 - \frac{w_5}{\tan\alpha_3}\right) \tag{A.13}$$

Figure A.7: Maximum width of truss 31

$$w_{31,1} = \sin\alpha_2 \cdot \left(l_5 - \frac{w_5}{\tan\alpha_2}\right) \tag{A.14}$$

$$\begin{aligned} w_{31,2} &= \sin\left(\frac{\pi}{2} - \alpha_2 + sign(a_{n4} - a_{n5}) \cdot \alpha_1\right) \\ \cdot \Bigg(\frac{l_1}{\cos\alpha_1} &- \frac{w_8}{\tan\left(\frac{\pi}{2} - \alpha_2 + sign(a_{n4} - a_{n5}) \cdot \alpha_1\right)} - sign(a_{n4} - a_{n5}) \\ &\cdot w_8 \cdot \tan\left(\frac{\pi}{2} - \alpha_2 + sign(a_{n4} - a_{n5}) \cdot \alpha_1\right) \Bigg) \end{aligned} \tag{A.15}$$

$$w_{8,1} = \frac{2a_1 - sign(a_{n4} - a_{n5}) \cdot l_1 \cdot \tan\alpha_1}{\cos\alpha_1} \tag{A.16}$$

The calculation of $w_{8,2}$ is explained in more detail in the following. The method of calculating this width is the same for struts in other nodes which also has the ability of rotating. The

maximum width $w_{8,2}$ has to take into account that truss 8 may rotate, and the method of finding this maximum width is dependent on the direction of rotation. This is shown in Figure A.8.

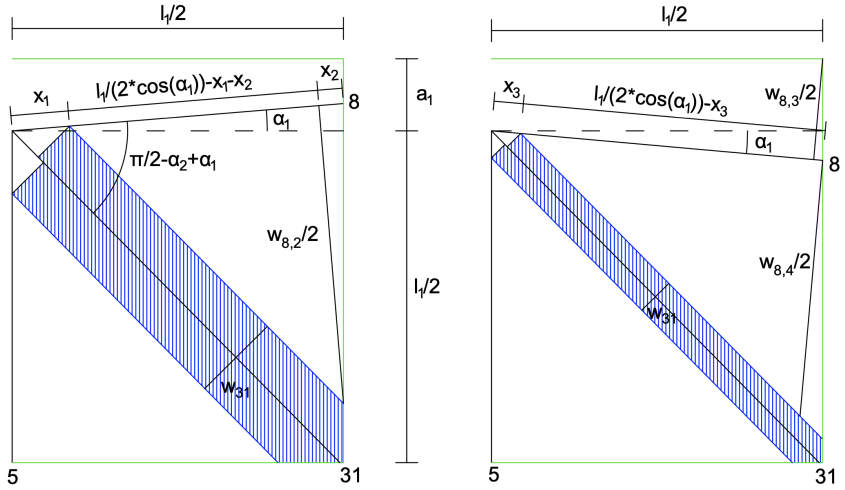

Figure A.8: Finding the maximum width.

The width $w_{8,4}$ in Figure A.8 can be written as:

$$w_{8,4} = \tan\left(\frac{\pi}{2} - \alpha_2 - \alpha_1\right) \cdot \left(\frac{l_1}{\cos\alpha_1} - \frac{w_{31}}{\sin\left(\frac{\pi}{2} - \alpha_2 - \alpha_1\right)}\right) \tag{A.17}$$

The width $w_{8,2}$ in Figure A.8 can be written as:

$$w_{8,2} = \tan\left(\frac{\pi}{2} - \alpha_2 + \alpha_1\right) \cdot \left(\frac{l_1}{\cos\alpha_1} - \frac{w_{31}}{\sin\left(\frac{\pi}{2} - \alpha_2 + \alpha_1\right)} - w_{8,2} \cdot \tan\alpha_1\right) \tag{A.18}$$

As $w_{8,2}$ appears on both sides of the equation, it can be rewritten to:

$$w_{8,2} = \frac{\tan\left(\frac{\pi}{2} - \alpha_2 + \alpha_1\right)}{1 + \tan\alpha_1 \cdot \tan\left(\frac{\pi}{2} - \alpha_2 + \alpha_1\right)} \cdot \left(\frac{l_1}{\cos\alpha_1} - \frac{w_{31}}{\sin\left(\frac{\pi}{2} - \alpha_2 + \alpha_1\right)}\right) \tag{A.19}$$

It is possible to include the equation for $w_{8,4}$ in the equation for $w_{8,2}$ and thus reducing the number of equations by one. First, the different sign of α_1 is taken account for by multiplying the angle with $sign(a_{n4} - a_{n5})$. In addition to this, the second term in the denominator of the first fraction in Equation A.19 is omitted for $w_{8,4}$ by multiplying it with the true-false statement $(a_{n4} > a_{n5})$. These changes results in:

$$\begin{aligned} w_{8,2} = & \frac{\tan\left(\frac{\pi}{2} - \alpha_2 + sign(a_{n4} - a_{n5}) \cdot \alpha_1\right)}{1 + \tan\alpha_1 \cdot \tan\left(\frac{\pi}{2} - \alpha_2 + \alpha_1\right) \cdot (a_{n4} > a_{n5})} \\ & \cdot \left(\frac{l_1}{\cos\alpha_1} - \frac{w_{31}}{\sin\left(\frac{\pi}{2} - \alpha_2 + sign(a_{n4} - a_{n5}) \cdot \alpha_1\right)}\right) \end{aligned} \tag{A.20}$$

$$w_{8,3} = \cos\alpha_1 \cdot (l_5 + l_1 \cdot \tan\alpha_1) \tag{A.21}$$

Change to similar nodes

Node 4	Node 3	Node 8	Node 9
Truss 4	Truss 2	Truss 18	Truss 20
Truss 5	Truss 5	Truss 17	Truss 17
Truss 3	Truss 30	Truss 19	Truss 34
Truss 31	Truss 7	Truss 33	Truss 15
Truss 8	Truss 6	Truss 14	Truss 16
Truss 1	Truss 1	Truss 17	Truss 17
a_1	a_2	a_3	a_4
a_{n4}	a_{n3}	a_{n8}	a_{n9}
a_{n5}	a_{n16}	a_{n6}	a_{n7}
a_{n3}	a_{n4}	a_{n9}	a_{n8}
a_{n16}	a_{n5}	a_{n7}	a_{n6}

Node 5

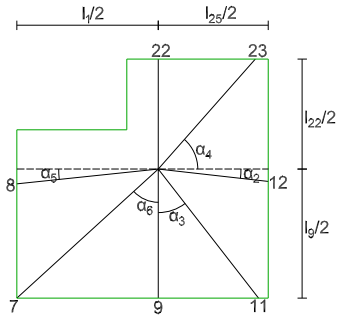

Figure A.9: Node 5.

Angles

$$\alpha_2 = \arctan\frac{abs(a_{n7} - a_{n5})}{l_{25}} \tag{A.22}$$

$$\alpha_3 = \arctan\frac{l_{25}}{l_9 + a_{n16} - a_{n6}} \tag{A.23}$$

$$\alpha_4 = \arccos\frac{l_{12}^2 + l_{23}^2 - l_{24}^2}{2l_{12}l_{23}} \tag{A.24}$$

$$\alpha_5 = \arctan\frac{abs(a_{n4} - a_{n5})}{l_1} \tag{A.25}$$

$$\alpha_6 = \arctan\frac{l_9 + a_{n16} - a_{n3}}{l_7} \tag{A.26}$$

Maximum allowed widths of struts

w_{22} :

$$w_{22,1} = 2a_6 \tag{A.27}$$

$$w_{22,2} = \tan\left(\frac{\pi}{2} - \alpha_4\right) \cdot \left(l_{22} - \frac{w_{23}}{\sin\frac{\pi}{2}}\right) \tag{A.28}$$

$$w_{22,3} = l_{25}/2 \tag{A.29}$$

w_{23} :

(a) **(b)**

Figure A.10: Maximum width of truss 23

$$w_{23,1} = \sin\left(\frac{\pi}{2} - \alpha_4\right) \cdot \left(l_{22} - \frac{w_{22}}{\tan\left(\frac{\pi}{2} - \alpha_4\right)}\right) \tag{A.30}$$

$$\begin{aligned} w_{23,2} &= \sin\left(\alpha_4 + sign(a_{n7} - a_{n5}) \cdot \alpha_2\right) \\ \cdot\left(\frac{l_{25}}{\cos\alpha_2} - \frac{w_{12}}{\tan\left(\alpha_4 + sign(a_{n7} - a_{n5}) \cdot \alpha_2\right)}\right. &+ \left. sign(a_{n5} - a_{n7}) \cdot w_{12} \cdot \tan\alpha_2\right) \end{aligned} \tag{A.31}$$

w_{12} :

(a) **(b)**

Figure A.11: Maximum width of truss 12

$$w_{12,1} = \frac{\tan\left(\alpha_4 + sign(a_{n7} - a_{n5}) \cdot \alpha_2\right)}{1 + \tan\alpha_2 \cdot \tan\left(\alpha_4 + sign(a_{n7} - a_{n5}) \cdot \alpha_2\right) \cdot (a_{n7} > a_{n5})} \cdot \left(\frac{l_{25}}{\cos\alpha_2} - \frac{w_{23}}{\sin\left(\alpha_4 + sign(a_{n7} - a_{n5}) \cdot \alpha_2\right)}\right) \tag{A.32}$$

$$w_{12,2} = \frac{\tan\left(\frac{\pi}{2} - \alpha_3 - sign(a_{n7} - a_{n5}) \cdot \alpha_2\right)}{1 + \tan\alpha_2 \cdot \tan\left(\frac{\pi}{2} - \alpha_3 - sign(a_{n7} - a_{n5}) \cdot \alpha_2\right) \cdot (a_{n5} > a_{n7})} \cdot \left(\frac{l_{25}}{\cos\alpha_2} - \frac{w_{11}}{\sin\left(\frac{\pi}{2} - \alpha_3 - sign(a_{n7} - a_{n5}) \cdot \alpha_2\right)}\right) \tag{A.33}$$

w_{11} :

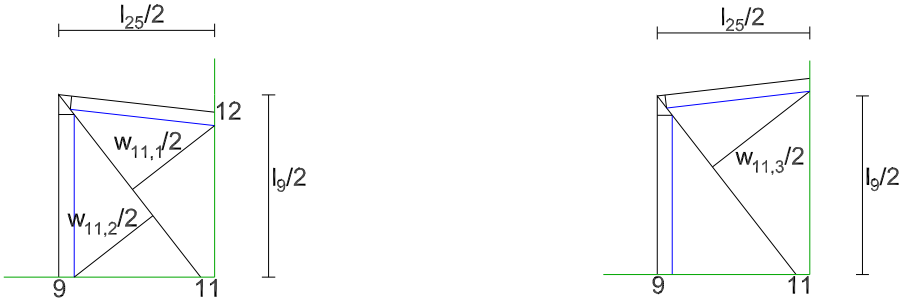

Figure A.12: Maximum width of truss 11

$$w_{11,1} = \sin\left(\frac{\pi}{2} - \alpha_3 - sign(a_{n7} - a_{n5}) \cdot \alpha_2\right) \cdot \left(\frac{l_{25}}{\cos\alpha_2} - \frac{w_{12}}{\tan\left(\frac{\pi}{2} - \alpha_3 - sign(a_{n7} - a_{n5}) \cdot \alpha_2\right)} + w_{12} \cdot \tan\alpha_2\right) \tag{A.34}$$

$$w_{11,2} = \sin\alpha_3(l_9 - \frac{w_9}{\tan\alpha_3}) \tag{A.35}$$

w_9 :

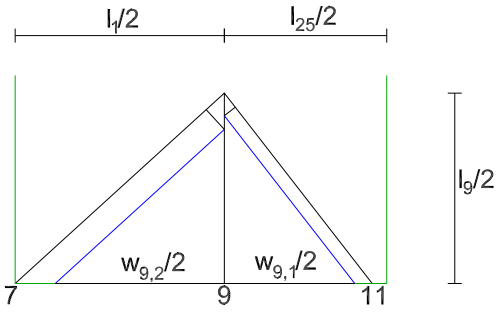

Figure A.13: Maximum width of truss 9

$$w_{9,1} = \tan\alpha_3(l_9 - \frac{w_{11}}{sin\alpha_3}) \tag{A.36}$$

$$w_{9,2} = \tan\alpha_6(l_9 - \frac{w_7}{sin\alpha_6}) \tag{A.37}$$

w_7 :

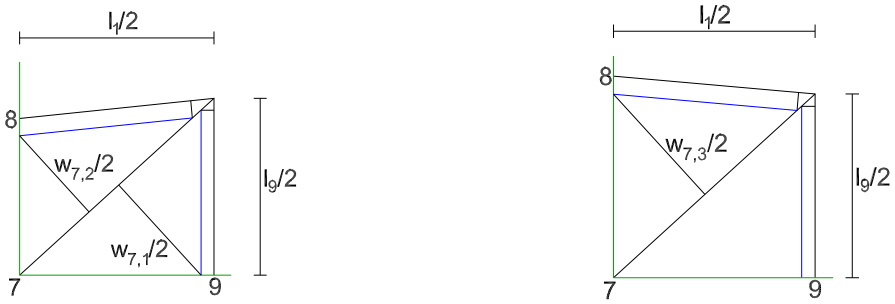

(a) **(b)**

Figure A.14: Maximum width of truss 7

$$w_{7,1} = \sin\alpha_4(l_9 - \frac{w_9}{\tan\alpha_4}) \tag{A.38}$$

$$w_{7,2} = \sin\left(\frac{\pi}{2} - \alpha_4 - sign(a_{n4} - a_{n5}) \cdot \alpha_5\right) \cdot \left(\frac{l_1}{\cos\alpha_5} - \frac{w_8}{\tan\left(\frac{\pi}{2} - \alpha_4 - sign(a_{n4} - a_{n5}) \cdot \alpha_5\right)} + sign(a_{n4} - a_{n5}) \cdot w_8 \cdot \tan\alpha_5\right) \tag{A.39}$$

w_8 :

(a) **(b)**

Figure A.15: Maximum width of truss 8

$$w_{8,1} = \frac{\tan\left(\frac{\pi}{2} - \alpha_6 - sign(a_{n4} - a_{n5}) \cdot \alpha_5\right)}{1 + \tan\alpha_5 \cdot \tan\left(\frac{\pi}{2} - \alpha_6 - sign(a_{n4} - a_{n5}) \cdot \alpha_5\right) \cdot (a_{n5} > a_{n4})} \cdot \left(\frac{l_1}{\cos\alpha_5} - \frac{w_7}{\sin\left(\frac{\pi}{2} - \alpha_6 - sign(a_{n4} - a_{n5}) \cdot \alpha_5\right)}\right) \tag{A.40}$$

$$w_{8,2} = (2a_1 + 2a_6 \tan\alpha_5)\cos\alpha_5 \cdot (a_{n4} > a_{n5}) + (2a_1 - l_1 \tan\alpha_5) \cdot (a_{n5} > a_{n4}) \quad \text{(A.41)}$$

$$w_{8,3} = \cos\alpha_5(l_9 + l_1 \cdot \tan\alpha_5) \quad \text{(A.42)}$$

Change to similar nodes

Node 5	Node 7
Truss 22	Truss 24
Truss 24	Truss 22
Truss 23	Truss 35
Truss 12	Truss 12
Truss 11	Truss 32
Truss 9	Truss 13
Truss 7	Truss 33
Truss 8	Truss 16
Truss 1	Truss 17
Truss 25	Truss 25
a_6	a_5
a_1	a_4
a_{n5}	a_{n7}
a_{n7}	a_{n5}
a_{n6}	a_{n16}
a_{n16}	a_{n6}
a_{n3}	a_{n8}
a_{n4}	a_{n9}

Node 12

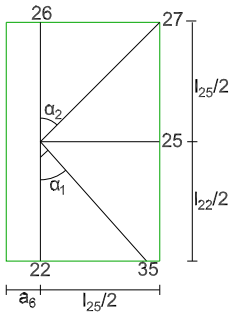

Figure A.16: Node 12.

Angles

$$\alpha_1 = \arctan \frac{l_{25}}{l_{22} + a_{n5} - a_{n7}} \tag{A.43}$$

$$\alpha_2 = \arccos \frac{l_{26}}{l_{27}} \tag{A.44}$$

Maximum allowed widths of struts

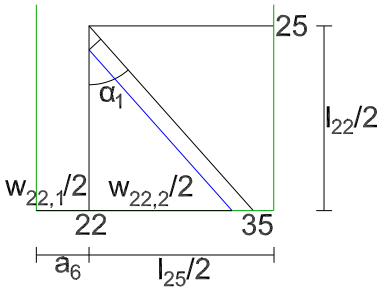

Figure A.17: Maximum width of truss 22

$$w_{22,1} = 2a_6 \tag{A.45}$$

$$w_{22,2} = \tan \alpha_1 \cdot \left(l_{22} - \frac{w_{35}}{\sin \alpha_1} \right) \tag{A.46}$$

$$w_{22,3} = l_{25} \tag{A.47}$$

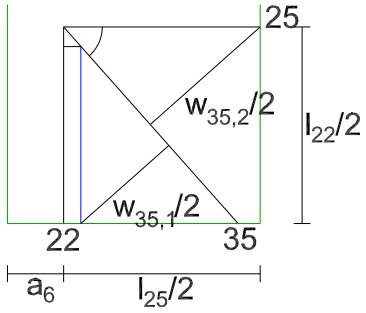

Figure A.18: Maximum width of truss 35

$$w_{35,1} = \sin \alpha_1 \cdot \left(l_{22} - \frac{w_{22}}{\tan \alpha_1} \right) \tag{A.48}$$

$$w_{35,2} = \sin \left(\frac{\pi}{2} - \alpha_1 \right) \cdot \left(l_{25} - \frac{w_{25}}{\tan \frac{\pi}{2} - \alpha_1} \right) \tag{A.49}$$

$$w_{27,1} = \sin \alpha_2 \cdot \left(l_{25} - \frac{w_{26}}{\tan \alpha_2} \right) \tag{A.50}$$

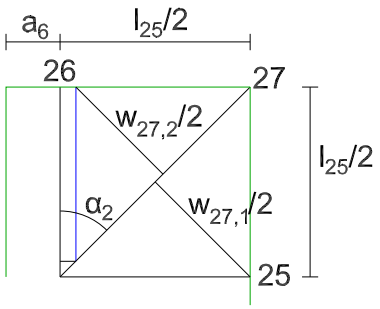

Figure A.19: Maximum width of truss 27

$$w_{27,2} = \sin\left(\frac{\pi}{2} - \alpha_2\right) \cdot \left(l_{25} - \frac{w_{25}}{\tan\left(\frac{\pi}{2} - \alpha_2\right)}\right) \tag{A.51}$$

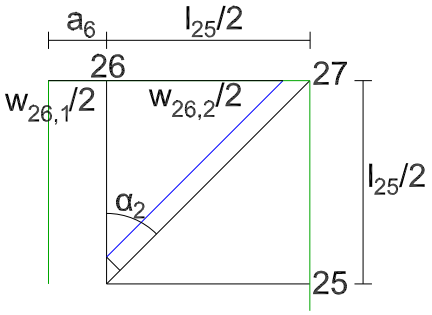

Figure A.20: Maximum width of truss 26

$$w_{26,1} = 2a_6 \tag{A.52}$$

$$w_{26,2} = \tan\alpha_2 \cdot \left(l_{25} - \frac{w_{27}}{\sin\alpha_2}\right) \tag{A.53}$$

$$w_{26,3} = l_{25} \tag{A.54}$$

Change to similar nodes

Node 12	Node 13
Truss 26	Truss 28
Truss 27	Truss 36
Truss 25	Truss 25
Truss 35	Truss 23
Truss 22	Truss 24
a_6	a_5
a_{n5}	a_{n7}
a_{n7}	a_{n5}

Node 16

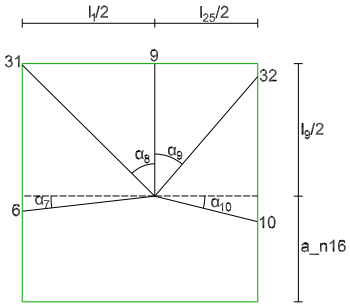

Figure A.21: Node 16.

Angles

$$\alpha_7 = \arctan \frac{abs(a_{n3} - a_{n16})}{l_1} \tag{A.55}$$

$$\alpha_8 = \arctan \frac{l_1}{l_9 + abs(a_{n5} - a_{n4})} \tag{A.56}$$

$$\alpha_9 = \arctan \frac{l_{25}}{l_9 + abs(a_{n5} - a_{n7})} \tag{A.57}$$

$$\alpha_1 0 = \arctan \frac{abs(a_{n6} - a_{n16})}{l_2 5} \tag{A.58}$$

Maximum allowed widths of struts

w_6 :

(a) **(b)**

Figure A.22: Maximum width of truss 6

$$w_{6,1} = \cos \alpha_7 \cdot \left(2a_{n16} + sign(a_{n3} - a_{n16}) \cdot l_1 \cdot \tan \alpha_7\right) \tag{A.59}$$

$$w_{6,2} = \frac{\tan\left(\frac{\pi}{2} - \alpha_8 + sign(a_{n16} - a_{n3}) \cdot \alpha_7\right)}{1 + \tan\left(\frac{\pi}{2} - \alpha_8 + sign(a_{n16} - a_{n3}) \cdot \alpha_7\right) \cdot \tan\alpha_7 \cdot (a_{n16} > a_{n3})} \cdot \left(\frac{l_1}{\cos\alpha_7} - \frac{w_{31}}{\sin\left(\frac{\pi}{2} - \alpha_8 + sign(a_{n16} - a_{n3}) \cdot \alpha_7\right)}\right) \tag{A.60}$$

w_{31} :

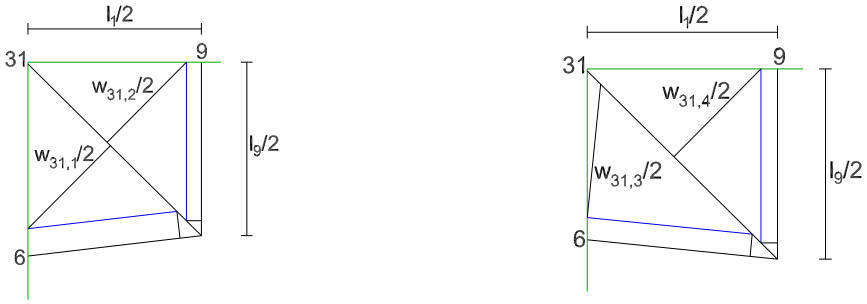

(a) **(b)**

Figure A.23: Maximum width of truss 31

$$w_{31,1} = \sin\left(\frac{\pi}{2} - \alpha_8 + sign(a_{n16} - a_{n3}) \cdot \alpha_7\right) \cdot \left(\frac{l_1}{\cos\alpha_7} - \frac{w_6}{\tan\left(\frac{\pi}{2} - \alpha_8 + sign(a_{n16} - a_{n3}) \cdot \alpha_7\right)} - sign(a_{n16} - a_{n3}) \cdot w_6 \tan\alpha_7\right) \tag{A.61}$$

$$w_{31,2} = \sin\alpha_8 \cdot \left(l_9 - \frac{w_9}{\tan\alpha_8}\right) \tag{A.62}$$

w_9 :

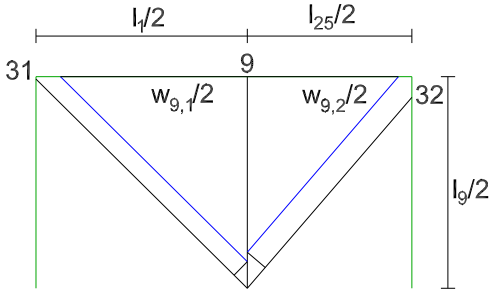

Figure A.24: Maximum width of truss 9

$$w_{9,1} = \tan\alpha_8 \left(l_9 - \frac{w_{31}}{\sin\alpha_8}\right) \tag{A.63}$$

$$w_{9,2} = \tan\alpha_9 \left(l_9 - \frac{w_{32}}{\sin\alpha_9}\right) \tag{A.64}$$

$$w_{9,3} = l_1 \tag{A.65}$$

$$w_{9,4} = l_{25} \tag{A.66}$$

w_{32} : The method for finding $w_{32,max}$ is the same as for $w_{31,max}$, but mirrored over truss 9.

$$w_{32,1} = \sin\alpha_9 \left(l_9 - \frac{w_9}{\tan\alpha_9} \right) \tag{A.67}$$

$$\begin{aligned} w_{32,2} &= \sin\left(\frac{\pi}{2} - \alpha_9 + sign(a_{n16} - a_{n6}) \cdot \alpha_{10}\right) \\ &\cdot \left(\frac{l_{25}}{\cos\alpha_{10}} - \frac{w_{10}}{\tan\left(\frac{\pi}{2} - \alpha_9 + sign(a_{n16} - a_{n6}) \cdot \alpha_{10}\right)} \right) \end{aligned} \tag{A.68}$$

w_{10} : The method for finding $w_{10,max}$ is the same as for $w_{6,max}$, but mirrored over truss 9.

$$\begin{aligned} w_{10,1} = \frac{\tan\left(\frac{\pi}{2} - \alpha_9 + sign(a_{n16} - a_{n6}) \cdot \alpha_{10}\right)}{1 + \tan\left(\frac{\pi}{2} - \alpha_9 + sign(a_{n16} - a_{n6}) \cdot \alpha_{10}\right) \cdot \tan\alpha_{10} \cdot (a_{n16} > a_{a_{n6}})} \\ \cdot \left(\frac{l_{25}}{\cos\alpha_{10}} - \frac{w_{32}}{\sin\left(\frac{\pi}{2} - \alpha_9 + sign(a_{n16} - a_{n6})\alpha_{10}\right)} \right) \end{aligned} \tag{A.69}$$

$$w_{10,2} = \cos\alpha_{10} \cdot \left(2a_{n16} - sign(a_{n16} - a_{n6}) \cdot l_{25} \tan\alpha_{10}\right) \tag{A.70}$$

Change to similar nodes

Node 16	Node 6
Truss 6	Truss 14
Truss 31	Truss 15
Truss 9	Truss 13
Truss 32	Truss 11
Truss 10	Truss 10
Truss 1	Truss 17
Truss 25	Truss 25
a_{n3}	a_{n8}
a_{n16}	a_{n6}
a_{n6}	a_{n16}
a_{n5}	a_{n7}
a_{n4}	a_{n9}
a_{n7}	a_{n5}

Appendix B

Matlab Code

The numbering of the trusses in the STMs are shown in Figure B.1. Figure B.2 shows the numbering of the nodes.

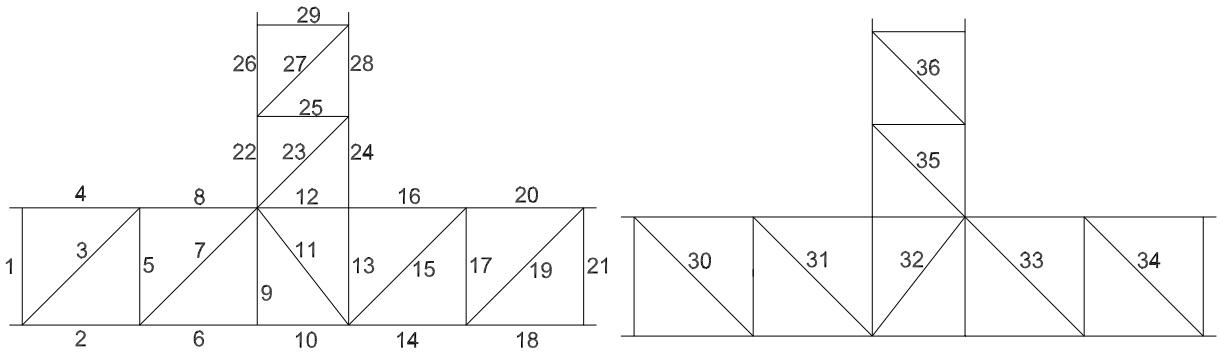

(a) **(b)**

Figure B.1: Numbering of trusses used in the STMs.

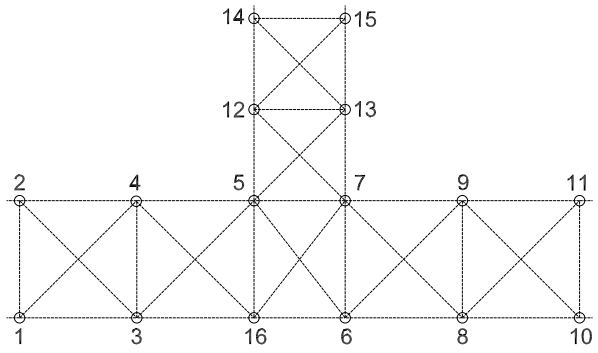

Figure B.2: Numbering of nodes used in the STMs.

Matlab Code

Main Script

```
%IMPORTANT: Make sure that the positive directions of forces and moments in
%input data coincides with the definition in this code

%The code runs faster if drawing of strut-and-tie model is turned off in
```

```
%line 95.

%Units: Length (mm), Force (N/m), Moment (Nmm/m), Area (mm^2), Stress (N/mm
    ^2)
clear
tic
%Available reinforcement (in bar diameter)
AR=[25,25;25,25;25,25];

%spacing longitudinal reinforcement
s=[200,200;200,200;200,200];

%Angle of shear force at end of D-region
theta=[45,45,45]*2*pi/360;

%Predefining
n_bars=[0,0;0,0;0,0];

%Geometry
h1=550; %Height of continuous wall
h2=450; %Height of intersecting wall
b=1000; %mm/m
h=[h1;h1;h2];
c=[50,50;50,50;50,50]; %Concrete cover
a=c+AR/2;

%Material data
fctm=4.1;
fyk=500;
fcm=58;
Ey=200*10^3;

%EC2 - Safety factors turned off for the analyses in the thesis
yc=1;
acc=1;
ys=1;

%Material data
fck=fcm; %The mean value is used in the thesis. Normally: fck=fcm-8MPa
fcd=acc/yc*fck;
fyd=fyk/ys;

%Predefining variables
Armering_opt=0;
n_bars_opt=0;
check_opt=0;

```

```
%Making matrix of variable trusses in the middle of the D-region
q=1;
for N9=1:-1:0
    for N11=1:-1:0
        for N13=1:-1:0
                N_var(q,:)=[N9,N11,N13,N11==0];
                q=q+1;
        end
    end
end

%Load cases
Rtot=[-3424,-2753,-742, 695,47,-671, 683*10^3,6*10^3,-689*10^3;
   -1701,-1699,950, -452,-498,-2, -467*10^3,480*10^3,-13*10^3;
   -2735,-3603,637, -894,257,868, -498*10^3,-141*10^3,639*10^3]*10^3; %
      includes all load combinations

%Finding the STMs
for i = 1:length(Rtot(:,1))
    U_opt=inf;
    %Extracting load case
    R=[Rtot(i,1:3)',Rtot(i,4:6)',Rtot(i,7:9)'];  %R=[N1,V1,M1;N2,V2,M2,N3,
       V3,M3]
    for j=1:length(N_var)

    %Choosing set of trusses for the STM
    N=[1,1,(R(1,2)>=0),1,1,1,(R(1,2)>=0),1,N_var(j,1),1,N_var(j,2),1,N_var(
       j,3),1,(R(2,2)<0),1,1,1,(R(2,2)<0),1,1,1,(R(3,2)<0),1,1,1,(R(3,2)<0)
       ,1,1,(R(1,2)<0),(R(1,2)<0),N_var(j,4),(R(2,2)>=0),(R(2,2)>=0),(R
       (3,2)>=0),(R(3,2)>=0)];

    %Optimization of the set of trusses
    [a_mid,Armering,n_bars_mid,U,check,w,check_force,N_STM,l,a_nodes] =
       Optimization(R,a,fck,fyd,h,b,s,theta,AR,c,n_bars,N,Ey);

    %Check of equilibrium, capacity of trusses and if the current STM is
    %the most efficient
    if  check==0 && check_force==0
        if U<U_opt
        U_opt=U;
        a_opt=a_mid;
        Armering_opt=Armering;
        n_bars_opt=n_bars_mid;
        check_opt=check;
        N_draw=N;
        end
    end
```

```
92      end
93
94      %Drawing the STM
95      draw_STM(N_draw,l,a_nodes) %increase speed of script by turning this
            off
96  end
97  toc
```

Optimization

```
1   function [a,As,n_bars,U,checked,w,check_force,N_STM,l,a_nodes] =
        Optimization(R,a,fck,fyd,h,b,s,theta,AR,c,n_bars,N,Ey)
2
3   %EC2 - Unused in the thesis
4   yc=1.5;
5   acc=0.85;
6   fcd=acc/yc*fck;
7
8
9   %Optimalization of strut placements
10      N_STM1=Forces_initial(R,N,theta,a,h); %Another Forces-function has to
            be used as the one used later requires already calculated forces
11      [N_STM,l,a_nodes,F,Fvv,Fv]=Forces(R,theta,a,h,N,N_STM1); %The STM is
            fixed according to the initial calculations in the line above.
12
13
14  %Sorting all forces in one array
15  F_nodes = [N_STM,F(1,:),F(2,:),F(3,:)];
16
17  %Trusses which are assessed in the optimization of the six sides
18  truss_numbers
        =[37,4,8,12,16;38,2,6,10,14;39,18,14,10,6;40,20,16,12,8;41,28,24,28,13;42,26,22,26,9]
         %In order to have equal amounts of entries in each row, the trusses are
         repeated in the discontinuous wall. This does not affect the process.
19
20  %Nodes which are assessed in the optimization of the six sides
21  node_numbers=[2,4,5,7;1,3,16,6;10,8,6,16;11,9,7,5;15,13,7,6;14,12,5,16];
22
23  %Predefining
24  check=zeros(3,2);
25
26  %Counter to make sure the while loop does not run indefinitely
27  z=0;
28
29  %Optimzation loop
30  while (sum(sum(check)) < sum(size(check))) && (z<200)
31      z=z+1;
```

```
32
33 %Checking which trusses that should be assessed
34 check_active=[1,1,1,(N_STM(8)>0)+(N_STM(8)<0)*(N_STM(12)<0),(N_STM(4)>0)*(
       N_STM(8)>0)*(N_STM(12)>0) ; 1,1,1,(N_STM(6)>0)+(N_STM(6)<0)*(N_STM(10)
       <0),(N_STM(6)>0)*(N_STM(10)>0)*(N_STM(14)>0) ; 1,1,1,(N_STM(14)>0)+(
       N_STM(14)<0)*(N_STM(10)<0),(N_STM(14)>0)*(N_STM(10)>0)*(N_STM(6)>0) ;
       1,1,1,(N_STM(16)>0)+(N_STM(16)<0)*(N_STM(12)<0),(N_STM(16)>0)*(N_STM(12)
       >0)*(N_STM(8)>0) ; 1,1,1,0,1 ; 1,1,1,0,1];
35
36 %Finding the force which determines placement of longitudinal trusses
37 N_check=F_nodes(truss_numbers).*check_active;
38
39 %Finding all necessary widths of struts
40 [~,w]=node_check(N_STM,F,l,b,a,a_nodes,fck);
41
42 %Maximum tension force if any. If not, maximum compression force
43 F_max = [max(N_check(1:2:5,:)') + (min(N_check(1:2:5,:)')-max(N_check
       (1:2:5,:)')).*(max(N_check(1:2:5,:)')<=0) ; max(N_check(2:2:6,:)') + (
       min(N_check(2:2:6,:)')-max(N_check(2:2:6,:)')).*(max(N_check(2:2:6,:)')
       <=0)]';
44
45 %Finding the necessary width which determines placement of longitudinal
46 %trusses
47 for j=1:3
48         w_opt(j,1)=max(max(w(node_numbers(2*j-1,:),truss_numbers(2*j-1,:)))
               );
49         w_opt(j,2)=max(max(w(node_numbers(2*j,:),truss_numbers(2*j,:))));
50 end
51
52 %Giving struts half of the cross section if necessary width is less than
53 %the available. If so, several calculations has to be updated
54 a = a + (0.25*[h,h]-a).*(2*a<w_opt).*(F_max<0);
55 [N_STM,l,a_nodes,F]=Forces(R,theta,a,h,N,N_STM);
56 F_nodes = [N_STM,F(1,:),F(2,:),F(3,:)];
57 check_active=[1,1,1,(N_STM(8)>0)+(N_STM(8)<0)*(N_STM(12)<0),(N_STM(4)>0)*(
       N_STM(8)>0)*(N_STM(12)<0) ; 1,1,1,(N_STM(6)>0)+(N_STM(6)<0)*(N_STM(10)
       <0),(N_STM(6)>0)*(N_STM(10)>0)*(N_STM(14)<0) ; 1,1,1,(N_STM(14)>0)+(
       N_STM(14)<0)*(N_STM(10)<0),(N_STM(14)>0)*(N_STM(10)>0)*(N_STM(6)<0) ;
       1,1,1,(N_STM(16)>0)+(N_STM(16)<0)*(N_STM(12)<0),(N_STM(16)>0)*(N_STM(12)
       >0)*(N_STM(8)<0) ; 1,1,1,0,1 ; 1,1,1,0,1];
58 N_check=F_nodes(truss_numbers).*check_active;
59 F_max = [max(N_check(1:2:5,:)') + (min(N_check(1:2:5,:)')-max(N_check
       (1:2:5,:)')).*(max(N_check(1:2:5,:)')<=0) ; max(N_check(2:2:6,:)') + (
       min(N_check(2:2:6,:)')-max(N_check(2:2:6,:)')).*(max(N_check(2:2:6,:)')
       <=0)]';
60 [~,w]=node_check(N_STM,F,l,b,a,a_nodes,fck);
61 for j=1:3
```

```
62          w_opt(j,1)=max(max(w(node_numbers(2*j-1,:),truss_numbers(2*j-1,:)))
                );
63          w_opt(j,2)=max(max(w(node_numbers(2*j,:),truss_numbers(2*j,:))));
64  end
65  %Necessary reinforcement area
66  As=(F_max>0).*(F_max./fyd)./(AR.^2*pi/4*b./s);
67
68  %Number of bars needed. Maximum two bars in each layer
69  n_bars=(F_max>0).*(floor(As) + ceil( (As-floor(As))./0.5) * 0.5);
70
71  %Calculating the new placement of longitudinal trusses
72  a=a.*(F_max<0) + (((c+floor(n_bars/2)/2.*AR) .* floor(n_bars/2)*2.*AR.^2*pi
        /4+(c + floor(n_bars/2).*AR+AR/2) .* rem(n_bars,2).*AR.^2*pi/4) ./ (
        floor(n_bars/2)*2.*AR.^2*pi/4 + rem(n_bars,2).*AR.^2*pi/4 + (F_max<0)))
        .*(F_max>0); %(z_i*A_:)/A_i The reason for the added F_max<0 in the
        denominator is to avoid dividing by zero. This added part is removed
        when everything is multiplied by (F_max>0).
73  a=a.*(F_max>0) + (a+(w_opt/2-a)./2).*(F_max<0);
74
75  %Calculating new forces
76  [N_STM,l,a_nodes,F]=Forces(R,theta,a,h,N,N_STM);
77  F_nodes = [N_STM,F(1,:),F(2,:),F(3,:)];
78
79  %Executing new check of widths of struts
80  check_active=[1,1,1,(N_STM(8)>0)+(N_STM(8)<0)*(N_STM(12)<0),(N_STM(4)>0)*(
        N_STM(8)>0)*(N_STM(12)<0) ; 1,1,1,(N_STM(6)>0)+(N_STM(6)<0)*(N_STM(10)
        <0),(N_STM(6)>0)*(N_STM(10)>0)*(N_STM(14)<0) ; 1,1,1,(N_STM(14)>0)+(
        N_STM(14)<0)*(N_STM(10)<0),(N_STM(14)>0)*(N_STM(10)>0)*(N_STM(6)<0) ;
        1,1,1,(N_STM(16)>0)+(N_STM(16)<0)*(N_STM(12)<0),(N_STM(16)>0)*(N_STM(12)
        >0)*(N_STM(8)<0) ; 1,1,1,0,0 ; 1,1,1,0,0];
81  N_check=F_nodes(truss_numbers).*check_active;
82  F_max = [max(N_check(1:2:5,:)') + (min(N_check(1:2:5,:)')-max(N_check
        (1:2:5,:)')).*(max(N_check(1:2:5,:)')<=0) ; max(N_check(2:2:6,:)') + (
        min(N_check(2:2:6,:)')-max(N_check(2:2:6,:)')).*(max(N_check(2:2:6,:)')
        <=0)]';
83  n_bars=(F_max>0).*(floor(As) + ceil( (As-floor(As))./0.5) * 0.5);
84  [~,w]=node_check(N_STM,F,l,b,a,a_nodes,fck);
85  for j=1:3
86          w_opt(j,1)=max(max(w(node_numbers(2*j-1,:),truss_numbers(2*j-1,:)))
                );
87          w_opt(j,2)=max(max(w(node_numbers(2*j,:),truss_numbers(2*j,:))));
88  end
89  %Check of both struts and ties
90  check=(F_max>0).*(F_max./fyd < n_bars.*b./s.*AR.^2/4*pi) + (F_max<0).*((2*a
        -w_opt).^2<1.0);
91
92  end
```

```
93
94  %Finding values for output of function
95  [checked,w]=node_check(N_STM,F,l,b,a,a_nodes,fck);
96
97  %Necessary reinforcement for output
98  As=N_STM/fyd.*(N_STM>0);
99
100 %Strain energy
101 U=sum(N_STM.*l.*N_STM./(As.*Ey+(As==0)).*(1-(As==0)));
102
103 %Check of equilibrium of forces
104 check_force = force_check(N_STM,F,Fv,theta,l,a_nodes);
105
106 end
```

Forces Initial

```
1   function [N_STM,l,a_nodes] = Forces_initial(R,N,theta,a,h)
2
3   %Placement of nodes
4   a_nodes = [0,0,0,0,a(3,2),a(3,1),a(3,1),0,0,0,0,a(3,2),a(3,1),a(3,2),a(3,1)
        ,a(3,2); %a_x: node 1-16
5        a(1,2),a(1,1),a(1,2),a(1,1),a(1,1),a(2,1),a(2,2),a(2,1),a(2,2),a(2,1),a
            (2,2),0,0,0,0, a(1,2)];%a_z: node 8-16
6
7   %Lengths of trusses
8   l1=h(1)-a(1,1)-a(1,2);
9   l2=l1;
10  l4=l1;
11  l3=sqrt(l1^2+l4^2);
12  l5=l1;
13  l6=sqrt(l1^2 + (a_nodes(2,16)-a_nodes(2,3))^2);
14  l8=sqrt(l1^2 + (a_nodes(2,5)-a_nodes(2,4))^2);
15  l7=sqrt(l1^2+(l5+a_nodes(2,4)-a_nodes(2,5))^2); %change du to other changes
16  l9=h(1) - a_nodes(2,16) - a_nodes(2,5);
17  l10=sqrt((a_nodes(2,16) - a_nodes(2,6))^2 + (h(3)-a_nodes(1,16)-a_nodes
        (1,6))^2); %the minus separates the height of the two nodes
18  l25=h(3)-a(3,1)-a(3,2);
19  l11=sqrt(l25^2 + (h(1)-a_nodes(2,5)-a_nodes(2,6)));
20  l12=sqrt((a_nodes(2,5) - a_nodes(2,7))^2 + (h(3)-a_nodes(1,5)-a_nodes(1,7))
        ^2); %the minus separates the height of the two nodes
21  l13=h(2) - a_nodes(2,6) - a_nodes(2,7);
22  l17=h(2)-a_nodes(2,1)-a_nodes(2,2);
23  l14=sqrt(l17^2+(a_nodes(2,6)-a_nodes(2,8))^2);
24  l16=sqrt(l17^2+(a_nodes(2,7)-a_nodes(2,9))^2);
25  l15=sqrt(l17^2+(l17+a_nodes(2,8)-a_nodes(2,6))^2);
26  l21=l17;
```

```
l18=l17;
l20=l17;
l19=sqrt(l17^2+l20^2);
l22=l25+a_nodes(2,5)-a_nodes(2,4);
l24=l25+a_nodes(2,7)-a_nodes(2,9);
l23=sqrt(l22^2+l25^2);
l26=l25;
l28=l25;
l27=sqrt(l25^2+l28^2);
l29=l25;
l32=sqrt(l25^2+(h(2)-a_nodes(2,7)-a_nodes(2,16))^2);
l30=sqrt(l1^2+l2^2);
l31=sqrt(l1^2+(l5+a_nodes(2,3)-a_nodes(2,16))^2);
l33=sqrt(l17^2+(l17+a_nodes(2,9)-a_nodes(2,7))^2);
l34=sqrt(l17^2+l18^2);
l35=sqrt(l24^2+l25^2);
l36=sqrt(l25^2+l26^2);

%Preallocating
F=zeros(3,2);
Fv=zeros(3,1);

%Distance from center of D-region to the three edges
x=[h(3)/2-a(3,2)+l1+l4+(h(1)/2-a(1,1)*(N(3)==1)-a(1,2)*(N(30)==1))/(tan(
    theta(1))),h(3)/2-a(3,1)+l17+l20+(h(2)/2-a(2,1)*(N(19)==1)-a(2,2)*(N(34)
    ==1))/(tan(theta(2))),h(1)/2-a_nodes(2,5)+l22+l26+(h(3)/2-a(3,1)*(N(36)
    ==1)-a(3,2)*(N(27)==1))/(tan(theta(3)))];

%Calculation of loads at edges
for i=1:length(R(:,1)) %Obtaining inital forces for the STM
    n=R(i,1);
    v=R(i,2);
    m=R(i,3)-x(i)*v*(1-2*(i==2)); %The last parentheses takes account of
        the difference in definition of positive directions
    Fvv=abs(v/tan(theta(i)));
    F(i,2)=n*(h(i)/2-a(i,1))/(h(i)-a(i,1)-a(i,2))+m/(h(i)-a(i,1)-a(i,2))+
        Fvv*(h(i)/2-a(i,1))/(h(i)-a(i,1)-a(i,2));
    F(i,1)=(n-n*(h(i)/2-a(i,1))/(h(i)-a(i,1)-a(i,2)))-m/(h(i)-a(i,1)-a(i,2)
        )+(Fvv-Fvv*(h(i)/2-a(i,1))/(h(i)-a(i,1)-a(i,2)));
    Fv(i)=-abs(v/sin(theta(i)));
end

%Calculation of truss forces
N1 = -Fv(1)*sin(theta(1))*(N(1)==1);
N30 = -N1*l30/l1*(N(30)==1);
N4 = (Fv(1)*cos(theta(1))*(N(30)==0)+F(1,1)-N(30)*l4/l30)*(N(4)==1);
N3 = -N1*l3/l1*(N(3)==1);
```

```
N2 = (F(1,2)-N3*l2/l3+Fv(1)*cos(theta(1))*(N(3)==0))*(N(2)==1);
N5 = (-N3*l5/l3-N30*l5/l30)*(N(5)==1);
N31 = -N5*l31/l5*(N(31)==1);
N8 = (N4+N3*l4/l3-N31*l8/l31)*(N(8)==1);
N7 = -N5*l7/l5*(N(7)==1);
N6 = (N2-N7*l6/l7+N30*l2/l30)*(N(6)==1);
N21 = -Fv(2)*sin(theta(2))*(N(21)==1);
N34 = -N21*l34/l21*(N(34)==1);
N18 = (F(2,1)+Fv(2)*cos(theta(2))*(N(34)==0)-N34*l18/l34)*(N(18)==1);
N19 = -N21*l19/l21*(N(19)==1);
N20 = (F(2,2)-N19*l20/l19+Fv(2)*cos(theta(2))*(N(19)==0))*(N(20)==1);
N17 = (-N19*l17/l19-N34*l17/l34)*(N(17)==1);
N33 = -N17*l33/l17*(N(33)==1);
N14 = (N18+N19*l18/l19-N33*l14/l33)*(N(14)==1);
N15 = -N17*l15/l17*(N(15)==1);
N16 = (N20-N15*l16/l15+N34*l20/l34)*(N(16)==1);
N29 = (-Fv(3)*sin(theta(3)))*(N(29)==1);
N36 = -N29*l36/l29*(N(36)==1);
N26 = (F(3,2)+Fv(3)*cos(theta(3))-N36*l26/l36)*(N(26)==1);
N27 = -N29*l27/l29*(N(27)==1);
N28 = (F(3,1)-N27*l28/l27+Fv(3)*cos(theta(3))*(N(27)==0))*(N(28)==1);
N25 = (-N27*l25/l27-N36*l25/l36)*(N(25)==1);
N35 = -N25*l35/l25*(N(35)==1);
N22 = (N26+N27*l26/l27-N35*l22/l35)*(N(22)==1);
N23 = -N25*l23/l25*(N(23)==1);
N24 = (N28-N23*l24/l23+N36*l28/l36)*(N(24)==1);
N13 = 1/(1+(N(10)==1)*(N(11)==1)*(N(32)==1)) * (N24+N35*l24/l35-N33*l13/l33
    -l13/l32*(N(32)==1)*(N6*l32/l10+N31*l6/l31*l32/l10+(-N14*l32/l10-N15*l14
    /l15*l32/l10+l32/l13*N15*l13/l15*(N(11)==1)))*(N(10)==1));
N11 = -(N13+N15*l13/l15)*l11/l13*(N(11)==1);
N10 = (N14+N15*l14/l15-N11*l10/l11)*(N(10)==1);
N32 = (N6*l32/l10+N31*l6/l31*l32/l10-N10*l32/l10)*(N(32)==1);
N12 = (N16+N33*l16/l33-N32*l12/l32-N35)*(N(12)==1);
N9 = (-N32*l9/l32-N31*l9/l31)*(N(9)==1);

%Sorting the lengths and forces in arrays
l=[l1,l2,l3,l4,l5,l6,l7,l8,l9,l10,l11,l12,l13,l14,l15,l16,l17,l18,l19,l20,
    l21,l22,l23,l24,l25,l26,l27,l28,l29,l30,l31,l32,l33,l34,l35,l36];
N_STM=[N1,N2,N3,N4,N5,N6,N7,N8,N9,N10,N11,N12,N13,N14,N15,N16,N17,N18,N19,
    N20,N21,N22,N23,N24,N25,N26,N27,N28,N29,N30,N31,N32,N33,N34,N35,N36];

end
```

Forces

```
function [N,l,a_nodes,F,Fvv,Fv] = Forces(R,theta,a,h,N,N_STM)
%Closing moment on left side - can be used for closing moment on right side
```

```
%by mirroring sectional forces.
%a=[50,50;50,50;50,50];
fyd=434;
fyd=500;
AR=[25,25];
b=1000;
s=[200,200];
c=[50,50];

%a7 - Placement of truss 10 if truss 6 & 14 are in compression while truss
%12 is in tension
a7=0;
a8=0;
if N_STM(10)>0
    As_a7=(N_STM(10)/fyd)/(AR(1,2)^2*pi/4*b/s(1,2)); %Necessary
        reinforcement area for the odd number force
    n_bars_a7=floor(As_a7) + ceil( (As_a7-floor(As_a7))/0.5) * 0.5; %Number
         of bars needed. Maximum two bars in each layer
    a7=((c(1,2)+floor(n_bars_a7/2)/2*AR(1,2)) * floor(n_bars_a7/2)*2*AR
        (1,2)^2*pi/4+(c(1,2) + floor(n_bars_a7/2)*AR(1,2)+AR(1,2)/2) * rem(
        n_bars_a7,2)*AR(1,2)^2*pi/4) / (floor(n_bars_a7/2)*2*AR(1,2)^2*pi/4
        + rem(n_bars_a7,2)*AR(1,2)^2*pi/4); %(z_i*A_i)/A_i
end
%a8 - Placement of truss 12 if truss 8 & 16 are in compression while truss
%12 is in tension
if N_STM(12)>0
    As_a8=(N_STM(12)/fyd)/(AR(1,1)^2*pi/4*b/s(1,1)); %Necessary
        reinforcement area for the odd number force
    n_bars_a8=floor(As_a8) + ceil( (As_a8-floor(As_a8))/0.5) * 0.5; %Number
         of bars needed. Maximum two bars in each layer
    a8=((c(1,1)+floor(n_bars_a8/2)/2*AR(1,1)) * floor(n_bars_a8/2)*2*AR
        (1,1)^2*pi/4+(c(1,1) + floor(n_bars_a8/2)*AR(1,1)+AR(1,1)/2) * rem(
        n_bars_a8,2)*AR(1,1)^2*pi/4) / (floor(n_bars_a8/2)*2*AR(1,1)^2*pi/4
        + rem(n_bars_a8,2)*AR(1,1)^2*pi/4); %(z_i*A_i)/A_i
end

a_nodes = [0,0,0,0,a(3,2),a(3,1),a(3,1),0,0,0,0,a(3,2),a(3,1),a(3,2),a(3,1)
    ,a(3,2); %a_x: node 1-16
    a(1,2),a(1,1),a(1,2),a(1,1), a(1,1)*((N_STM(8)>0)+(N_STM(8)<0)*(N_STM
        (12)<0))+a(2,2)*(N_STM(16)>0)*(N_STM(12)>0)*(N_STM(8)<0) + a8*(N_STM
        (12)>0)*(N_STM(8)<0)*(N_STM(16)<0) , a(2,1)*((N_STM(14)>0)+(N_STM
        (14)<0)*(N_STM(10)<0))+a(1,2)*(N_STM(6)>0)*(N_STM(10)>0)*(N_STM(14)
        <0)+a7*(N_STM(10)>0)*(N_STM(6)<0)*(N_STM(14)<0) , a(2,2)*((N_STM(16)
        >0)+(N_STM(16)<0)*(N_STM(12)<0))+a(1,1)*(N_STM(8)>0)*(N_STM(12)>0)*(
        N_STM(16)<0)+a8*(N_STM(12)>0)*(N_STM(8)<0)*(N_STM(16)<0) , a(2,1),a
        (2,2),a(2,1),a(2,2),0,0,0,0, a(1,2)*((N_STM(6)>0)+(N_STM(6)<0)*(
        N_STM(10)<0))+a(2,1)*(N_STM(14)>0)*(N_STM(10)>0)*(N_STM(6)<0)+a7*(
```

```
        N_STM(10)>0)*(N_STM(6)<0)*(N_STM(14)<0)];

%Truss lengths needed for the following correction
l1=h(1)-a(1,1)-a(1,2);
l17=h(2)-a(2,1)-a(2,2);
l25=h(3)-a(3,1)-a(3,2);

%Correcting for nonactive trusses
a_nodes(2,6)=(a_nodes(2,16)-a_nodes(2,8))*l17/(l17+l25)*(N(15)==0)*(N(13)
    ==0)*(N(11)==0)*(a_nodes(2,6)~=a_nodes(2,16)) + (a_nodes(2,8)-a_nodes
    (2,16))*l25/(l17+l25)*(N(15)==0)*(N(13)==0)*(N(11)==0)*(a_nodes(2,6)~=
    a_nodes(2,8)) + a_nodes(2,6)*(1-(N(15)==0)*(N(13)==0)*(N(11)==0)*(
    a_nodes(2,6)~=a_nodes(2,16))*(a_nodes(2,6)~=a_nodes(2,8)));
a_nodes(2,16)=(a_nodes(2,6)-a_nodes(2,3))*l1/(l1+l25)*(N(31)==0)*(N(9)==0)
    *(N(32)==0)*(a_nodes(2,16)~=a_nodes(2,6)) + (a_nodes(2,3)-a_nodes(2,6))*
    l25/(l1+l25)*(N(31)==0)*(N(9)==0)*(N(32)==0)*(a_nodes(2,16)~=a_nodes
    (2,3)) + a_nodes(2,16)*(1-(N(31)==0)*(N(9)==0)*(N(32)==0)*(a_nodes(2,16)
    ~=a_nodes(2,6))*(a_nodes(2,16)~=a_nodes(2,3)));

%The rest of the truss lengths
l2=l1;
l4=l1;
l3=sqrt(l1^2+l4^2);
l5=l1;
l6=sqrt(l1^2 + (a_nodes(2,16)-a_nodes(2,3))^2);
l8=sqrt(l1^2 + (a_nodes(2,5)-a_nodes(2,4))^2);
l7=sqrt(l1^2+(l5+a_nodes(2,4)-a_nodes(2,5))^2);
l9=h(1) - a_nodes(2,16) - a_nodes(2,5);
l10=sqrt((a_nodes(2,16) - a_nodes(2,6))^2 + (h(3)-a_nodes(1,16)-a_nodes
    (1,6))^2); %the minus separates the height of the two nodes
l25=h(3)-a(3,1)-a(3,2);
l11=sqrt(l25^2 + (h(1)-a_nodes(2,5)-a_nodes(2,6))^2);
l12=sqrt((a_nodes(2,5) - a_nodes(2,7))^2 + (h(3)-a_nodes(1,5)-a_nodes(1,7))
    ^2); %the minus separates the height of the two nodes
l13=h(2) - a_nodes(2,6) - a_nodes(2,7);
l17=h(2)-a(2,1)-a(2,2);
l14=sqrt(l17^2+(a_nodes(2,6)-a_nodes(2,8))^2);
l16=sqrt(l17^2+(a_nodes(2,7)-a_nodes(2,9))^2);
l15=sqrt(l17^2+(l17+a_nodes(2,8)-a_nodes(2,6))^2);
l21=l17;
l18=l17;
l20=l17;
l19=sqrt(l17^2+l20^2);
l22=l25+(a_nodes(2,5)-a_nodes(2,7))*(a_nodes(2,5)>a_nodes(2,7));
l24=l25+(a_nodes(2,7)-a_nodes(2,5))*(a_nodes(2,7)>a_nodes(2,5));
l23=sqrt(l22^2+l25^2);
l26=l25;
```

```
l28=l25;
l27=sqrt(l25^2+l28^2);
l29=l25;
l32=sqrt(l25^2+(h(2)-a_nodes(2,7)-a_nodes(2,16))^2);
l30=sqrt(l1^2+l2^2);
l31=sqrt(l1^2+(l5+a_nodes(2,3)-a_nodes(2,16))^2);
l33=sqrt(l17^2+(l17+a_nodes(2,9)-a_nodes(2,7))^2);
l34=sqrt(l17^2+l18^2);
l35=sqrt(l24^2+l25^2);
l36=sqrt(l25^2+l26^2);



%Preallocating
F=zeros(3,2);
Fv=zeros(3,1);

%Distance from center of D-region to the three edges
x=[h(3)/2-a(3,2)+l1+l4+(h(1)/2-a(1,1)*(N(3)==1)-a(1,2)*(N(30)==1))/(tan(
    theta(1))),h(3)/2-a(3,1)+l17+l20+(h(2)/2-a(2,1)*(N(19)==1)-a(2,2)*(N(34)
    ==1))/(tan(theta(2))),h(1)/2-a_nodes(2,5)+l22+l26+(h(3)/2-a(3,1)*(N(36)
    ==1)-a(3,2)*(N(27)==1))/(tan(theta(3)))];

%Calculation of loads at edges
for i=1:length(R(:,1)) %Obtaining inital forces for the STM
    n=R(i,1);
    v=R(i,2);
    m=R(i,3)-x(i)*v*(1-2*(i==2)); %The last parentheses takes account of
        the difference in definition of positive directions
    Fvv=abs(v/tan(theta(i)));
    F(i,2)=n*(h(i)/2-a(i,1))/(h(i)-a(i,1)-a(i,2))+m/(h(i)-a(i,1)-a(i,2))+
        Fvv*(h(i)/2-a(i,1))/(h(i)-a(i,1)-a(i,2));
    F(i,1)=(n-n*(h(i)/2-a(i,1))/(h(i)-a(i,1)-a(i,2)))-m/(h(i)-a(i,1)-a(i,2)
        )+(Fvv-Fvv*(h(i)/2-a(i,1))/(h(i)-a(i,1)-a(i,2)));
    Fv(i)=-abs(v/sin(theta(i)));
end

%Calculation of truss forces
N(1) = -Fv(1)*sin(theta(1))*(N(1)==1);
N(30) = -N(1)*l30/l1*(N(30)==1);
N(4) = (Fv(1)*cos(theta(1))*(N(30)==0)+F(1,1)-N(30)*l4/l30)*(N(4)==1);
N(3) = -N(1)*l3/l1*(N(3)==1);
N(2) = (F(1,2)-N(3)*l2/l3+Fv(1)*cos(theta(1))*(N(3)==0))*(N(2)==1);

N(5)=-1/(1+((a_nodes(2,5)-a_nodes(2,4))*(N(30)==0)*(N(31)==1)+(a_nodes
    (2,16)-a_nodes(2,3))*(N(3)==0)*(N(7)==1))/(l5+a_nodes(2,4)-a_nodes(2,5)-
    a_nodes(2,16)+a_nodes(2,3))) * (N(3)*l5/l3+N(30)*l5/l30+(a_nodes(2,5)-
```

```
    a_nodes(2,4))/l1*(N(4)+N(3)*l4/l3+(a_nodes(2,5)-a_nodes(2,4))/(l5+
    a_nodes(2,3)-a_nodes(2,16)-a_nodes(2,5)+a_nodes(2,4))*(N(4)+N(3)*l4/l3)
    *(N(31)==1))*(N(30)==0)+(a_nodes(2,16)-a_nodes(2,3))/l1*(N(2)+N(30)*l2/
    l30+(a_nodes(2,16)-a_nodes(2,3))/(l5+a_nodes(2,4)-a_nodes(2,5)-a_nodes
    (2,16)+a_nodes(2,3))*(N(2)+N(30)*l2/l30)*(N(7)==1))*(N(3)==0))*(N(5)==1)
    ;
N(31)=-l31/(l5+a_nodes(2,3)-a_nodes(2,16)-a_nodes(2,5)+a_nodes(2,4))*(N(5)
    +(a_nodes(2,5)-a_nodes(2,4))/l1*(N(4)+N(3)*l4/l3))*(N(31)==1);
N(7)=-l7/(l5+a_nodes(2,4)-a_nodes(2,5)-a_nodes(2,16)+a_nodes(2,3))*(N(5)+(
    a_nodes(2,16)-a_nodes(2,3))/l1*(N(2)+N(30)*l2/l30))*(N(7)==1);
N(6)=(N(2)+N(30)*l2/l30-N(7)*l1/l7)*l6/l1*(N(6)==1);
N(8)=(N(4)+N(3)*l4/l3-N(31)*l1/l31)*l8/l1*(N(8)==1);

N(21) = -Fv(2)*sin(theta(2))*(N(21)==1);
N(34) = -N(21)*l34/l21*(N(34)==1);
N(18) = (F(2,1)+Fv(2)*cos(theta(2))*(N(34)==0)-N(34)*l18/l34)*(N(18)==1);
N(19) = -N(21)*l19/l21*(N(19)==1);
N(20) = (F(2,2)-N(19)*l20/l19+Fv(2)*cos(theta(2))*(N(19)==0))*(N(20)==1);

N(17)=-1/(1+((a_nodes(2,7)-a_nodes(2,9))*(N(19)==0)*(N(15)==1)+(a_nodes
    (2,6)-a_nodes(2,8))*(N(34)==0)*(N(33)==1))/(l17+a_nodes(2,9)-a_nodes
    (2,7)-a_nodes(2,6)+a_nodes(2,8))) * (N(34)*l17/l34+N(19)*l17/l19+(
    a_nodes(2,7)-a_nodes(2,9))/l17*(N(20)+N(34)*l20/l34+(a_nodes(2,7)-
    a_nodes(2,9))/(l17+a_nodes(2,8)-a_nodes(2,6)-a_nodes(2,7)+a_nodes(2,9))
    *(N(20)+N(34)*l20/l34)*(N(15)==1))*(N(19)==0)+(a_nodes(2,6)-a_nodes(2,8)
    )/l17*(N(18)+N(19)*l18/l19+(a_nodes(2,6)-a_nodes(2,8))/(l17+a_nodes(2,9)
    -a_nodes(2,7)-a_nodes(2,6)+a_nodes(2,8))*(N(18)+N(19)*l18/l19)*(N(33)
    ==1))*(N(34)==0))*(N(17)==1);
N(15)=-l15/(l17+a_nodes(2,8)-a_nodes(2,6)-a_nodes(2,7)+a_nodes(2,9))*(N(17)
    +(a_nodes(2,7)-a_nodes(2,9))/l17*(N(20)+N(34)*l20/l34))*(N(15)==1);
N(33)=-l33/(l17+a_nodes(2,9)-a_nodes(2,7)-a_nodes(2,6)+a_nodes(2,8))*(N(17)
    +(a_nodes(2,6)-a_nodes(2,8))/l17*(N(18)+N(19)*l18/l19))*(N(33)==1);
N(14)=(N(18)+N(19)*l18/l19-N(33)*l17/l33)*l14/l17*(N(14)==1);
N(16)=(N(20)+N(34)*l20/l34-N(15)*l17/l15)*l16/l17*(N(16)==1);

N(29) = (-Fv(3)*sin(theta(3)))*(N(29)==1);
N(36) = -N(29)*l36/l29*(N(36)==1);
N(26) = (F(3,2)+Fv(3)*cos(theta(3))*(N(36)==0)-N(36)*l26/l36)*(N(26)==1);
N(27) = -N(29)*l27/l29*(N(27)==1);
N(28) = (F(3,1)-N(27)*l28/l27+Fv(3)*cos(theta(3))*(N(27)==0))*(N(28)==1);
N(25) = (-N(27)*l25/l27-N(36)*l25/l36)*(N(25)==1);
N(35) = -N(25)*l35/l25*(N(35)==1);
N(22) = (N(26)+N(27)*l26/l27-N(35)*l24/l35)*(N(22)==1);
N(23) = -N(25)*l23/l25*(N(23)==1);
N(24) = (N(28)-N(23)*l22/l23+N(36)*l28/l36)*(N(24)==1);

N(10)=l10/l25*((N(6)*l1/l6+N(31)*l1/l31-N(32)*l25/l32)*(N(32)==0)*(N(11)
```

```
    ~=0)+(N(14)*l17/l14+N(15)*l17/l15-N(11)*l25/l11)*(N(11)==0))*(N(10)==1);
N(12)=l12/l25*((N(8)*l1/l8+N(7)*l1/l7-N(23)*l25/l23-N(11)*l25/l11)*(N(11)
    ==0)*(N(32)~=0)+(N(16)*l17/l16+N(33)*l17/l33-N(35)*l25/l35-N(32)*l25/l32
    )*(N(32)==0))*(N(12)==1);
N(9)=(-(N(6)*(a_nodes(2,3)-a_nodes(2,16))/l6+N(31)*(l5+a_nodes(2,3)-a_nodes
    (2,16))/l31+N(10)*(a_nodes(2,6)-a_nodes(2,16))/l10)*(N(32)==0)+(N(22)+N
    (23)*l22/l23+N(12)*(a_nodes(2,5)-a_nodes(2,7))/l12+N(8)*(a_nodes(2,5)-
    a_nodes(2,4))/l8-N(7)*(l5+a_nodes(2,4)-a_nodes(2,5))/l7)*(N(11)==0)*(N
    (32)~=0))*(N(9)==1);
N(13)=(-(N(14)*(a_nodes(2,8)-a_nodes(2,6))/l14+N(15)*(l17+a_nodes(2,8)-
    a_nodes(2,6))/l15+N(10)*(a_nodes(2,16)-a_nodes(2,6))/l10)*(N(11)==0)+(N
    (24)+N(35)*l24/l35+N(12)*(a_nodes(2,7)-a_nodes(2,5))/l12+N(16)*(a_nodes
    (2,7)-a_nodes(2,9))/l16-N(33)*(l17+a_nodes(2,9)-a_nodes(2,7))/l33)*(N
    (32)==0)*(N(11)~=0))*(N(13)==1);
N(11)=-l11/(l13+a_nodes(2,7)-a_nodes(2,5)) * ((N(14)*(a_nodes(2,8)-a_nodes
    (2,6))/l14+N(15)*(l13+a_nodes(2,7)-a_nodes(2,9))/l15+N(13)+N(10)*(
    a_nodes(2,16)-a_nodes(2,6))/l10)*(N(9)~=0)+(N(7)*(l5+a_nodes(2,4)-
    a_nodes(2,5))/l7+N(8)*(a_nodes(2,4)-a_nodes(2,5))/l8+N(12)*(a_nodes(2,7)
    -a_nodes(2,5))/l12-N(22)-N(23)*l22/l23)*(N(9)==0))*(N(11)==1);
N(32)=-l32/(l9+a_nodes(2,5)-a_nodes(2,7)) * ((N(6)*(a_nodes(2,3)-a_nodes
    (2,16))/l6+N(31)*(l9+a_nodes(2,5)-a_nodes(2,4))/l31+N(9)+N(10)*(a_nodes
    (2,6)-a_nodes(2,16))/l10)*(N(13)~=0)+(N(33)*(l17+a_nodes(2,9)-a_nodes
    (2,7))/l33+N(16)*(a_nodes(2,9)-a_nodes(2,7))/l16+N(12)*(a_nodes(2,5)-
    a_nodes(2,7))/l12-N(24)-N(35)*l24/l35)*(N(13)==0))*(N(32)==1);

%%Sorting the lengths in array
l=[l1,l2,l3,l4,l5,l6,l7,l8,l9,l10,l11,l12,l13,l14,l15,l16,l17,l18,l19,l20,
    l21,l22,l23,l24,l25,l26,l27,l28,l29,l30,l31,l32,l33,l34,l35,l36];

end
```

Node Check

```
function [checked,w] = node_check(N_STM,F,l,b,a,a_nodes,fck)

%EC2 - Safety factors turned off in the thesis
yc=1;
acc=1;
%Material data
fcm=58; %Used as concrete strength in the thesis
fck=50; %For the calculation of upsilon. The imported fck is equal to fcm
    in the thesis, which means that fck has to be redefined
fcd=acc/yc*fcm;

%EC2 6.5.4
upsilon=1-fck/250;
k1=1;
```

```
k2=0.85;
k3=0.75;


%Here, the variable "node" indicates the active trusses in each node. The
%six forces representing the sectional forces are arranged from 37-42.
node=[1,1,1,zeros(1,33),0,1,zeros(1,4);%1
    1,0,0,1,zeros(1,25),1,zeros(1,6),1,zeros(1,5);%2
    0,1,0,0,1,1,1,zeros(1,22),1,zeros(1,6),zeros(1,6);%3
    0,0,1,1,1,0,0,1,zeros(1,22),1,zeros(1,5),zeros(1,6);%4
    zeros(1,6),1,1,1,0,1,1,zeros(1,9),1,1,zeros(1,13),zeros(1,6);%5
    zeros(1,9),1,1,0,1,1,1,zeros(1,21),zeros(1,6);%6
    zeros(1,11),1,1,0,0,1,zeros(1,7),1,zeros(1,7),1,1,0,1,0,zeros(1,6);%7
    zeros(1,13),1,0,0,1,1,1,zeros(1,13),1,0,0,0,zeros(1,6);%8
    zeros(1,14),1,1,1,0,0,1,zeros(1,13),1,0,0,zeros(1,6);%9
    zeros(1,17),1,0,0,1,zeros(1,12),1,0,0,0,0,1,0,0,0;%10
    zeros(1,18),1,1,1,zeros(1,15),zeros(1,3),1,0,0;%11
    zeros(1,21),1,0,0,1,1,1,zeros(1,7),1,0,zeros(1,6);%12
    zeros(1,22),1,1,1,0,0,1,zeros(1,7),1,zeros(1,6);%13
    zeros(1,25),1,0,0,1,zeros(1,6),1,zeros(1,5),1;%14
    zeros(1,26),1,1,1,zeros(1,7),zeros(1,4),1,0;%15
    zeros(1,5),1,0,0,1,1,zeros(1,20),1,1,zeros(1,4),zeros(1,6)];%16


%Making a common array for all forces in order to carry out the lines below
    .
F_nodes = [N_STM,F(1,:),F(2,:),F(3,:)];

%Checking number of ties anchored in each node
n_tension = sum(((node.*F_nodes)>0)');

%Max. allowed nodal stress
sigma_Rd_max = ((n_tension>1)'*k3+(n_tension==1)'*k2+(n_tension==0)'*k1)*
    fcd*upsilon; %Max. allowed nodal stress

%Necessary width
w = -(node.*F_nodes)./(b.*sigma_Rd_max);

%storing the w matrix while temporarily changing all signs to positive
w_store = w;
w=w.*(w>0);


%Calcuation of maximum allowed widths in nodes. s1,s2,... are the angles
%between various trusses. They are named alpha1,alpha2,... in thesis

%node1
```

```
wmax(1,38) = 2*a(1,2); %F2
wmax(1,2) = min([2*a(1,2) , tan(pi/4)*(l(1)-w(1,3)/sin(pi/4))]);
wmax(1,3) = min([sin(pi/4)*(l(1)-w(1,1)/tan(pi/4)) , sin(pi/4)*(l(1)-w(1,2)
    /tan(pi/4))]);
wmax(1,1) = 0;

%node2
wmax(2,37) = 2*a(1,1); %F1
wmax(2,4) = min([2*a(1,1) , tan(pi/4)*(l(1)-w(2,30)/sin(pi/4))]);
wmax(2,30) = min([sin(pi/4)*(l(1)-w(2,1)/tan(pi/4)) , sin(pi/4)*(l(1)-w
    (2,4)/tan(pi/4))]);
wmax(2,1) = 0;

%node3
s1=acos(l(1)/l(6));
s2=atan(l(1)/(l(5)+a_nodes(2,5)-a_nodes(2,4)));
s3=acos(l(5)/l(30));

wmax(3,2) = min([2*a(1,2) , tan(pi/4)*(l(1)-w(3,30)/sin(pi/4)) , l(5)]);
wmax(3,30) = min([sin(pi/2-s3)*(l(1)-w(3,2)/tan(pi/2-s3)) , sin(s3)*(l(5)-w
    (3,5)/tan(s3))]);
wmax(3,5) = 0;
wmax(3,7) = min([sin(s2)*(l(5)-w(3,5)/tan(s2)) , sin(pi/2-s2+sign(a_nodes
    (2,3)-a_nodes(2,16))*s1)*(l(1)/cos(s1)-w(3,6)/tan(pi/2-s2+sign(a_nodes
    (2,3)-a_nodes(2,16))*s1)-sign(a_nodes(2,3)-a_nodes(2,16))*w(3,6)*tan(pi
    /2-s2+sign(a_nodes(2,3)-a_nodes(2,16))*s1))]);
wmax(3,6) = min([(2*a(1,2)-sign(a_nodes(2,3)-a_nodes(2,16)))/cos(s1) , tan(
    pi/2-s2+sign(a_nodes(2,3)-a_nodes(2,16))*s1)/(1+tan(pi/2-s2+s1)*tan(s1)
    *(a_nodes(2,16)>a_nodes(2,3)))*(l(1)/cos(s1)-w(3,7)/sin(pi/2-s2+sign(
    a_nodes(2,3)-a_nodes(2,16))*s1)) , cos(s1)*(l(5)+l(1)*tan(s1))]);

%node4
s1=acos(l(1)/l(8));
s2=atan(l(1)/(l(5)+a_nodes(2,16)-a_nodes(2,3)));
s3=acos(l(5)/l(3));

wmax(4,4) = min([2*a(1,1) , tan(pi/4)*(l(1)-w(4,3)/sin(pi/4)) , l(5)]);
wmax(4,3) = min([sin(pi/2-s3)*(l(1)-w(4,4)/tan(pi/2-s3)) , sin(s3)*(l(5)-w
    (4,5)/tan(s3))]);
wmax(4,5) = 0;
wmax(4,31) = min([sin(s2)*(l(5)-w(4,5)/tan(s2)) , sin(pi/2-s2+sign(a_nodes
    (2,4)-a_nodes(2,5))*s1)*(l(1)/cos(s1)-w(4,8)/tan(pi/2-s2+sign(a_nodes
    (2,4)-a_nodes(2,5))*s1)-sign(a_nodes(2,4)-a_nodes(2,5))*w(4,8)*tan(pi/2-
    s2+sign(a_nodes(2,4)-a_nodes(2,5))*s1))]);
wmax(4,8) = min([(2*a(1,1)-sign(a_nodes(2,4)-a_nodes(2,5)))/cos(s1) , tan(
    pi/2-s2+sign(a_nodes(2,4)-a_nodes(2,5))*s1)/(1+tan(pi/2-s2+s1)*tan(s1)*(
    a_nodes(2,5)>a_nodes(2,4)))*(l(1)/cos(s1)-w(4,31)/sin(pi/2-s2+sign(
```

```
    a_nodes(2,4)-a_nodes(2,5))*s1)) , cos(s1)*(l(5)+l(1)*tan(s1))]);
91
92  %node 5
93  s2=atan(abs(a_nodes(2,7)-a_nodes(2,5))/l(25));
94  s3=atan(l(25)/(l(9)+a_nodes(2,16)-a_nodes(2,6)));
95  s4=acos((l(12)^2+l(23)^2-l(24)^2)/(2*l(12)*l(23)));
96  s5=atan(abs(a_nodes(2,4)-a_nodes(2,5))/l(1));
97  s6=acos((l(9)+a_nodes(2,16)-a_nodes(2,3))/l(7));
98
99  wmax(5,22) =min([2*a(3,2) , tan(pi/2-s4)*(l(22)-w(5,23)/sin(pi/2-s4)) , l
        (25)]);
100 wmax(5,23) =min([sin(pi/2-s4)*(l(22)-w(5,22)/tan(pi/2-s4)) , sin(s4+sign(
        a_nodes(2,7)-a_nodes(2,5))*s2)*(l(25)/cos(s2)-w(5,12)/tan(s4+sign(
        a_nodes(2,7)-a_nodes(2,5))*s2)-sign(a_nodes(2,7)-a_nodes(2,5))*w(5,12)*
        tan(s2))]);
101 wmax(5,12) =min([tan(s4+sign(a_nodes(2,7)-a_nodes(2,5))*s2)/(1+tan(s2)*tan(
        s4+s2)*(a_nodes(2,7)>a_nodes(2,5)))*(l(25)/cos(s2)-w(5,23)/sin(s4+sign(
        a_nodes(2,7)-a_nodes(2,5))*s2)) , tan(pi/2-sign(a_nodes(2,7)-a_nodes
        (2,5))*s2-s3)/(1+tan(s2)*tan(pi/2+s2-s3)*(a_nodes(2,5)>a_nodes(2,7)))*(l
        (25)/cos(s2)-w(5,11)/sin(pi/2-sign(a_nodes(2,7)-a_nodes(2,5))*s2-s3))]);
102 wmax(5,11) =min([sin(pi/2-sign(a_nodes(2,7)-a_nodes(2,5))*s2-s3)*(l(25)/cos
        (s2)-w(5,12)/tan(pi/2-sign(a_nodes(2,7)-a_nodes(2,5))*s2-s3)+sign(
        a_nodes(2,7)-a_nodes(2,5))*w(5,12)*tan(s2)) , sin(s3)*(l(9)-w(5,9)/tan(
        s3))]);
103 wmax(5,9) =min([tan(s3)*(l(9)-w(5,11)/sin(s3)) , tan(s4)*(l(9)-w(5,7)/sin(
        s4))]);
104 wmax(5,7) =min([sin(s6)*(l(9)-w(5,9)/tan(s6)) , sin(pi/2-s4-sign(a_nodes
        (2,4)-a_nodes(2,5))*s5)*(l(1)/cos(s5)-w(5,8)/tan(pi/2-s4-sign(a_nodes
        (2,4)-a_nodes(2,5))*s5)+sign(a_nodes(2,4)-a_nodes(2,5))*w(5,8)*tan(s5))
        ]);
105 wmax(5,8) =min([tan(pi/2-sign(a_nodes(2,4)-a_nodes(2,5))*s5-s4)/(1+tan(pi
        /2+s5-s4)*tan(s5)*(a_nodes(2,5)>a_nodes(2,4)))*(l(1)/cos(s5)-w(5,7)/sin(
        pi/2-sign(a_nodes(2,4)-a_nodes(2,5))*s5-s4)) , (2*a(1,1)+2*a(3,2)*tan(s5
        ))*cos(s5)*(a_nodes(2,4)>a_nodes(2,5))+(2*a(1,1)-l(1)*tan(s5))*(a_nodes
        (2,5)>=a_nodes(2,4)) , cos(s5)*(l(9)+l(1)*tan(s5))]);
106
107 %node 6
108 s7=atan(abs(a_nodes(2,8)-a_nodes(2,6))/l(17));
109 s8=atan(l(17)/(l(17)+a_nodes(2,5)-a_nodes(2,4)));
110 s9=atan(l(25)/(l(13)+a_nodes(2,5)-a_nodes(2,7)));
111 s10=atan(abs(a_nodes(2,16)-a_nodes(2,6))/l(25));
112
113 wmax(6,14) = min([cos(s7)*(2*a_nodes(2,6)+sign(a_nodes(2,8)-a_nodes(2,6))*l
        (17)*tan(s7)) , tan(pi/2-s8-sign(a_nodes(2,8)-a_nodes(2,6))*s7)/(1+tan(
        pi/2-s8+s7)*tan(s7)*(a_nodes(2,6)>a_nodes(2,8)))*(l(17)/cos(s7)-w(6,15)/
        sin(pi/2-s8-sign(a_nodes(2,8)-a_nodes(2,6))*s7)) , cos(s7)*(l(13)+l(17)*
        tan(s7))]);
```

```
114 wmax(6,15) = min([sin(pi/2-sign(a_nodes(2,8)-a_nodes(2,6))*s7-s8)*(l(17)/
        cos(s7)-w(6,14)/tan(pi/2-sign(a_nodes(2,8)-a_nodes(2,6))*s7-s8)+sign(
        a_nodes(2,8)-a_nodes(2,6))*w(6,14)*tan(s7)) , sin(s8)*(l(13)-w(6,13)/tan
        (s8))]);
115 wmax(6,13) = min([tan(s8)*(l(13)-w(6,15)/sin(s8)) , tan(s9)*(l(13)-w(6,11)/
        sin(s9)) , l(17) , l(25)]);
116 wmax(6,11) = min([sin(s9)*(l(13)-w(6,13)/tan(s9)) , sin(pi/2-sign(a_nodes
        (2,16)-a_nodes(2,6))*s10-s9)*(l(25)/cos(s10)-w(6,10)/tan(pi/2-sign(
        a_nodes(2,16)-a_nodes(2,6))*s10-s9)+sign(a_nodes(2,16)-a_nodes(2,6))*w
        (6,10)*tan(s10))]);
117 wmax(6,10) = min([cos(s10)*(2*a_nodes(2,6)+sign(a_nodes(2,16)-a_nodes(2,6))
        *l(25)*tan(s10)) , tan(pi/2-s9-sign(a_nodes(2,16)-a_nodes(2,6))*s10)/(1+
        tan(pi/2-s9-sign(a_nodes(2,16)-a_nodes(2,6))*s10)*tan(s10)*(a_nodes(2,6)
        >a_nodes(2,16)))*(l(25)/cos(s10)-w(6,11)/sin(pi/2-s9-sign(a_nodes(2,16)-
        a_nodes(2,6))*s10)) , cos(s10)*(l(13)+l(25)*tan(s10))]);
118
119 %node 7
120 s2=atan(abs(a_nodes(2,5)-a_nodes(2,7))/l(25));
121 s3=atan(l(25)/(l(13)+a_nodes(2,6)-a_nodes(2,16)));
122 s4=acos((l(12)^2+l(35)^2-l(22)^2)/(2*l(12)*l(35)));
123 s5=atan(abs(a_nodes(2,9)-a_nodes(2,7))/l(17));
124 s6=acos((l(13)+a_nodes(2,6)-a_nodes(2,8))/l(33));
125
126 wmax(7,24) =min([2*a(3,1) , tan(pi/2-s4)*(l(24)-w(7,35)/sin(pi/2-s4)) , l
        (25)]);
127 wmax(7,35) =min([sin(pi/2-s4)*(l(24)-w(7,24)/tan(pi/2-s4)) , sin(s4+sign(
        a_nodes(2,5)-a_nodes(2,7))*s2)*(l(25)/cos(s2)-w(7,12)/tan(s4+sign(
        a_nodes(2,5)-a_nodes(2,7))*s2)-sign(a_nodes(2,5)-a_nodes(2,7))*w(7,12)*
        tan(s2))]);
128 wmax(7,12) =min([tan(s4+sign(a_nodes(2,5)-a_nodes(2,7))*s2)/(1+tan(s2)*tan(
        s4+s2)*(a_nodes(2,5)>a_nodes(2,7)))*(l(25)/cos(s2)-w(7,35)/sin(s4+sign(
        a_nodes(2,5)-a_nodes(2,7))*s2)) , tan(pi/2-sign(a_nodes(2,5)-a_nodes
        (2,7))*s2-s3)/(1+tan(s2)*tan(pi/2+s2-s3)*(a_nodes(2,7)>a_nodes(2,5)))*(l
        (25)/cos(s2)-w(7,32)/sin(pi/2-sign(a_nodes(2,5)-a_nodes(2,7))*s2-s3))]);
129 wmax(7,32) =min([sin(pi/2-s2-s3)*(l(25)/cos(s2)-w(7,12)/tan(pi/2-s2-s3)+
        sign(a_nodes(2,5)-a_nodes(2,7))*w(7,12)*tan(s2)) , sin(s3)*(l(13)-w
        (7,13)/tan(s3))]);
130 wmax(7,13) =min([tan(s3)*(l(13)-w(7,32)/sin(s3)) , tan(s4)*(l(13)-w(7,33)/
        sin(s4))]);
131 wmax(7,33) =min([sin(s6)*(l(13)-w(7,13)/tan(s6)) , sin(pi/2-s4-sign(a_nodes
        (2,9)-a_nodes(2,7))*s5)*(l(1)/cos(s5)-w(7,16)/tan(pi/2-s4-sign(a_nodes
        (2,9)-a_nodes(2,7))*s5)+sign(a_nodes(2,9)-a_nodes(2,7))*w(7,16)*tan(s5))
        ]);
132 wmax(7,16) =min([tan(pi/2-sign(a_nodes(2,9)-a_nodes(2,7))*s5-s4)/(1+tan(pi
        /2+s5-s4)*tan(s5)*(a_nodes(2,7)>a_nodes(2,9)))*(l(1)/cos(s5)-w(7,33)/sin
        (pi/2-sign(a_nodes(2,9)-a_nodes(2,7))*s5-s4)) , (2*a(2,2)+2*a(3,1)*tan(
        s5))*cos(s5)*(a_nodes(2,9)>a_nodes(2,7))+(2*a(2,2)-l(17)*tan(s5))*(
```

```
    a_nodes(2,7)>=a_nodes(2,9)) , cos(s5)*(l(13)+l(1)*tan(s5))]);
133
134 %node8
135 s1=acos(l(17)/l(14));
136 s2=atan(l(17)/(l(17)+a_nodes(2,7)-a_nodes(2,9)));
137 s3=acos(l(17)/l(19));
138
139 wmax(8,18) = min([2*a(2,1) , tan(pi/4)*(l(17)-w(4,19)/sin(pi/4)) , l(17)]);
140 wmax(8,19) = min([sin(pi/2-s3)*(l(17)-w(8,18)/tan(pi/2-s3)) , sin(s3)*(l
    (17)-w(8,17)/tan(s3))]);
141 wmax(8,17) = 0;
142 wmax(8,33) = min([sin(s2)*(l(17)-w(8,17)/tan(s2)) , sin(pi/2-s2+sign(
    a_nodes(2,8)-a_nodes(2,6))*s1)*(l(17)/cos(s1)-w(8,14)/tan(pi/2-s2+sign(
    a_nodes(2,8)-a_nodes(2,6))*s1)-sign(a_nodes(2,8)-a_nodes(2,6))*w(8,14)*
    tan(pi/2-s2+sign(a_nodes(2,8)-a_nodes(2,6))*s1))]);
143 wmax(8,14) = min([(2*a(2,1)-sign(a_nodes(2,8)-a_nodes(2,6)))/cos(s1) , tan(
    pi/2-s2+sign(a_nodes(2,8)-a_nodes(2,6))*s1)/(1+tan(pi/2-s2+s1)*tan(s1)*(
    a_nodes(2,6)>a_nodes(2,8)))*(l(17)/cos(s1)-w(8,33)/sin(pi/2-s2+sign(
    a_nodes(2,8)-a_nodes(2,6))*s1)) , cos(s1)*(l(17)+l(17)*tan(s1))]);
144
145 %node9
146 s1=acos(l(17)/l(16));
147 s2=atan(l(17)/(l(17)+a_nodes(2,6)-a_nodes(2,8)));
148 s3=acos(l(17)/l(34));
149
150 wmax(9,20) = min([2*a(2,2) , tan(pi/4)*(l(17)-w(4,34)/sin(pi/4)) , l(17)]);
151 wmax(9,34) = min([sin(pi/2-s3)*(l(17)-w(9,20)/tan(pi/2-s3)) , sin(s3)*(l
    (17)-w(9,17)/tan(s3))]);
152 wmax(9,17) = 0;
153 wmax(9,15) = min([sin(s2)*(l(17)-w(9,17)/tan(s2)) , sin(pi/2-s2+sign(
    a_nodes(2,9)-a_nodes(2,7))*s3)*(l(17)/cos(s1)-w(9,16)/tan(pi/2-s2+sign(
    a_nodes(2,9)-a_nodes(2,7))*s3)-sign(a_nodes(2,9)-a_nodes(2,7))*w(9,16)*
    tan(pi/2-s2+sign(a_nodes(2,9)-a_nodes(2,7))*s3))]);
154 wmax(9,16) = min([(2*a(2,2)-sign(a_nodes(2,9)-a_nodes(2,7)))/cos(s1) , tan(
    pi/2-s2+sign(a_nodes(2,9)-a_nodes(2,7))*s1)/(1+tan(pi/2-s2+s1)*tan(s1)*(
    a_nodes(2,7)>a_nodes(2,9)))*(l(17)/cos(pi/2-s2)-w(9,15)/sin(pi/2-s2+sign
    (a_nodes(2,9)-a_nodes(2,7))*s1)) , cos(s1)*(l(17)+l(17)*tan(s1))]);
155
156 %node10
157 wmax(10,39) = 2*a(2,1);%F3
158 wmax(10,18) = min([2*a(2,1) , tan(pi/4)*(l(21)-w(10,34)/sin(pi/4))]);
159 wmax(10,34) = min([sin(pi/4)*(l(21)-w(10,21)/tan(pi/4)) , sin(pi/4)*(l(21)-
    w(10,18)/tan(pi/4))]);
160 wmax(10,21) = 0;
161
162 %node11
163 wmax(11,40) = 2*a(2,2);%F4
```

```
wmax(11,20) = min([2*a(2,2) , tan(pi/4)*(l(21)-w(11,19)/sin(pi/4))]);
wmax(11,19) = min([sin(pi/4)*(l(21)-w(11,21)/tan(pi/4)) , sin(pi/4)*(l(21)-
    w(11,20)/tan(pi/4))]);
wmax(11,21) = 0;

%node12
s1=atan(l(25)/(l(22)+a_nodes(2,5)-a_nodes(2,7)));
s2=acos(l(26)/l(27));

wmax(12,22) = min([2*a(3,2) , tan(s1)*(l(22)-w(12,35)/sin(s1)) , l(25)]);
wmax(12,35) = min([sin(s1)*(l(22)-w(12,22)/tan(s1)) , sin(pi/2-s1)*(l(25)-w
    (12,25)/tan(pi/2-s1))]);
wmax(12,25) = 0;
wmax(12,27) = min([sin(s2)*(l(25)-w(12,26)/tan(s2)) , sin(pi/2-s2)*(l(25)-w
    (12,25)/tan(pi/2-s2))]);
wmax(12,26) = min([2*a(3,2) , tan(s2)*(l(25)-w(12,27)/sin(s2)) , l(25)]);

%node13
s1=atan(l(25)/(l(24)+a_nodes(2,7)-a_nodes(2,5)));
s2=acos(l(28)/l(36));

wmax(13,24) = min([2*a(3,1) , tan(s1)*(l(24)-w(13,23)/sin(s1)) , l(25)]);
wmax(13,23) = min([sin(s1)*(l(24)-w(13,24)/tan(s1)) , sin(pi/2-s1)*(l(25)-w
    (13,25)/tan(pi/2-s1))]);
wmax(13,25) = 0;
wmax(13,36) = min([sin(s2)*(l(25)-w(13,28)/tan(s2)) , sin(pi/2-s2)*(l(25)-w
    (13,25)/tan(pi/2-s2))]);
wmax(13,28) = min([2*a(3,1) , tan(s2)*(l(25)-w(13,36)/sin(s2)) , l(25)]);

%node14
wmax(14,42) = 2*a(3,2);%F6
wmax(14,26) = min([2*a(3,2) , tan(pi/4)*(l(25)-w(14,36)/sin(pi/4))]);
wmax(14,36) = min([sin(pi/4)*(l(25)-w(14,26)/tan(pi/4)) , sin(pi/4)*(l(29)-
    w(14,29)/tan(pi/4))]);
wmax(14,29) = 0;

%node15
wmax(15,41) = 2*a(3,1);%F5
wmax(15,28) = min([2*a(3,1) , tan(pi/4)*(l(25)-w(15,27)/sin(pi/4))]);
wmax(15,27) = min([sin(pi/4)*(l(25)-w(15,28)/tan(pi/4)) , sin(pi/4)*(l(29)-
    w(15,29)/tan(pi/4))]);
wmax(15,29) = 0;

%node 16
s7=atan(abs(a_nodes(2,3)-a_nodes(2,16))/l(1));
s8=atan(l(1)/(l(1)+a_nodes(2,5)-a_nodes(2,4)));
s9=atan(l(25)/(l(9)+a_nodes(2,5)-a_nodes(2,7)));
```

```
s10=atan(abs(a_nodes(2,6)-a_nodes(2,16))/l(25));

wmax(16,6) = min([cos(s7)*(2*a_nodes(2,16)+sign(a_nodes(2,3)-a_nodes(2,16))*l(1)*tan(s7)) , tan(pi/2-s8-sign(a_nodes(2,3)-a_nodes(2,16))*s7)/(1+tan(pi/2-s8+s7)*tan(s7)*(a_nodes(2,16)>a_nodes(2,3)))*(l(1)/cos(s7)-w(16,31)/sin(pi/2-s8-sign(a_nodes(2,3)-a_nodes(2,16))*s7)) , cos(s7)*(l(9)+l(1)*tan(s7))]);
wmax(16,31) = min([sin(pi/2-sign(a_nodes(2,3)-a_nodes(2,16))*s7-s8)*(l(1)/cos(s7)-w(16,6)/tan(pi/2-sign(a_nodes(2,3)-a_nodes(2,16))*s7-s8)+sign(a_nodes(2,3)-a_nodes(2,16))*w(16,6)*tan(s7)) , sin(s8)*(l(9)-w(16,9)/tan(s8))]);
wmax(16,9) = min([tan(s8)*(l(9)-w(16,31)/sin(s8)) , tan(s9)*(l(9)-w(16,32)/sin(s9)) , l(1) , l(25)]);
wmax(16,32) = min([sin(s9)*(l(9)-w(16,9)/tan(s9)) , sin(pi/2-sign(a_nodes(2,6)-a_nodes(2,16))*s10-s9)*(l(25)/cos(s10)-w(16,10)/tan(pi/2-sign(a_nodes(2,6)-a_nodes(2,16))*s10-s9)+sign(a_nodes(2,6)-a_nodes(2,16))*w(16,10)*tan(s10))]);
wmax(16,10) = min([cos(s10)*(2*a_nodes(2,16)+sign(a_nodes(2,6)-a_nodes(2,16))*l(25)*tan(s10)) , tan(pi/2-s9-sign(a_nodes(2,6)-a_nodes(2,16))*s10)/(1+tan(pi/2-s9-sign(a_nodes(2,6)-a_nodes(2,16))*s10)*tan(s10)*(a_nodes(2,16)>a_nodes(2,6)))*(l(25)/cos(s10)-w(16,32)/sin(pi/2-s9-sign(a_nodes(2,6)-a_nodes(2,16))*s10)) , cos(s10)*(l(9)+l(25)*tan(s10))]);



%Setting the lowest value of wmax from the two nodes of each strut as wmax
%in both nodes
wmax=(wmax~=0).*min((wmax==0).*max(wmax)+wmax);

%w=0 in ties
w=w_store;
w=w.*((node.*F_nodes)<0);

%A check is conducted widths and the two trusses which are not allowed to
%be ties (11 & 32)
checked=sum(sum((w./(wmax+(wmax==0)).*(1-(wmax==0)))>1.01))+(N_STM(11)>0)+(N_STM(32)>0);

end
```

Force Check

```
function check = force_check(N,F,Fv,theta,l,a_nodes)

%Predefining
eq=0*a_nodes;

```

```
%Node 1
eq(1,1)=N(2)+N(3)*l(2)/l(3)-F(1,2)-Fv(1)*cos(theta(1))*(N(3)==0);
eq(2,1)=N(1)+N(3)*l(1)/l(3)+Fv(1)*sin(theta(1))*(N(3)==0);
%Node 2
eq(1,1)=N(4)+N(30)*l(4)/l(30)-F(1,1)-Fv(1)*cos(theta(1))*(N(30)==0);
eq(2,1)=N(1)+N(30)*l(1)/l(30)+Fv(1)*sin(theta(1))*(N(30)==0);
%Node 3
eq(1,3)=N(6)*l(1)/l(6)+N(7)*l(1)/l(7)-N(30)*l(1)/l(30)-N(2);
eq(2,3)=N(30)*l(5)/l(30)+N(5)+N(7)*(l(5)+a_nodes(2,4)-a_nodes(2,5))/l(7)+N
    (6)*(a_nodes(2,16)-a_nodes(2,3))/l(6);
%Node 4
eq(1,4)=N(8)*l(1)/l(8)+N(31)*l(1)/l(31)-N(3)*l(1)/l(3)-N(4);
eq(2,4)=N(3)*l(5)/l(3)+N(5)+N(31)*(l(5)+a_nodes(2,3)-a_nodes(2,16))/l(31)+N
    (8)*(a_nodes(2,5)-a_nodes(2,4))/l(8);
%Node 5
eq(1,5)=N(12)*l(25)/l(12)+N(23)*l(25)/l(23)+N(11)*l(25)/l(11)-N(8)*l(1)/l
    (8)-N(7)*l(1)/l(7);
eq(2,5)=N(22)-N(9)+N(23)*l(22)/l(23)+N(12)*(a_nodes(2,5)-a_nodes(2,7))/l
    (12)-N(11)*(l(13)+a_nodes(2,7)-a_nodes(2,5))/l(11)-N(7)*(l(5)+a_nodes
    (2,4)-a_nodes(2,5))/l(7)+N(8)*(a_nodes(2,5)-a_nodes(2,4))/l(8);
%Node 6
eq(1,6)=-N(15)*l(17)/l(15)+N(11)*l(25)/l(11)+N(10)*l(25)/l(10)-N(14)*l(17)/
    l(14);
eq(2,6)=N(13)+N(15)*(l(17)+a_nodes(2,8)-a_nodes(2,6))/l(15)+N(11)*(l(13)+
    a_nodes(2,7)-a_nodes(2,5))/l(11)+N(14)*(a_nodes(2,8)-a_nodes(2,6))/l(14)
    +N(10)*(a_nodes(2,16)-a_nodes(2,6))/l(10);
%Node 7
eq(1,7)=N(12)*l(25)/l(12)+N(35)*l(25)/l(35)+N(32)*l(25)/l(32)-N(16)*l(17)/l
    (16)-N(33)*l(17)/l(33);
eq(2,7)=N(24)-N(13)+N(35)*l(24)/l(35)+N(12)*(a_nodes(2,7)-a_nodes(2,5))/l
    (12)-N(32)*(l(9)+a_nodes(2,5)-a_nodes(2,7))/l(32)-N(33)*(l(17)+a_nodes
    (2,9)-a_nodes(2,7))/l(33)+N(16)*(a_nodes(2,7)-a_nodes(2,9))/l(16);
%Node 8
eq(1,8)=N(14)*l(17)/l(14)+N(33)*l(17)/l(33)-N(19)*l(17)/l(19)-N(18);
eq(2,8)=N(19)*l(17)/l(19)+N(17)+N(33)*(l(17)+a_nodes(2,9)-a_nodes(2,7))/l
    (33)+N(14)*(a_nodes(2,6)-a_nodes(2,8))/l(14);
%Node 9
eq(1,9)=N(16)*l(17)/l(16)+N(15)*l(17)/l(15)-N(34)*l(17)/l(34)-N(20);
eq(2,9)=N(34)*l(17)/l(34)+N(17)+N(15)*(l(17)+a_nodes(2,8)-a_nodes(2,6))/l
    (15)+N(16)*(a_nodes(2,7)-a_nodes(2,9))/l(16);
%Node 10
eq(1,10)=F(2,1)+Fv(2)*cos(theta(2))*(N(34)==0)-N(34)*l(18)/l(34)-N(18);
eq(2,10)=Fv(2)*sin(theta(2))*(N(34)==0)+N(21)+N(34)*l(21)/l(34);
%Node 11
eq(1,11)=F(2,2)+Fv(2)*cos(theta(2))*(N(19)==0)-N(19)*l(20)/l(19)-N(20);
eq(2,11)=Fv(2)*sin(theta(2))*(N(19)==0)+N(21)+N(19)*l(21)/l(19);
%Node 12
```

```
eq(1,12)=N(27)*l(25)/l(27)+N(25)+N(35)*l(25)/l(35);
eq(2,12)=N(26)+N(27)*l(26)/l(27)-N(35)*l(24)/l(35)-N(22);
%Node 13
eq(1,13)=N(36)*l(25)/l(36)+N(25)+N(23)*l(25)/l(23);
eq(2,13)=N(28)+N(36)*l(28)/l(36)-N(23)*l(22)/l(23)-N(24);
%Node 14
eq(1,14)=N(29)+Fv(3)*sin(theta(3))*(N(36)==0)+N(36)*l(29)/l(36);
eq(2,14)=F(3,2)+Fv(3)*cos(theta(3))*(N(36)==0)-N(26)-N(36)*l(26)/l(36);
%Node 15
eq(1,15)=N(29)+Fv(3)*sin(theta(3))*(N(27)==0)+N(27)*l(29)/l(27);
eq(2,15)=F(3,1)+Fv(3)*cos(theta(3))*(N(27)==0)-N(28)-N(27)*l(28)/l(27);
%Node 16
eq(1,16)=-N(31)*l(1)/l(31)+N(32)*l(25)/l(32)+N(10)*l(25)/l(10)-N(6)*l(1)/l
    (6);
eq(2,16)=N(9)+N(31)*(l(5)+a_nodes(2,3)-a_nodes(2,16))/l(31)+N(32)*(l(13)+
    a_nodes(2,6)-a_nodes(2,16))/l(32)+N(6)*(a_nodes(2,3)-a_nodes(2,16))/l(6)
    +N(10)*(a_nodes(2,6)-a_nodes(2,16))/l(10);

%Check of forces in nodes
check=sum(sum(abs(eq)>max(abs(N))*4*10^(-3)));
end
```

Draw STM

```
function draw_STM(N,l,a_nodes)




base_x = [0 0 l(4) l(4)+l(1) l(4)+l(1)+l(25) l(4)+l(1)+l(25)+l(17) l(4)+l
    (1)+l(25)+l(17)+l(20) l(4)+l(1)+l(25)+l(17)+l(20) l(4)+l(1)+l(25)+l(17)+
    l(20)-l(18) l(4)+l(1)+l(25)+l(20)-l(18) l(4)+l(1)+l(20)-l(18) l(4)+l(20)
    -l(18) l(4)+l(20)-l(18)-l(2)];
base_y = [a_nodes(2,1) a_nodes(2,1)+l(1) a_nodes(2,3)+l(5) a_nodes(2,16)+l
    (9) a_nodes(2,6)+l(13) a_nodes(2,8)+l(17) a_nodes(2,10)+l(21) a_nodes
    (2,10) a_nodes(2,8) a_nodes(2,6) a_nodes(2,16) a_nodes(2,3) a_nodes(2,1)
    ];

top_x = [l(4)+l(1) l(4)+l(1) l(4)+l(1) l(4)+l(1)+l(29) l(4)+l(1)+l(29) l(4)
    +l(1)+l(29) l(4)+l(1)];
top_y = [a_nodes(2,16)+l(9) a_nodes(2,16)+l(9)+l(22) a_nodes(2,16)+l(9)+l
    (22)+l(26) a_nodes(2,16)+l(9)+l(22)+l(26) a_nodes(2,16)+l(9)+l(22)+l(26)
    -l(28) a_nodes(2,16)+l(9)+l(22)+l(26)-l(28)-l(24) a_nodes(2,16)+l(9)];
shear_left_x = [0 l(2)*(N(3)==1) l(2)*(N(3)==1) (l(2)+l(1))*(N(3)==1) (l(2)
    +l(1))*(N(30)==0) (l(2)+l(1))*(N(30)==0)+l(2)*(N(30)==1) (l(2)+l(1))*(N
    (30)==0)+l(2)*(N(30)==1) (l(2)+l(1))*(N(30)==0)+(l(2)+l(1))*(N(30)==1) (
    l(2)+l(1))*(N(30)==0)+(l(2)+l(1))*(N(30)==1) (l(2)+l(1))*(N(30)==0)+(l
```

```
    (2)+l(1))*(N(30)==1)];
shear_left_y = [a_nodes(2,1) a_nodes(2,1)*(N(3)==0)+(a_nodes(2,3)+l(5))*(N
    (3)==1) a_nodes(2,1)*(N(3)==0)+a_nodes(2,3)*(N(3)==1) a_nodes(2,1)*(N(3)
    ==0)+(a_nodes(2,16)+l(9))*(N(3)==1) (a_nodes(2,16)+l(9))*(N(30)==0)+(
    a_nodes(2,1)+l(1))*(N(30)==1) (a_nodes(2,16)+l(9))*(N(30)==0)+a_nodes
    (2,3)*(N(30)==1) (a_nodes(2,16)+l(9))*(N(30)==0)+(a_nodes(2,3)+l(5))*(N
    (30)==1) (a_nodes(2,16)+l(9))*(N(30)==0)+a_nodes(2,16)*(N(30)==1) ((
    a_nodes(2,16)+l(9))*(N(30)==0)+a_nodes(2,16)*(N(30)==1))*(N(9)==0)+
    a_nodes(2,16)*(N(9)==1) ((a_nodes(2,16)+l(9))*(N(30)==0)+a_nodes(2,16)*(
    N(30)==1))*(N(9)==0)+(a_nodes(2,16)+l(9))*(N(9)==1)];

shear_right_x = [(l(4)+l(1)+l(25)+l(17)+l(20)) (l(4)+l(1)+l(25)+l(17)+l(20)
    )*(N(34)==0)+(l(4)+l(1)+l(25)+l(17))*(N(34)==1) (l(4)+l(1)+l(25)+l(17)+l
    (20))*(N(34)==0)+(l(4)+l(1)+l(25)+l(17))*(N(34)==1) (l(4)+l(1)+l(25)+l
    (17)+l(20))*(N(34)==0)+(l(4)+l(1)+l(25))*(N(34)==1) (l(4)+l(1)+l(25))*(N
    (19)==0)+(l(4)+l(1)+l(25)+l(17)+l(20))*(N(19)==1) (l(4)+l(1)+l(25))*(N
    (19)==0)+(l(4)+l(1)+l(25)+l(17))*(N(19)==1) (l(4)+l(1)+l(25))*(N(19)==0)
    +(l(4)+l(1)+l(25)+l(17))*(N(19)==1) (l(4)+l(1)+l(25))*(N(19)==0)+(l(4)+l
    (1)+l(25))*(N(19)==1) (l(4)+l(1)+l(25))*(N(19)==0)+(l(4)+l(1)+l(25))*(N
    (19)==1) (l(4)+l(1)+l(25))*(N(19)==0)+(l(4)+l(1)+l(25))*(N(19)==1)];

shear_right_y = [a_nodes(2,10) a_nodes(2,10)*(N(34)==0)+(a_nodes(2,8)+l(17)
    )*(N(34)==1) a_nodes(2,10)*(N(34)==0)+a_nodes(2,8)*(N(34)==1) a_nodes
    (2,10)*(N(34)==0)+(a_nodes(2,6)+l(13))*(N(34)==1) (a_nodes(2,6)+l(13))*(
    N(19)==0)+(a_nodes(2,10)+l(21))*(N(19)==1) (a_nodes(2,6)+l(13))*(N(19)
    ==0)+a_nodes(2,8)*(N(19)==1) (a_nodes(2,6)+l(13))*(N(19)==0)+(a_nodes
    (2,8)+l(17))*(N(19)==1) (a_nodes(2,6)+l(13))*(N(19)==0)+a_nodes(2,6)*(N
    (19)==1) ((a_nodes(2,6)+l(13))*(N(19)==0)+a_nodes(2,6)*(N(19)==1))*(N
    (13)==0)+a_nodes(2,6)*(N(13)==1) ((a_nodes(2,6)+l(13))*(N(19)==0)+
    a_nodes(2,6)*(N(19)==1))*(N(13)==0)+(a_nodes(2,6)+l(13))*(N(13)==1)];
shear_top_x = [(l(2)+l(1)) l(2)+l(1)+l(25)*(N(36)==1) l(2)+l(1) l(2)+l(1)+l
    (25)*(N(36)==1) l(2)+l(1)+l(25) l(2)+l(1)+l(25)*(N(36)==1) l(2)+l(1)+l
    (25) l(2)+l(1)+l(25)*(N(36)==1)];
shear_top_y = [a_nodes(2,16)+l(9)+l(22)+l(26) (a_nodes(2,16)+l(9)+l(22)+l
    (26))*(N(36)==0)+(a_nodes(2,6)+l(13)+l(24))*(N(36)==1) (a_nodes(2,16)+l
    (9)+l(22)+l(26))*(N(36)==0)+(a_nodes(2,16)+l(9)+l(22))*(N(36)==1) (
    a_nodes(2,16)+l(9)+l(22)+l(26))*(N(36)==0)+(a_nodes(2,6)+l(13))*(N(36)
    ==1) (a_nodes(2,6)+l(13))*(N(36)==1)+(a_nodes(2,6)+l(13)+l(24)+l(28))*(N
    (27)==1) (a_nodes(2,6)+l(13))*(N(36)==1)+(a_nodes(2,16)+l(9)+l(22))*(N
    (27)==1) (a_nodes(2,6)+l(13))*(N(36)==1)+(a_nodes(2,6)+l(13)+l(24))*(N
    (27)==1) (a_nodes(2,6)+l(13))*(N(36)==1)+(a_nodes(2,16)+l(9))*(N(27)==1)
    ];

int_11_x = [(l(2)+l(1))*(N(11)==1) (l(2)+l(1)+l(25))*(N(11)==1)];
int_11_y = [a_nodes(2,1)*(N(11)==0)+(l(9)+a_nodes(2,16))*(N(11)==1) a_nodes
    (2,1)*(N(11)==0)+a_nodes(2,6)*(N(11)==1)];
int_32_x = [(l(2)+l(1))*(N(32)==1) (l(2)+l(1)+l(25))*(N(32)==1)];
```

```
23 int_32_y = [a_nodes(2,1)*(N(32)==0)+a_nodes(2,16)*(N(32)==1) a_nodes(2,1)*(
       N(32)==0)+(l(13)+a_nodes(2,6))*(N(32)==1)];
24
25
26 figure
27 hold on
28 plot(base_x, base_y,'-k')
29 plot(top_x, top_y,'-k')
30 plot(shear_left_x, shear_left_y,'-k')
31 plot(shear_right_x, shear_right_y,'-k')
32 plot(shear_top_x, shear_top_y,'-k')
33 plot(int_11_x, int_11_y,'-k')
34 plot(int_32_x, int_32_y,'-k')
35 xlim([-100,(l(1)*2.5+l(25)+l(17)*2.5)])
36 ylim([-100,(max(l(9),l(13))+l(25)*2.5)])
37
38 end
```

Mikael Rosendahl

Comparison of Strut-and-Tie Modeling and Nonlinear Finite Element Analysis Approaches for Concrete Connections

NTNU
Norwegian University of
Science and Technology